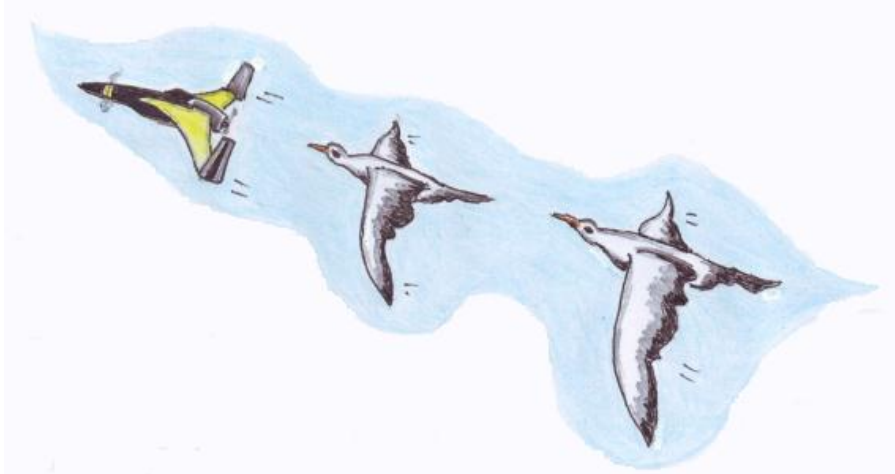


*Predicting the Structural Performance  
of Composite Structures Under  
Cycling Loading*



Christos Kassapoglou



# **Predicting the Structural Performance of Composite Structures Under Cyclic Loading**



# PREDICTING THE STRUCTURAL PERFORMANCE OF COMPOSITE STRUCTURES UNDER CYCLIC LOADING

## PROEFSCHRIFT

ter verkrijging van de graad van doctor  
aan de Technische Universiteit Delft,  
op gezag van de Rector Magnificus prof. ir. K.C.A.M. Luyben,  
voorzitter van het College voor Promoties,  
in het openbaar te verdedigen op maandag 7 mei 2012 om 10:00 uur  
door

Christos KASSAPOGLOU

master of science in Aeronautics and Astronautics,  
master of science in Mechanical Engineering,  
Massachusetts Institute of Technology, Cambridge MA, USA  
geboren te Athene Griekenland

Dit proefschrift is goedgekeurd door de promotor:

Prof. dr. Z. Gürdal

Samenstelling promotiecommissie:

Rector Magnificus	voorzitter
Prof. dr. Z. Gürdal	Technische Universiteit Delft, promotor
Prof. dr. ir. R. Benedictus	Technische Universiteit Delft
Prof. dr. P.A. Lagacé	Massachusetts Institute of Technology
Prof. dr. K.L. Reifsnider	The University of South Carolina
Prof. dr. ir. M.J.L. van Tooren	Technische Universiteit Delft
Prof. dr. M.R. Wisnom	University of Bristol

Keywords: fatigue analysis, composite materials, damage, probability of failure, residual strength

ISBN XXX-XX-XXXX-XXX-X

Copyright ©2012 by Christos Kassapoglou

All rights reserved. No part of the material protected by the copyright notice may be reproduced or utilized in any form or by any means, electronic or mechanical, including photocopying, recording or by any information storage and retrieval system, without the prior written permission by the author.

*Into this Universe and Why not knowing  
Nor Whence, like Water willy-nilly flowing;  
And out of it, as Wind along the Waste,  
I know not Whither, willy-nilly blowing.*

Rubaiyat of Omar Khayyäm  
Translated by Edward Fitzgerald

*Je n'ai fait celle-ci plus longue que parce que je n'ai pas eu le loisir  
de la faire plus courte*

Blaise Pascal, Lettres Provinciales, Lettre XVI



---

## Summary

The increased use of advanced composite materials on primary aircraft structure has brought back to the forefront the question of how such structures perform under repeated loading. In particular, when damage or other stress risers are present, tests have shown that the load to cause failure after a given number of cycles is a decreasing function of these cycles. This is a result of damage that was already present in the structure or was created during cyclic loading. In composites, multiple types of damage may be present in the structure at the same time such as matrix cracks, fiber kinks, delaminations, broken fibers, etc. These types of damage may interact and transition from one type to another and are, ultimately, responsible for structural failure. In trying to predict the number of cycles to failure of a composite structure it is, therefore, necessary to understand how damage is created, how it evolves and how different types of damage may interact or coalesce. A first step in that direction, using what is one of the simplest models that can be used, is the subject of this thesis.

The number of cycles to failure is related to the residual strength of the structure for constant amplitude loading. A simple first-order model is postulated that determines the residual strength at any point during the fatigue life as a function of the residual strength at any earlier point in time. For constant amplitude loading, the resulting expression relates the maximum applied load, the number of cycles, the cycles to failure corresponding to the applied load, and the residual strength at the beginning of a test, to the residual strength at the end of the test. With the residual strength known as a function of cycles, a cycle-by-cycle probability of failure is introduced. It is shown that, if the static (or residual) strength follows a two-parameter Weibull distribution, the cycle-by-cycle probability of failure is constant and independent of the number of cycles. For the case of constant cycle-by-cycle probability of failure, the number of cycles to failure is determined as the value that maximizes the likelihood of failure. The resulting expression is in terms of the cycle-by-cycle probability of failure. If the residual strength distribution is known, the cycles to failure can be expressed in terms of parameters of this distribution. Simple closed-form expressions are obtained for two-parameter Weibull distributions. For other types of distributions (normal or lognormal for example) no closed form expressions were found. The effect of R ratio is incorporated using a simple proportional relation that accounts for the load excursion being different from that for  $R=0$ . The predictions of this approach for constant amplitude loading situations were compared to test results in the literature for a wide variety of laminates, materials, and loading conditions. While in some cases the agreement of test results with predictions was excellent, in others the discrepancy clearly suggested that the analytical

---

model must be improved.

The analytical model was also used to construct Goodman diagrams and determine omission levels for tests. Comparison of analytically predicted Goodman diagrams to test results showed good agreement in the tension-dominated portion of the diagram but some disagreement in the compression-dominated portion. This is attributed to the simplicity of the model which does not accurately capture interaction of failure modes when both tension and compression loads are present.

The omission level is the load level below which no damage is created, no growth of existing damage is observed, and no failure occurs for a prescribed number of cycles. This allows shortening of test programs by eliminating cycles with loads below the omission level. Comparisons of predictions to test results showed very good agreement over a wide variety of tests, materials, R ratios, notches, and layups.

The model, in its simplest form, was then extended to spectrum loading cases. This was done by creating an equivalence between different load levels and applied cycles by matching the residual strength at the end of each load level. For this approach to work, the failure mode and damage type dominating the fatigue life must be the same for the two (or more) load segments of interest. This then allows a single quantity, the residual strength, to accurately describe the damage state. Simple closed form expressions were obtained for the number of cycles or load segments to failure under spectrum loading. Comparisons with test results showed good agreement for tension-dominated spectra but major discrepancies for compression-dominated spectra again pointing to the need for improving the model to account for interaction of multiple failure modes and types of damage.

The main reason for the discrepancies between test results and analytical predictions was the constant cycle-by-cycle probability of failure that resulted from the original assumptions in the model. If there is one dominant failure mode the cycle-by-cycle probability of failure is constant. However, when more than one types of damage or failure modes are present, their interaction and the resulting load redistribution in the structure changes the cycle-by-cycle probability of failure. The model was, therefore, modified by assuming that the probability of failure is constant over a limited number of cycles until another failure mode or damage type occurs and changes the residual strength and the cycle-by-cycle probability of failure. This can become quite complex even for the apparently simple case of a uni-directional laminate under tension where, during cyclic loading, weak fibers fail and their load is redistributed to adjacent fibers. The main difficulty is then in creating an analytical model that can accurately determine stresses throughout the structure as damage evolves and, on the basis of these stresses, predict the residual strength.

The improved model was applied to two cases, a uni-directional laminate

---

and a cross-ply laminate of the form  $[0_m/90_n]_s$  under tension-tension fatigue. For the uni-directional laminate, the improved predictions for cycles to failure were in excellent agreement with test results. For the cross-ply laminate, the accuracy of the predictions ranged from excellent to poor depending on the ratio of the thickness of internal  $90^\circ$  plies to that of the surrounding  $0^\circ$  plies. The main issue in this case is that the analytical model developed for predicting stresses around matrix cracks and the associated load redistribution in the laminate are not very accurate as the crack density increases beyond a certain point. More accurate analytical modeling of this situation is expected to improve the predictions for cycles to failure.

The analysis method proposed here is still in its infancy. In its simplest form, it is shown to work well in many cases but not well in others. What is important is that a framework for performing fatigue analysis of composites is presented, which relies on the residual strength and how that varies with cycles as damage is created and evolves. Essentially, what is proposed here is a wear-out model. Wear-out models have been proposed before. The main difference and potential improvement here is that there is no need for curve fitting test data or experimentally determined fatigue parameters. The equations governing the model are determined analytically and, in some cases, in closed form. While the model needs further improvements mainly in how the creation of different types of damage is predicted and how their interaction and evolution is accounted for, it is very promising because it provides a general and purely analytical methodology to predict cycles to failure under constant amplitude or spectrum loading.



---

## Samenvatting

Door het toenemende gebruik van geavanceerde composieten materialen in primaire vliegtuigconstructies is de vraag opnieuw gerezen hoe zulke constructies zich gedragen onder cyclische belasting. Experimenten hebben aangetoond dat de belasting, die leidt tot breuk na een bepaald aantal cycli, afneemt met het aantal cycli wanneer beschadiging of andere spanningsverhogers in het spel zijn. Dit is het gevolg van de beschadiging die reeds aanwezig was in de constructie of die ontstaan is tijdens de cyclische belasting. Verschillende soorten van beschadigingen kunnen tegelijkertijd aanwezig zijn in de constructie, waaronder scheurtjes in de matrix, een kink in de vezels, delaminaties, gebroken vezels, enz. Deze soorten van beschadigingen kunnen interageren en veranderen van het ene type naar het andere en zijn uiteindelijk verantwoordelijk voor het bezwijken van de constructie. Wanneer men tracht het aantal cycli te voorspellen, dat leiden tot het bezwijken van een composieten constructie, is het dan ook noodzakelijk om te begrijpen hoe de beschadigingen ontstaan. De eerste stap in die richting, gebruik makend van een van de eenvoudigste modellen die gebruikt kunnen worden, is het onderwerp van deze thesis.

Het aantal cycli dat leidt tot bezwijken is gerelateerd aan de structurele reststerkte onder een belasting met constante amplitude. Een eenvoudig eerste ordemodel, dat de reststerkte bepaalt op elk punt in de vermoeiingscurve als functie van de reststerkte op elk moment eerder in de tijd, wordt aangenomen. Voor een belasting met constante amplitude wordt er een uitdrukking opgesteld die de maximale opgelegde belasting, het aantal cycli, het aantal cycli die leiden tot bezwijken onder de opgelegde belasting en de reststerkte aan het begin van de test relateert aan de reststerkte aan het einde van de test. De kans op bezwijken voor elke cyclus wordt berekend op basis van de reststerkte als functie van de cycli. Als de statische (of rest-) sterkte voldoet aan een Weibullverdeling met twee variabelen, dan is aangetoond dat kans op bezwijken bij elke cyclus constant is en onafhankelijk van het aantal cycli. In het geval dat de kans op bezwijken per cyclus constant is, dan wordt het aantal cycli dat leidt tot bezwijken bepaald door de waarde die de kans op bezwijken maximaliseert. De resulterende uitdrukking kan worden geschreven in termen van de kans op bezwijken per cyclus. Wanneer de reststerkteverdeling gekend is, kan het aantal cycli dat leidt tot bezwijken uitgedrukt worden in termen van de parameters van deze verdeling. Eenvoudige analytische uitdrukkingen zijn afgeleid voor Weibullverdelingen met twee variabelen. Analytische uitdrukkingen werden niet gevonden voor andere soort verdelingen, zoals normaalverdelingen of lognormale verdelingen. De invloed van de R-verhouding is meegenomen door gebruik te maken van een eenvoudige recht evenredige relatie die in acht neemt

---

dat de belastingsuitschieter verschillend is van deze bij  $R=0$ . De voorspellingen van deze aanpak, bij situaties waar de amplitude van de belasting constant was, zijn vergeleken met testresultaten uit de literatuur voor een heel aantal laminaten, materialen en types belasting. Hoewel er gevallen waren waar de overeenkomst tussen de testresultaten en de voorspellingen excellent was, waren er andere gevallen waar de discrepanties duidelijk aantoonde dat het analytische model verbeterd moest worden.

Het analytische model werd ook gebruikt om Goodman diagrammen te creëren en om te bepalen welke testen weggelaten konden worden. Een vergelijking tussen de Goodman diagrammen die gecreëerd waren met het analytische model toonde aan dat er een goede overeenstemming was voor het gedeelte van het diagram dat gedomineerd wordt door trekspanning, maar er ontstond een zeker verschil in het gedeelte van het diagram dat gedomineerd werd door drukspanningen. Dit wordt toegeschreven aan de eenvoud van het model wat niet in staat is om op een accurate manier de interactie tussen de bezwijkvormen te beschrijven wanneer zowel trek- als drukbelastingen aanwezig zijn.

Het weglatingsniveau is het belastingsniveau onder hetwelk er geen beschadigingen worden gecreëerd, er geen groei van bestaande beschadigingen geobserveerd wordt en waarbij er geen bezwijken optreedt voor een voorgeschreven aantal cycli. Hierdoor kan het testprogramma verkort worden omdat de cycli met belastingen onder het weglatingsniveau weggelaten kunnen worden. Vergelijking van de voorspellingen met de testresultaten toonde een goede overeenkomst aan voor een groot aantal testen, materialen,  $R$ -verhoudingen, beschadigingen en vezelvolgordes.

Het model in zijn meest eenvoudige vorm werd vervolgens uitgebreid met spectrale belastinggevallen. Dit werd bewerkstelligd door verschillende belastingniveaus en toegepaste cycli gelijkwaardig te stellen door de reststerktes aan het eind van elk belastingniveau overeen te laten komen. Om dit te bewerkstelligen moeten de bezwijkvormen en beschadigingstypes die de vermoeiing domineren hetzelfde zijn voor twee of meer relevante belastingsegmenten. Dit zorgt er voor dat slechts een parameter, namelijk de reststerkte, de beschadiging op een accurate manier kan beschrijven. Eenvoudige analytische uitdrukkingen werden afgeleid voor het aantal cycli of belastingsegmenten onder spectrale belasting. Een vergelijking met experimentele resultaten toonde aan dat er een goede overeenkomst is voor spectra die gedomineerd worden door trekspanningen maar grote afwijkingen werden er gevonden voor spectra die gedomineerd werden door drukspanningen, hetgeen opnieuw wijst op de noodzaak om het model te verbeteren en de interactie van verschillende bezwijkvormen en beschadigingstypes mee te kunnen nemen.

De belangrijkste oorzaak van de verschillen tussen testresultaten en analytische voorspellingen was de constante kans op bezwijken per cyclus in

---

het oorspronkelijke model. Indien er slechts een dominante bezwijkvorm is, dan is de kans op bezwijken per cyclus constant. Echter, wanneer er meerdere beschadigingstypes of bezwijkvormen zijn, veranderen hun interactie en de resulterende structurele belastingherverdeling de kans op bezwijken per cyclus. Daarom werd het model aangepast waarbij werd aangenomen dat de kans op bezwijken constant was voor een beperkt aantal cycli totdat er een nieuwe bezwijkvorm of beschadigingstype opdook en de reststerkte en kans op bezwijken per cyclus veranderde. Dit kan redelijk ingewikkeld worden zelfs voor het schijnbaar eenvoudige geval van een uni-directioneel laminaat dat belast wordt op trek waarin tijdens het uitharden zwakke vezels bezwijken en hun belasting herverdeeld wordt over de aanliggende vezels. De grootste moeilijkheid bevindt zich in het opstellen van het analytische model dat op een accurate manier de spanningen kan berekenen in de constructie wanneer de beschadigingen evolueren en op basis van die spanningen de reststerkte kan voorspellen.

Het verbeterde model werd toegepast op twee gevallen, een uni-directioneel laminaat en een laminaat met vezels loodrecht op elkaar in de vorm  $[0_m/90_n]_s$  onder een trek-trek vermoeiingsbelasting. Voor het uni-directioneel laminaat bleken de verbeterde voorspellingen voor het aantal cycli die leiden tot bezwijken goed overeen te komen met testresultaten. In het geval van het laminaat met loodrechte vezels varieerde nauwkeurigheid van de voorspellingen van excellent tot matig, afhankelijk van de verhouding tussen de dikte van de interne  $90^\circ$  laagjes en de omliggende  $0^\circ$  laagjes. Het belangrijkste probleem in dit geval is het feit dat het analytische model, dat ontwikkeld was om spanningen rond matrixscheurtjes en de resulterende spanningsherverdeling te berekenen in het laminaat, niet erg nauwkeurig was omdat de scheurdichtheid toeneemt vanaf een bepaald punt. Verwacht wordt dat een meer accurate analytische modellering van deze situatie de voorspelling voor het aantal cycli, dat leidt tot bezwijken, zal verbeteren.

De analytische methode die hier wordt voorgesteld staat nog steeds in de kinderschoenen. Het is aangetoond dat het model, in zijn meest essentiële vorm, goed functioneert voor talrijke gevallen, maar niet goed functioneert voor andere gevallen. Het belangrijkste is dat er een raamwerk om een vermoeiingsanalyse voor composieten uit te voeren, is voorgesteld. Dit raamwerk is gebaseerd op de reststerkte en hoe deze varieert met het aantal cycli terwijl beschadigingen ontstaan en evolueren. Wat hier eigenlijk voorgesteld wordt is een wear-out model. Dit type model is reeds vroeger voorgesteld. Het belangrijkste verschil en mogelijke verbetering is dat er in dit geval geen noodzaak is om meetgegevens of experimenteel bepaalde vermoeiingsparameters af te leiden uit grafieken. De vergelijkingen die het model beschrijven zijn afgeleid op een analytische manier en, in sommige gevallen, in een vergelijking. Hoewel het model verder verbeterd moet

---

worden, hoofdzakelijk op het vlak van hoe het ontstaan van verschillende beschadigingstypes voorspeld wordt en hoe hun interactie en evolutie in rekening gebracht worden, is het erg veelbelovend omdat het een algemene en zuiver analytische methode is om het aantal cycli te voorspellen die leiden tot bezwijken onder een belasting met constante amplitude of spectrale belasting.

---

## Acknowledgements

Now that I have come full circle and completed a PhD thesis 34 years after I started my Bachelor's I look back and realize that I would never have gotten here if it weren't for some far-sighted and, thankfully, stubborn people who helped me all along. What follows is not necessarily in order of importance.

First and foremost, Paul Lagacé who started as my Master's thesis advisor 29 years ago (I finished both MS degrees 28 years ago by the way) and now graciously accepted to be a member of my PhD thesis committee. Throughout the years and, in particular, the past few years when this work started taking shape, his insightful comments and suggestions were invaluable not the least of which was that baseball can be exciting especially when the Red Sox win the World Series. I am indebted to him for not giving up on me.

Furthermore, I am grateful to Zafer Gürdal for insisting that I do this and helping me all along. I still can't figure out how he manages to combine superb engineering and academic rigor with intuition that is almost never wrong. I have learned a lot and look forward to more lessons.

The remaining committee members, Michel van Tooren, Michael Wisnom, Kenneth Reifsnider, and Rinze Benedictus are the best members one could hope for. I am convinced the quality of this thesis would suffer a lot if it weren't for their excellent, and sometimes tough, comments. I am honored.

In addition to the above, there is a group of people to whom I am grateful. Myriam Kaminski was instrumental in setting up some of the work on cross-ply laminates. Roeland de Breuker, a scholar's scholar, translated the propositions and the summary to Dutch. Miranda Aldham-Breary helped me tremendously in getting my English to read (and sound) as English should. Finally, the two gurus Djim Molenkamp and Willem Eerland were instrumental in putting some professionalism in the layout and appearance of my work. My heartfelt thanks!



# Contents

<b>1</b>	<b>Introduction</b>	<b>1</b>
1.1	Background . . . . .	1
1.2	Previous Work . . . . .	6
1.3	Outline . . . . .	10
<b>2</b>	<b>Analytical model for determining the cycles to failure under constant amplitude loading</b>	<b>13</b>
2.1	Damage state in a composite structure after repeated loading relation to residual strength . . . . .	14
2.2	Determination of cycles to failure relation to residual strength . . . . .	18
2.2.1	Cycle-by-cycle probability of failure . . . . .	18
2.2.2	Determination of cycles to failure . . . . .	27
2.3	Effect of R Ratio . . . . .	32
2.3.1	Tension-tension ( $0 < R < 1$ ) or compression-compression ( $R > 1$ ) cases. . . . .	33
2.3.2	Tension-compression cases ( $R < 0$ ) . . . . .	36
<b>3</b>	<b>Comparison of analytical predictions with test results - implications</b>	<b>39</b>
3.1	Residual strength comparison . . . . .	39
3.2	Applied stress level to cause failure after N cycles (S-N curves) . . . . .	40
3.3	Goodman diagrams . . . . .	46
3.4	Evaluation-shortcomings of the method as presented so far . . . . .	52
3.5	Summary . . . . .	54
<b>4</b>	<b>Applications of the proposed model to establish reliability-based design curves and omission levels and reduced number of test cycles</b>	<b>55</b>
4.1	Determination of number of lifetimes testing for B-basis reliability . . . . .	55
4.2	Determination of omission levels in test programs . . . . .	60
4.3	An exchange rule for reduced equivalent number of cycles . . . . .	64
4.4	Summary . . . . .	67
<b>5</b>	<b>Extension of the analytical model to situations with spectrum loading</b>	<b>69</b>
5.1	Model development . . . . .	70
5.1.1	Residual strength as a function of applied load segments . . . . .	70
5.1.2	Cumulative damage law . . . . .	73
5.1.3	Implications of the spectrum loading model . . . . .	77

---

5.1.4	Number of block repetitions to cause failure . . . . .	78
5.2	Comparison with test results and discussion . . . . .	80
5.2.1	Two-load segment case: test versus analytical predictions	80
5.2.2	Four load segment case: test versus analytical predictions	86
5.2.3	Discussion . . . . .	88
<b>6</b>	<b>Enhancements to the analytical model for prediction of cycles to failure</b>	<b>93</b>
6.1	Description of improved model . . . . .	94
6.2	Application 1: uni-directional laminate under tension-tension loading . . . . .	99
6.2.1	Effect of fiber diameter variation and fiber waviness on fiber strength . . . . .	100
6.2.2	Effect of flaws on fiber strength . . . . .	103
6.2.3	Analysis procedure . . . . .	106
6.2.4	Comparison with test results . . . . .	109
6.3	Application 2 - cross-ply laminate under tension-tension loading	110
6.3.1	Determination of stresses in a cross-ply laminate with matrix cracks under tension . . . . .	112
6.3.2	Comparison of analytically determined stresses to finite element results . . . . .	115
6.3.3	Predictions of cycles to failure compared to test results	117
6.4	Discussion . . . . .	118
<b>7</b>	<b>Conclusions and recommendations</b>	<b>123</b>
7.1	Conclusions . . . . .	124
7.2	Recommendations . . . . .	125

## List of Figures

1.1	Typical S-N curves for Composite and Metal (normalized) . . .	2
1.2	Typical S-N curves for composite and metal (not normalized) .	2
1.3	Damage created during fatigue loading (tension-tension loading)	4
1.4	Flaw growth as a function of cycles . . . . .	6
2.1	S-N curve and residual strength curve . . . . .	15
2.2	Probability density distribution for compression strength of typical Graphite/Epoxy (two-parameter Weibull: $\alpha = 10.375$ $\beta = 1447.1$ MPa) . . . . .	20
2.3	Cumulative distribution function for compression strength of typical Graphite/Epoxy (two-parameter Weibull: $\alpha = 10.375$ $\beta$ $= 1447.1$ MPa) . . . . .	21
2.4	Evolution of residual strength probability density distribution with cycles when a constant cyclic stress $\sigma$ ( $\sigma > \sigma_E$ ) is applied	23
2.5	Change of shape parameter (scatter) of residual strength as a function of cycles . . . . .	23
2.6	$[0_m / 90_n / 0_m]$ laminate with matrix crack in $90^\circ$ plies . . . .	25
2.7	Stresses in the $0^\circ$ ply between two successive matrix cracks . .	26
2.8	Edge delaminations developing in a laminate under tensile loading	27
2.9	Probability that the structure failed between 1 and N cycles as a function of N . . . . .	28
2.10	S-N curves predicted by Eqs 2.30 and 2.32 . . . . .	31
2.11	Cyclic loading for $R = 0$ . . . . .	33
2.12	Cases where $0 < R < 1$ or $R > 1$ . . . . .	33
2.13	Modification of probability density distribution when $R \neq 0$ . .	35
2.14	Typical cyclic load for $R < 0$ . . . . .	36
3.1	Analysis versus test for uni-directional AS4/3501-6 (R=0) . . .	41
3.2	Analysis versus test for $[(\pm 45/0_2)_2]_s$ T800/5245 (R=0.1 and R=0.5) . . . . .	42
3.3	Analysis versus test for $[(\pm 45/0_2)_2]_s$ T800/5245 (R=-1) . . . .	42
3.4	Analysis versus test for $[(\pm 45/0_2)_2]_s$ T800/5245 (R=10) . . . .	43
3.5	Analysis versus test for $[0_2 / \pm 45/0_2 / \pm 45/90]_s$ Celion 6000/ H795E BMI (R=-1) . . . . .	44
3.6	Tension-Torsion case (tension=torsion and R=0) for woven glass fabric . . . . .	44

---

3.7	Onset of delamination load for skin/stiffener pull-off configuration (R=0.1, material: IM6/3501-6) . . . . .	45
3.8	Onset of edge delamination for $[35_2/-35_2/0_2/90_2]_s$ AS4/PEEK (R=0.1) . . . . .	46
3.9	Onset of delamination for quasi-isotropic glass/epoxy (R=0.1) .	47
3.10	Tension-Compression (R=-1.66) failure of T300/914 bolted joints	48
3.11	Relationship between Weibull shape parameter and Coefficient of Variation (CV) . . . . .	49
3.12	Typical Goodman diagram for open hole specimens ( $CV_{ten} = 7\%$ , $CV_{comp} = 10\%$ ) . . . . .	50
3.13	Predicted Goodman diagram versus test results . . . . .	51
3.14	Effect of type of statistical distribution on theoretical predictions for $[0_2/\pm 45/0_2/\pm 45/90]_s$ Celion 6000/ H795E BMI (R=-1)	53
4.1	Fatigue tests on uni-directional AS4/3501-6 Graphite/Epoxy Scatter of fatigue tests. . . . .	56
4.2	Mean and B-Basis curves for the data in Figure 4.1 . . . . .	57
4.3	Ratios of Mean and Modal lives to B-Basis life as a function of $p$	59
4.4	Omission level for one million cycles. Test results and analytical prediction . . . . .	63
4.5	Reduction in number of test cycles as a function of increase in applied load . . . . .	66
5.1	Schematic of loading spectrum as a function of cycles . . . . .	69
5.2	Combinations of cycles and loads giving the same residual strength at the end of two load segments . . . . .	71
5.3	Comparison of present method to (linear) Miner's rule predictions (two load segment case) . . . . .	76
5.4	Schematic of repeating blocks making up a spectrum . . . . .	79
5.5	S-N curve for E-glass/epoxy . . . . .	81
5.6	Residual strength: Analysis versus test (Case 1) . . . . .	82
5.7	Residual strength: Analysis versus test (Case 2) . . . . .	83
5.8	Residual strength: Analysis versus test (Case 3) . . . . .	83
5.9	Residual strength: Analysis versus test (Case 4) . . . . .	84
5.10	Comparison of predictions to test results for two-segment spectrum loading of cross-ply fiberglass laminates . . . . .	86
5.11	Spectrum loading predictions compared to test results . . . . .	88
5.12	All $0^\circ$ laminate with a hole: Damage creation when tension-tension is applied first followed by compression-compression . .	90
5.13	All $0^\circ$ laminate with a hole: Damage creation when compression-compression is applied first followed by tension-tension . . . . .	91

---

6.1	Example of damage tracking and interaction in a composite structure consisting of two sections, i and j. . . . .	96
6.2	Different damage scenarios leading to the same residual strength when starting with identical specimens. . . . .	98
6.3	Wavy fiber in a uni-directional composite . . . . .	101
6.4	Schematic of strength of fibers in a uni-directional ply (width of each bar is proportional to number of fibers with strength in the corresponding range) . . . . .	104
6.5	Analytical predictions compared to test results for uni-directional laminate ( $R \approx 0$ ) . . . . .	109
6.6	Matrix cracks caused in a cross-ply laminate under tension . .	111
6.7	Normal stress $\sigma_x$ in $90^\circ$ ply compared to finite element results .	116
6.8	Crack density versus applied stress for cross-ply laminates Test versus theory . . . . .	117
6.9	Stresses in a $[0/90_2/0]$ laminate under tension with two matrix cracks in the $90^\circ$ plies . . . . .	120
6.10	Analytical predictions compared to test results for $[0/90_2]_s$ AS4/3501-6 laminate . . . . .	121
6.11	Analytical predictions compared to test results for $[0_2/90_2]_s$ AS4/3501-6 laminate . . . . .	121
6.12	Analytical predictions compared to test results for $[0/90_4]_s$ AS4/3501-6 laminate . . . . .	122



*List of Tables*

3.1	Comparison of residual strength predictions to test results . . .	40
4.1	B-Basis, modal, and mean cycles to failure for various p values	59
4.2	Ratio of Mean to B-Basis and Modal to B-Basis lives . . . . .	60
5.1	Cases for residual strength comparison . . . . .	82
5.2	Cases for spectrum loading comparison on fiberglass . . . . .	85
5.3	Cases for spectrum loading comparison on Graphite/BMI material	87



# 1

## *Introduction*

### **1.1 Background**

Under cyclic loading, the strength and stiffness of composite and metal structures degrade. Damage is created and may grow throughout a structure eventually leading to failure. This damage formation and subsequent growth is accompanied by strength and stiffness degradation and forms the basic mechanism driving structural fatigue. There are, however, several important differences between how metal and composite materials behave under cyclic loading and one should carefully define the terms to be used when referring to the performance of composites under repeated loading.

The first important difference is in the failure stress versus cycles (S-N) curve. The S-N curve relates a certain load or stress level S to the number of cycles to failure N. It can be used to determine the maximum load amplitude S of N load cycles before the structure fails. For composites, S-N curves tend to be much shallower than those for metals. The loss of strength for a given number of cycles is significantly smaller in composites. A typical example is shown in Figure 1.1 where the continuous lines represent best fits to the test data. For both curves in Figure 1.1 the damage present at the beginning of the tests resulted in a ratio of notched static failure strength to un-notched static failure strength of 1.5. The composite specimens were sandwich with two plain weave fabric plies and 12.7mm honeycomb core. The unnotched static strength was 367MPa (failure due to facesheet wrinkling). The Aluminum specimens were standard hourglass specimens with specially machined notch having the same unnotched to notched static strength ratio of 1.5.

When the applied stress is normalized by the static strength, the quasi-isotropic (QI) sandwich composite appears to be superior to the 7075-T6 Aluminum. The Al data shown in Figure 1.1 were taken from [1]. For the composites sandwich specimens, the required damage level before the fatigue test started was determined by impacting various specimens at different energy levels and statically testing them to failure. The impact energy that led to a compression after impact (static) strength to undamaged strength ratio of 1.5 was used to impact the fatigue test specimens. In addition, both the metal and composite specimens are loaded in their critical failure mode, the composite in compression after impact ( $R = \sigma_{min}/\sigma_{max} \approx 10$ ) and the metal in notched tension ( $R = 0$ ).

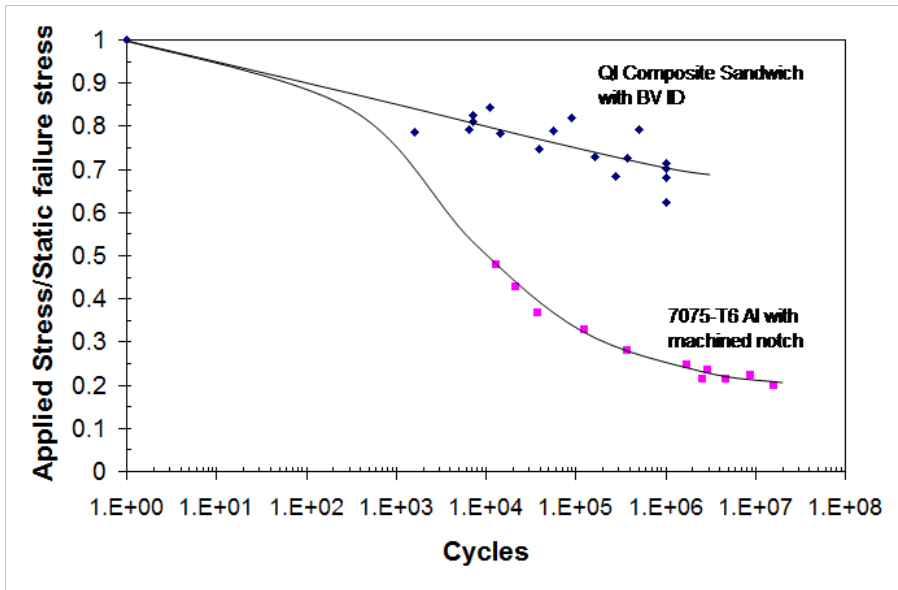


Figure 1.1: Typical S-N curves for Composite and Metal (normalized)

A more instructive comparison can be drawn if the data shown in Figure 1.1 are plotted without normalizing the strength as shown in Figure 1.2.

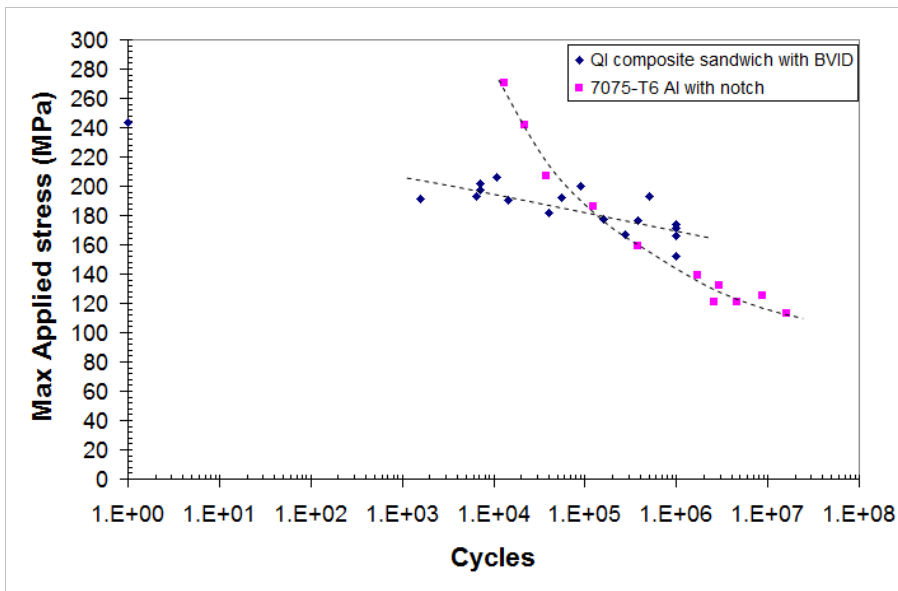


Figure 1.2: Typical S-N curves for composite and metal (not normalized)

It is now evident, as can be seen from Figure 1.2, that for low cycle fatigue, metals can be better than QI composites. The two curves cross at about  $10^5$  cycles. Beyond  $10^5$  cycles the curve for the metal is below the curve for the composite and thus, in terms of the stress level needed to reach a given number of cycles, the composite outperforms the metal.

The relative “shallowness” of the composite S-N curves has led many to suggest that composites have no fatigue problems and, even, infinite fatigue lives. While some test data seem to suggest no strength degradation of unidirectional laminates under tension-tension loading, (at least up to 1 million cycles) generalizing this to multiple materials and different stacking sequences and loadings can be misleading and, in fact, dangerous. For example, it can be seen from Figure 1.1 that the applied compression stress cannot exceed 70% of the static strength for a QI composite to last one million cycles. This means that, if composite structures are not properly designed to account for strength reduction under repeated loading, once damaged, they may fail prematurely. Conversely, for structures that undergo relatively few cycles in a lifetime ( $< 10^5 - 2 \cdot 10^5$ ), as do many fuselage parts, a good static design typically also covers the fatigue requirement, while for parts that see a large number of cycles in a lifetime ( $> 10^6$ ) such as vibrating parts of the fuselage, engine parts, rotor and wind turbine blades, performance under fatigue loads may be the critical condition for designing the structure [2,3]. This sensitivity to cyclic loading is particularly pronounced for constant amplitude loading and load spectra dominated by constant amplitude load segments. Composite parts undergoing spectrum loading with multiple load segments of different amplitudes are less sensitive.

The second important difference between composites and metals, evident from Figure 1.1, is that composites exhibit greater scatter than metals. This means that a design curve or value for a composite with a specified reliability will be a fraction of the mean strength that is lower than the corresponding fraction for the equivalent metal design.

The third important difference between composites and metals is how the fatigue process evolves within these materials. While in a metal damage progression, which is in the form of crack initiation and growth, is self-similar with one or more cracks growing parallel to their original orientation under repeated loading, in composites, multiple complex types of damage can be present and interact.

In general, damage in composites first manifests in the form of matrix cracks in plies with fibers not aligned with the load(s). Under repeated loading, these cracks multiply and grow. Depending on the loading and stacking sequence however, these cracks may either branch out to adjacent plies or form delaminations at ply interfaces. Upon further loading, the matrix cracks and delaminations grow, and which type of damage will dominate is a function of

loading, part geometry, and stacking sequence, as well as constituent (mainly resin) properties. Stress concentrations at the tips of matrix cracks and/or delaminations can also lead to fiber breakage. A hand-drawn schematic showing representative types of damage in a composite is shown in Figure 1.3.

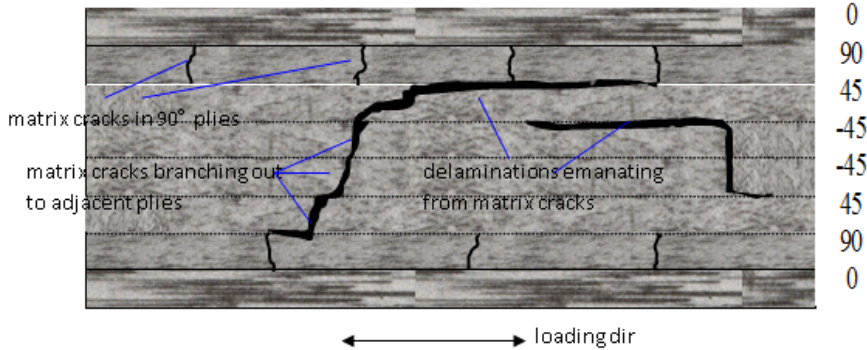


Figure 1.3: Damage created during fatigue loading (tension-tension loading)

Understanding damage creation and evolution in a composite structure involves analysis and testing over a great range of scales, from the fiber diameter scale,  $7\ \mu\text{m}$  for typical carbon fibers, where surface cracks on the fiber surface or flaws in the fiber/matrix interface may act as stress concentration points, to the ply scale,  $0.15\ \text{mm}$ , with matrix cracks, voids, and delaminations at the ply interfaces, to the macro-scale, on the order of centimeters, where large scale delaminations and fiber breakage occur and may lead to final failure. While a complete understanding of these effects requires modeling across all these scales, the focus in the present work will be on scales in the range of a few hundred fiber diameters to the macro scale with the assumption that the process of damage nucleation at lower scales has already taken place during fabrication. In a sense, this assumes the presence of inherent flaws such as fiber surface cracks, fiber/matrix disbonds, etc. It is a convenient assumption that simplifies the analytical modeling, and one that can be relaxed when models at the smaller scales are necessary. The approach presented here is still applicable at different scales; only the appropriate models will change.

The multiple types of damage present in composites during fatigue loading complicate modeling of the structure and, as mentioned earlier, depart significantly from those found in metals where a single type of damage, a crack, grows in a self-similar mode. Determining the number of cycles to failure for a composite structure under a given loading, requires tracking the evolution of all possible types of damage and their effect on the strength and stiffness of the structure.

This multiplicity of damage types, and the fact that the type(s) of damage that dominate performance and lead to failure can, in fact, change with cyclic loading, make a growth-based modeling of damage tolerance of composites difficult and not cost-efficient. While in metals, a crack may grow in a stable fashion over a large number of cycles permitting economical inspection methods and intervals to be established, in composites, certain types of damage such as delamination or a through cracks may arrest or grow very fast without presenting any useful region of stable growth to allow for structural monitoring on the basis of damage tolerance. This is illustrated in Figure 1.4 where typical growth curves for composites and metals are provided. In the composite, a typical sandwich fuselage skin 15 cm wide by 30 cm long with a cross-crack through the thickness of one facesheet approximately 2 cm across is loaded in tension-tension ( $R=0.05$ ) with maximum stress equal to 67% of the static strength of the specimen. During the cyclic test, there is some growth in jumps, evidenced by the fact that the data do not follow a smooth curve, until approximately 160000 cycles. This growth is characterized by some crack growth but mostly by the creation and growth of delaminations. After 160000 cycles, rapid growth and final failure follow at about 370000 cycles. This means that the only region where some inspection intervals might reliably be established is between 20000 and 150000 cycles. This region is very narrow. Since at least three inspection intervals should be established, each inspection interval would correspond to about 43000 cycles. For many applications, this translates to a few hundred or, at most one thousand flight hours. Grounding an aircraft for detailed inspection looking for delamination growth at these intervals is not economical. Conversely, 7075-T6 Aluminum has a well defined region of stable growth between 2000 and 500000 cycles (data taken from [4]). The inspection intervals in this case would be longer and thus more economical.

As seen from Figure 1.4, damage growth in composites is, usually, sudden and unstable as implied by the steep slope at the end of the curve. This coupled with their increased scatter during fatigue loading, which increases the cost and reduces the accuracy, makes growth-based damage tolerance of composites non-economical (in most cases). In the past, this has led to damage tolerance designs where no growth of damage typical of what is expected to occur during service was permitted in the structure. Such an approach results in weight penalties because the structure must be designed ensuring that damage of a certain size will not grow under service loads. This does not mean that, under certain circumstances, stable growth of damage in composites cannot occur and economically feasible inspection intervals cannot be established. Unfortunately, these situations are quite limited and, in general, a “no-growth” approach is used. The “no-growth” approach has been shown to be both reliable and economically feasible [5,6].

In the above discussion, fiber-reinforced composites were considered as

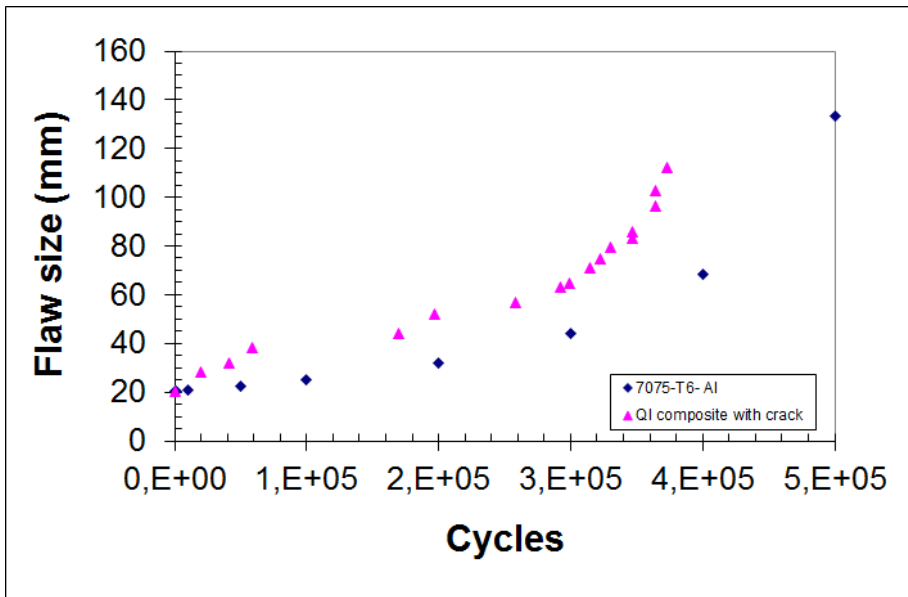


Figure 1.4: Flaw growth as a function of cycles

the only material present. Some of the differences between metals and composites become less pronounced when they are combined to create fiber metal laminates. A good overview of the behavior of fiber metal laminates is given by Schijve [7]. It should be noted that the emphasis in this thesis is on fiber-reinforced composite laminates without any metal layers in the stacking sequence.

## 1.2 Previous Work

Given the important differences mentioned above between composites and metals, it became clear early on, that fatigue analysis methods specific to composites would have to be developed if accurate models were to be used to predict the structural performance of composites under cyclic loads. If the ultimate goal is the design of safe, economically viable composite aircraft with quantified and statistically meaningful service lives, the methods developed should (a) provide an understanding of the degradation of structural properties of composite structures under fatigue loading, (b) link this understanding to the certification or qualification requirements via rational interpretation of these requirements as they apply to composites and unaffected by the prevailing experience on metal structures and (c) provide a methodology that can associate a specific design and loading scenario with an accurately measured and/or predicted number of cycles to failure with an associated

reliability level. An overview of this entire problem with its implications for composite, as opposed to metal, structures, is provided by Rouchon [8]. To put things into perspective, it helps to examine, in rough chronological order, the development of fatigue analysis methods for composites. At the beginning, the work was concentrated on isolating the different types of damage and quantifying their effect on the strength and stiffness of composite structures [9–18]. A good summary of the damage mechanisms is given by Talreja in his book [9]. The simpler case of uni-directional composites under fatigue loading was examined by Lorenzo and Hahn [10]. Different mechanisms and damage accumulation were studied by Charewics and Daniel [11] and Reifsnider et al [12]. An attempt to combine various effects of stacking sequence and loading on the creation of damage and its subsequent effect on residual strength was made by Reifsnider and Stinchcomb [13] using the concept of a critical element. This concept was successfully applied to un-notched laminates and was later extended to notched laminates by Bakis et al [14]. At this point, understanding of the micromechanics of damage creation was advanced enough to attempt modeling of fiber, matrix, and their interface [15], as well as laminates with holes under compression [16, 17] and, the most complex situation where in-plane and out-of-plane effects combine to cause damage, [18].

As a result of its inherent complexity, impact damage modeling under fatigue loading led to the creation of multiple models with limited success [19, 20]. As a result of these efforts it became obvious that understanding delamination creation and growth under fatigue loading would be instrumental to obtaining more accurate fatigue models for impacted laminates. To this end, OBrien and others have made numerous contributions [21–26] based mostly on energy release rate approaches.

Continuing along these lines, Subramanian, Reifsnider, and Stinchcomb [27] attempted to include the effects of fiber-matrix interface to track damage creation at smaller scales than previously used. Fatigue of matrix-dominated laminates was examined by Yang, Lee, and Sheu [28, 29] monitoring stiffness degradation as a function of cycles. Compression fatigue methodologies were developed by Badaliane and Dill [30] and Ratwani and Kan [31]. Schaff and Davidson extended their work for constant amplitude fatigue loading [32] to spectrum loading [33]. Implications of damage accumulation for design of fatigue-sensitive composite structures were discussed by Kedward and Beaumont [34]. Philippidis and Vassilopoulos [35] studied the effect of multi-axial loading on fatigue of composites. Whitney [36, 37] and Sendeckyj [38] addressed important aspects of the statistical treatment of test data and interpretation of model parameters in fatigue models. Studying primarily tension-dominated fatigue loading, Schulte [39–41] observed, among other things, that tougher resins lead to longer lives, transverse cracks in  $90^\circ$  plies transition to adjacent  $0^\circ$  plies, and intersecting longitudinal cracks tend to

create delaminations.

The complexity of the phenomena involved required correspondingly complex and computationally intensive analytical models. These models were not efficient enough to be used for design purposes and simplified methods (with rather limited applicability) were developed by Ronold and Echtenmeyer [42], Chamis and Ginty [43], and Lee and Harris [44].

It was soon recognized that the simplified models would not capture the material behavior correctly and would not be sufficiently accurate over a wider range of applications. Investigators turned to improved modeling of damage and its progress under cyclic loading. Diao et al, [45], use a statistical model to predict probability of failure for cross-ply laminates. A shear lag model is used to estimate stiffness reduction and the associated load redistribution from 90 to 0 plies. The model makes an attempt to predict both matrix cracks in the 90 plies and delaminations at the 0/90 ply interface triggered by these cracks. The approach gives good agreement with test results for several types of cross-ply laminates but requires a basic fatigue curve for 90° plies and a strength degradation model for the critical element of the structure. This model requires two curve-fitting parameters.

Turon et al [46] model delaminations during high cycle fatigue by linking the crack growth rate  $da/dN$  with evolution of a damage variable obtained using a cohesive model. This model works well but requires experimentally determined Paris law parameters for the growth rate law of the material.

In another recent attempt, Lian and Yao [47] use a finite element model with built-in stiffness and strength degradation to predict fatigue lives of glass/epoxy composite laminates. Their model requires the basic S-N curves for longitudinal, transverse, and shear loading as inputs. In addition, each element in the finite element model is randomly assigned material properties representative of the experimental scatter of the material. The predictions are in very good agreement with test results, except for cases where local out-of-plane loading dominate damage creation and failure. For these cases, no basic S-N curves are obtained for incorporation into the analytical model.

Effects of different fiber architectures and fiber volumes have been examined, mostly experimentally. One example is work by Mandell et al [48] focusing on wind turbine applications. They show a significant improvement in fatigue life with increasing fiber volume fraction. They also show that the fiber architecture can have a big effect. For example, stitched laminates have a significant advantage over unstitched laminates.

Kawai and Koizumi, [49], have developed a semi-empirical approach to determine constant life diagrams. For the method to work, reference S-N curves, obtained by fitting test data, are necessary. On the same subject of constant life diagram determination, Vassilopoulos et al, [50], examine the use of piecewise linear models to obtain the complete constant life diagram and

find that the results compare favorably with other methods and, in several cases, give the most accurate answers.

Filis et al, [51], have studied the load cycle-mix damage events with emphasis on fiber dominated composites. They show that two-level block test data can be used to account for damage accumulation in composites. This can then be extended to multi-block tests. Preliminary comparisons of their predictions with test data showed that the approach is very promising.

Heuristic arguments about material behavior ahead of a delamination front, combined with a Paris-type law for crack growth, are used by Andersons et al [52] to obtain good predictions of delamination growth as a function of cycles for various materials. As in almost all the models discussed so far, this model involves the use of curve-fitted parameters (such as the constants in the Paris law).

Kim and Hwang [53] propose a semi-empirical method to correlate fatigue performance of composites with property degradation caused by impact damage. The assumption is that at any given point during fatigue life, the stiffness and strength reduction of the composite will equal that caused by the impact of a specific energy level.

Post et al [54] combine a phenomenological residual strength model with an empirical model to track damage accumulation in a Monte Carlo simulation to predict the remaining strength in a composite structure.

Shivakumara et al [55] have developed a predictive model for the complete growth history of a delamination in a composite under cyclic loading. They use basic static and fatigue tests to obtain several model parameters needed in their equation for the delamination growth rate  $da/dN$ .

Boerstra, [56], proposes using a set of equations relating mean and vibratory stress to fatigue life to obtain constant life diagrams for composites. A number of constants, mostly exponents in the equations, different for tension and compression, have to be determined experimentally before the model can be used.

Harper and Hallett, [57] concentrate on improving the numerical techniques based on cohesive elements. They have developed a fatigue degradation law by relating energy release rates to Paris law data. Once the model was calibrated, very good agreement with Mode I, Mode II, and mixed mode fatigue test results was observed.

Of particular interest to the method presented in this thesis is the work of Verhoef, [58], where he attempts to relate the residual strength of a structure to the probability of failure during fatigue cycling, which is analogous to the approach in the present work. In the approach by Verhoef, [58], the structure is divided into elements which have a certain probability of failure. The state of damage and loading determines which elements will fail and when. Once an element fails, load is redistributed and the probability of failure changes. The

probability of failure is linked to the residual strength but it is not analytically determined nor is there a solid analytical method for residual strength and probability of failure link. In addition, the damage state and its relation to residual strength are not quantified. Test results are used to fill in the analysis gaps in the approach.

The above discussion covers only some of the more representative attempts to model damage creation, growth, and failure during fatigue loading of composites. The main conclusions to be drawn from the above summary are:

- (a) all models require some combination of fatigue testing of representative plies, or elements with some semi-empirical constants obtained by curve-fitting some test results.
- (b) there is no comprehensive analytical model for composites that can be used to predict fatigue behavior where all the parameters or variables involved can be calculated analytically or from static tests. As a result, the applicability of existing models is restricted and using them requires expensive and time consuming experiments and computation.

The conclusion, and the motivation for the present work, is that there is a need for analytical models for fatigue of composites that do not include empirical, or semi-empirical parameters and require no fatigue testing to obtain basic behavior. A new model is needed, based, as much as possible, on modeling of physical processes and understanding how the strength and stiffness of a composite structure change with cyclic loading and damage creation and growth.

The approach will be based on the residual strength of the structure and how that changes with cyclic loads. This is coupled with the determination of a cycle-by-cycle probability of failure and a model that predicts the number of cycles with the maximum likelihood of failure. This is used to predict cycles to failure under constant amplitude loading. Under spectrum loading, the residual strength of the structure is first determined as the applied cyclic loads change. This is then used in conjunction with the model for constant amplitude loading to predict the number of spectrum cycles or load blocks to failure.

### 1.3 Outline

The basic concepts for constructing a model to predict cycles to failure under constant amplitude loading are presented in Chapter 2. These include a residual strength model to predict the strength of a composite structure after a certain number of cycles, and the cycle-by-cycle probability of failure. Under

certain assumptions, the cycle-by-cycle probability of failure can be calculated in closed form and related to the static strength of the structure. Closed form equations used to predict cycles to failure for different loading cases are presented.

The model developed in Chapter 2 is compared to experimental results in Chapter 3. The two main ingredients of the analytical model are isolated and comparisons to test results are done separately, first for the residual strength and then for cycles to failure. This will help in identifying where any model weaknesses are most pronounced. In addition, constant life diagrams (Goodman diagrams) are constructed and compared to test results. A wide variety of laminate stacking sequences, materials, and loadings are used for comparison. As a result, all major types of damage, matrix cracks, fiber splitting, delaminations, and fiber breakage are included in the test results. This gives a good understanding of the range of applicability of the model presented in Chapter 2 in its simplest form. It also points to weaknesses of the model which will be evaluated further in Chapter 6.

A summary of how the model can be used to answer important questions in production programs of composite structures is provided in Chapter 4. The first is the determination of number of test cycles needed on a single specimen or component, to establish B-Basis reliability. The second is the determination of the omission level corresponding to one million cycles. This is the load level below which a composite structure can be cycled up to one million cycles with no creation of damage, no growth of existing damage, and no failure. The results of both applications are compared to test results.

The basic model of Chapter 2 for constant amplitude loading is extended to spectrum loading in Chapter 5. Closed form expressions are developed for cycles or blocks to failure. Predictions are compared to test results to establish the accuracy of the model.

Throughout the first five chapters, the shortcomings of the analytical model are presented and discussed. The main shortcoming is the fact that the model uses a constant cycle-by-cycle probability of failure. This is a valid assumption as long as the type of damage created does not change. While there are many cases in which this assumption is valid, there are also numerous cases where this is no longer valid. An approach to rectify this shortcoming is presented in Chapter 6. First, the general approach is presented and then two special cases, one for a uni-directional laminate and one for a cross-ply laminate, are examined in detail.

Finally, the main conclusions and recommendations are summarized in Chapter 7.



# 2

## *Analytical model for determining the cycles to failure under constant amplitude loading*

It became obvious from the discussion in the previous chapter that, to predict the number of cycles to failure of a composite structure accurately, the type(s) of damage created during cyclic loading, their interaction, and their effect on the strength of the structure must be accurately modelled. The formation and evolution of damage is complicated by the multiplicity of failure modes and their interaction. Depending on the stacking sequence, geometry and loading, any combination of matrix cracks, fiber kinking, delaminations, failure of the fiber matrix interface, and fiber failures may occur in almost any sequence (see for example [10–19]). Usually, matrix cracks (tension dominated loading) or fiber kinking and micro-buckling (compression dominated loading) are among the first failure modes that occur followed by delaminations emanating at matrix cracks or in regions of high stresses such as free edges and plydrops. Subsequently, more matrix cracks are created and/or branching of matrix cracks to adjacent plies occur while delaminations extend. Stress concentrations caused by the matrix cracks and delaminations eventually cause fibers to break. Accumulation of fiber breakage leads to final failure of the structure.

Developing a general model that accounts for all types of damage and failure modes and their interactions is complicated and requires modeling the correct sequence of damage creation, which depends on stacking sequence, geometry, loading, the presence of notches, etc. In this chapter, the approach is simplified assuming one type of damage dominates the behavior. This will help describe the features of the analytical model better and will isolate some important characteristics of the analysis. In subsequent chapters some of the obvious limitations of the model will be discussed (Chapters 3-5) and enhancements to the model accounting for additional types of damage created during cyclic loading, will be proposed in Chapter 6.

To develop the model, it is assumed that a single type of damage exists. Exactly what that damage is does not matter as long as it is the same that causes failure under static loading. The damage present determines the static strength under static loading or the residual strength after fatigue loading. This direct relation between the state of damage and the strength of the structure forms the basis of the analytical model. More specifically, residual

strength is selected here as the critical design parameter. The approach is then aimed at determining:

- the damage state of a composite structure after repeated loading
- the relation between the damage state and the (residual) strength of the structure after repeated loading
- the relation between the residual strength and cycles to failure given a damage state in the structure

The above points are discussed in some detail in what follows.

## **2.1 Damage state in a composite structure after repeated loading relation to residual strength**

At a sufficiently small scale, there will always be some damage present in an “as-manufactured” composite structure. This may be in the form of surface cracks or flaws in individual fibers, small disbonds between fibers and matrix, or other flaws at the matrix/fiber interface. In the present model, these types of damage are considered to be part of the pristine structure and are partially responsible for the experimental scatter observed during tests of static strength. These types of damage along with tiny voids, or resin-rich and resin-poor areas act as nucleation sites for the creation of larger-scale damage which is the damage of interest discussed in the present work. One of the most common combinations of damage occurring in composites is matrix cracks and delaminations. Usually, in-plane stresses exceeding the matrix strength cause matrix cracks while out-of-plane stresses lead to delaminations [59]. Under cyclic loading the two may interact [60]. Local geometry changes such as plydrops may contribute in promoting delamination growth in one location and slowing it down or arresting it in another [60]. However, damage growth of one type of damage, matrix cracks, versus the other delaminations, may change with cycles, even for the same stacking sequence [60].

Sufficient number of load repetitions, even if the load intensity is relatively low, will lead to damage creation in a composite structure. As mentioned in chapter 1, typically, the first type of damage is matrix cracks in off-axis plies. These cracks may branch out to neighboring plies and/or, at sufficiently high crack density, lead to delaminations at ply interfaces. The stress concentrations at the tips of matrix cracks and delaminations eventually lead to fiber breakage and subsequent collapse of the structure.

Given a state of damage, there is a load at which either (a) the structure will fail, or (b) the next type of damage will be initiated. This load will be loosely termed residual strength. Note that this term is used here in a broader sense as

it does not necessarily refer to final failure but also covers local failure. It will also be assumed that there is a one-to-one correspondence between residual strength, as defined here, and damage state. If after repeated loading the damage state  $D$  reached in the structure corresponds to a residual strength  $\sigma_r$ , then if one started from a pristine structure and applied repeated loads such that the residual strength reached the value  $\sigma_r$ , the corresponding damage state will be  $D$ . This assumption may not be valid in complex structures where it is possible that different damage states lead to the same residual strength. The implications of this will be discussed later in section 6.1.

It should be noted that the model developed here is a wear-out model with similarities to the "strength-life equal rank assumption" wear-out model first presented by Hahn and Kim [61] and later formulated into a rigorous approach to fit fatigue data by Sendekyj [62]. The main difference from these models is that no curve fitting of test data is required and the model parameters are analytically determined.

The relationship between residual strength and load required to cause failure after  $n$  cycles is shown schematically in Fig. 2.1.

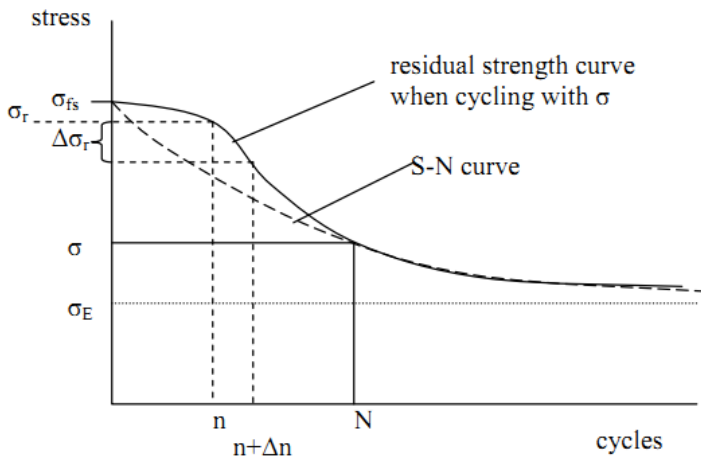


Figure 2.1: S-N curve and residual strength curve

Suppose that a constant amplitude load with maximum stress  $\sigma$  ( $R=\sigma_{min}/\sigma_{max}=0$ ) is applied to a composite structure. The corresponding cycles to failure when  $\sigma$  is applied are  $N$ . This means that if the test is stopped at any cycle level  $n < N$  the structure would not have failed and would still be able to carry load. At this point, a strength test on the structure would show a failure strength  $\sigma_r$  as shown in Fig. 2.1 with  $\sigma_r > \sigma$ . So, during cycling, the curve for the residual strength  $\sigma_r$  decreases from the static failure strength  $\sigma_{fs}$

at one cycle, to  $\sigma$  after  $N$  cycles. The residual strength curve is always above the S-N curve coinciding with it only at two points, when  $n = 1$  and  $n = N$ .

It is now postulated that, given the damage state  $D$  in a composite structure, the subsequent damage created by cycling at load  $\sigma$  changes the residual strength by an amount that is only a function of the number of cycles and the residual strength level corresponding to  $D$ . One of the simplest relations of this type is:

$$\Delta\sigma_r = (A\sigma_r + B)\Delta n \quad (2.1)$$

which states that if a structure has residual strength  $\sigma_r$  after  $n$  cycles, the change in residual strength  $\Delta\sigma_r$  when  $\Delta n$  more cycles are applied at the same load level  $\sigma$  is proportional to the cycle level  $\Delta n$  with constant of proportionality a linear function of the current residual strength level  $\sigma_r$ .

Eq. 2.1 is an assumption partially validated by test results presented in chapters 3.1 and 5.2.1. The problem with test results on residual strength is that they are limited and have significant scatter. More tests are necessary to better quantify the validity of this equation. The equation has the advantage of simplicity at the same time capturing what is intuitively expected, that the state of damage at some point during the life will affect the state of damage at subsequent stages. Other expressions can be used, with the added difficulty of additional unknown constants appearing in the solution for the determination of which there is no immediately available information. Still, other forms of Eq. 2.1 should be investigated. For the purposes of this work, this simplest form is considered sufficient for developing basic trends.

In the limit, for infinitesimal changes in cycles and residual strength, and with proper assumptions on continuity of the functions involved, one can rewrite Eq. 2.1 as:

$$\frac{d\sigma_r}{dn} - A\sigma_r = B \quad (2.2)$$

with  $A$  and  $B$  unknown constants.

The solution to Eq. 2.2 is

$$\sigma_r = Ce^{An} - \frac{B}{A} \quad (2.3)$$

with  $C$  another unknown constant.

The following three conditions are now imposed:

(a) At  $n = 0$ , before cycling, the residual strength equals the static failure strength  $\sigma_{fs}$  (see Fig. 2.1). This leads to:

$$\sigma_{fs} = C - \frac{B}{A} \quad (2.4)$$

(b) One cycle before failure when  $s$  is applied, at  $n = N - 1$ , the residual strength equals  $\sigma$ , i.e., the structure would fail at the next cycle at applied stress  $\sigma$ . This gives the condition:

$$\sigma = Ce^{A(N-1)} - \frac{B}{A} \quad (2.5)$$

(c) For very large  $n$ , with applied load  $\sigma$ , the residual strength tends to the endurance limit  $\sigma_E$ , see Fig. 2.1. The endurance limit is the stress level below which any applied stress will cause no fatigue failure no matter how many cycles are applied. Assuming  $A$  is negative, this condition requires that:

$$\sigma_E = -\frac{B}{A} \quad (2.6)$$

Eqs. 2.4-2.6 form a system of three equations in the three unknowns  $A$ ,  $B$ , and  $C$ . Solving the system gives:

$$\begin{aligned} A &= \frac{1}{N-1} \ln \left( \frac{\sigma - \sigma_E}{\sigma_{fs} - \sigma_E} \right) \\ B &= \frac{\sigma_E}{N-1} \ln \left( \frac{\sigma - \sigma_E}{\sigma_{fs} - \sigma_E} \right) \\ C &= \sigma_{fs} - \sigma_E \end{aligned} \quad (2.7)$$

Note that since  $\sigma < \sigma_{fs}$ , the logarithm in the right hand side of Eq. 2.7 is negative which makes  $A$  negative in agreement with the prior assumption.

With  $A$ ,  $B$ , and  $C$  known from Eq. 2.7, one can substitute in Eq. 2.3 to obtain, after some manipulation:

$$\sigma_r = (\sigma_{fs} - \sigma_E) \left( \frac{\sigma - \sigma_E}{\sigma_{fs} - \sigma_E} \right)^{\frac{n}{N-1}} + \sigma_E \quad (2.8)$$

It is now assumed that the endurance limit  $\sigma_E$  is zero. That is, any stress level repeated for a sufficient number of cycles will, eventually, lead to failure of the structure. Depending on loading, material, and stacking sequence, composites do exhibit non-zero endurance limits, however, accurate determination of endurance limit requires testing beyond  $500 \cdot 10^6$  cycles and is quite difficult [63]. In addition, test data by Samborskys et al [64] at very high cycles shows no clear evidence of an endurance limit up to  $10^8$  cycles for laminates and  $10^{10}$  cycles for fiber strands. This is supported by very high cycle data obtained by D. van Delft at TUDelft. For the purposes of this study, which deals with constant amplitude cycles up to  $100 \cdot 10^6$ , setting the endurance limit equal to zero will, at most, introduce a small error.

Then, Eq. 2.8 is simplified to:

$$\sigma_r = \sigma_{fs} \left( \frac{\sigma}{\sigma_{fs}} \right)^{\frac{n}{N-1}} \quad (2.9)$$

or, rearranging:

$$\sigma_r = \sigma^{\frac{n}{N-1}} \sigma_{fs}^{\frac{N-n-1}{N-1}} \quad (2.10)$$

Eq. 2.10 relates the residual strength after  $n$  cycles to the applied stress  $\sigma$ , the static strength  $\sigma_{fs}$  and the cycles to failure  $N$  when  $\sigma$  is applied. Note that, while the static strength can be determined from simple tests or analysis, the number of cycles to failure  $N$  is, at this point unknown.

In general, if  $N$  is constant, it can be shown that Eq. 2.10 is a decreasing function of  $n$ . This means that the residual strength predicted by this model will never increase. However, there are cases [65], such as open hole tension specimens with combinations of 0 and angle plies (0 aligned with the loading direction) where the residual strength increases, as much as 50%, as longitudinal cracks forming in the 0 plies reduce the stress concentration and then decreases once other forms of damage are created in the angle plies and/or weak fibers in the 0 plies start to fail. The rigorous way to incorporate this effect in the model would be to replace the residual strength Eq. 2.2 with a more general equation that would account for this effect.

## 2.2 Determination of cycles to failure relation to residual strength

### 2.2.1 Cycle-by-cycle probability of failure

Consider a composite structure under constant amplitude loading with maximum applied stress  $\sigma$ . For simplicity, it is assumed that the structure starts from the pristine condition with static strength  $\sigma_{fs}$ . The approach is the same if the structure starts from an already damaged state, after it has been cycled for a number of cycles  $n_o$ , with a proper redefinition of terms such that the static strength is the residual strength of the structure  $\sigma_{ro}$  after  $n_o$  cycles.

Assume now that the static strength of the structure follows a two-parameter Weibull distribution. This is a fairly standard assumption for composite structures where strength for a wide variety of loading and stacking sequences is shown to follow two-parameter Weibull, normal, or log-normal distribution [66]. It will be shown in this section that, as long as the damage during cyclic loading stays the same, the Weibull parameters of the static strength distribution will also determine the residual strength after any number of cycles.

The probability density function for a two-parameter Weibull distribution is given by:

$$f(X) = \frac{\alpha}{\beta} \left( \frac{X}{\beta} \right)^{\alpha-1} e^{-\left(\frac{X}{\beta}\right)^\alpha} \quad (2.11)$$

where  $X$  is the variable (strength in this case) and  $\alpha$  and  $\beta$  are the two parameters of the distribution.  $\alpha$  is the shape parameter and  $\beta$  is the scale parameter. The shape parameter  $\alpha$  is a measure of the data scatter. The larger the value of  $\alpha$  the lower will be the scatter. It will be shown later (section 3.3) that the shape parameter is inversely proportional to the coefficient of variation ( $CV = \text{standard deviation}/\text{mean}$ ). The scale parameter  $\beta$  shifts the entire distribution to the left or to the right. From this perspective, the scale parameter is analogous to the mean of a normal distribution. However, unlike the normal distribution where the mean coincides with the 50th percentile, the scale parameter of a Weibull distribution, is the 63.2 percentile of the distribution.

As an example, the two-parameter Weibull probability density distribution, Eq. 2.11, for the compression strength of typical uni-directional graphite/epoxy with mean strength 1379 MPa and CV 11%, corresponding to a value of  $a=10.375$  is shown in Fig. 2.2.

One important aspect, of immediate implications for the model under development, is the probability  $p$  that the strength of a specimen or structure be lower than a given value  $X_o$ . With reference to Figure 2.2, this probability is the area under the curve to the left of  $X_o$  (shaded region) divided by the total area under the curve.

An equivalent way to see this is to use the cumulative distribution function  $F(X)$  which for a two-parameter Weibull distribution is given by:

$$f(X) = 1 - e^{-\left(\frac{X}{\beta}\right)^\alpha} \quad (2.12)$$

The cumulative distribution function for the same example of Figure 2.2 is plotted in Figure 2.3.

Given a strength value on the x-axis, the curve can be used to read off the y axis the probability  $p$  that the strength of a specimen is less than that value. For example, for the same  $X_o$  value as in Figure 2.2, the dashed horizontal line gives a probability of about 0.05. That is, the probability that the strength of any specimen from this population is less than  $X_o$  ( $\approx 1100$  MPa) is 5%.

Replacing  $X$  with  $\sigma$  in the above discussion, the model for determining cycles to failure can now be presented. The main objective at this point is to determine the probability of failure  $p$  when  $\sigma$  is applied, i.e. the probability that the strength is less than the applied load  $\sigma$ , for a number of cycles  $n$ .

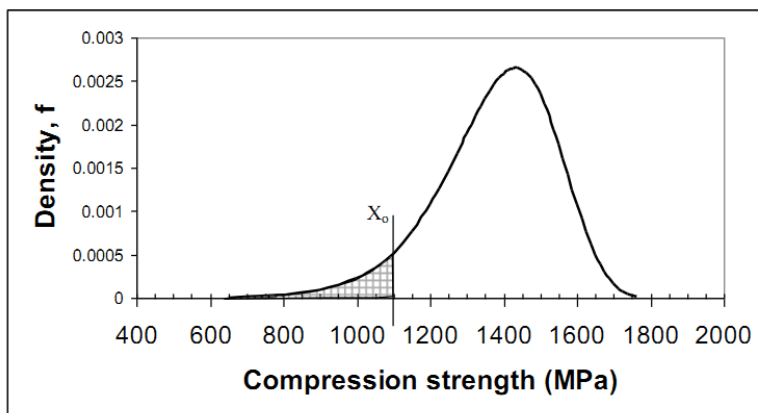


Figure 2.2: Probability density distribution for compression strength of typical Graphite/Epoxy (two-parameter Weibull:  $\alpha = 10.375$   $\beta = 1447.1$  MPa)

The residual strength after  $n$  cycles of maximum applied stress  $\sigma$  is given by Eq. 2.10. In order to determine the probability  $p$  that the residual strength  $\sigma_r$  is less than the applied stress  $\sigma$ , the type of statistical distribution corresponding to Eq. 2.10 must be determined given the fact that the static strength  $\sigma_{fs}$  follows a two-parameter Weibull distribution.

As can be seen from Eq. 2.10, the statistical variable,  $\sigma_{fs}$ , is raised to the power:

$$q = \frac{N - n - 1}{N - 1} \quad (2.13)$$

It can be shown [67] that raising a two parameter Weibull variable to a power  $q$  results in a new distribution that is also a two-parameter Weibull with shape parameter  $\alpha_{new}$  and scale parameter  $\beta_{new}$  given by:

$$\alpha_{new} = \frac{\alpha}{q} \quad \beta_{new} = \beta^q \quad (2.14)$$

That is, the new scale parameter is the original scale parameter raised to the same power  $q$  and the new shape parameter is the original one divided by  $q$ .

This means that the quantity

$$\sigma_{fs}^{\frac{N-n-1}{N-1}}$$

in Eq. 2.10 is a two-parameter Weibull variate with

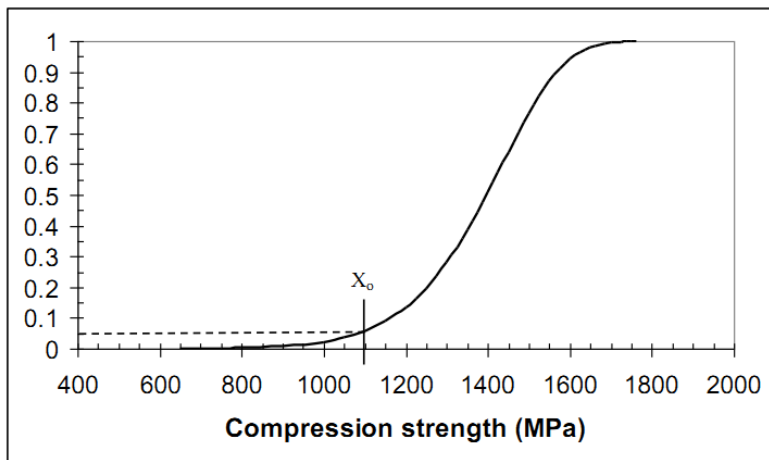


Figure 2.3: Cumulative distribution function for compression strength of typical Graphite/Epoxy (two-parameter Weibull:  $\alpha = 10.375$   $\beta = 1447.1$  MPa)

$$\alpha_{new} = \frac{\alpha(N-1)}{N-n-1} \quad \beta_{new} = \beta^{\frac{N-n-1}{N-1}} \quad (2.15)$$

In addition, the same quantity

$$\sigma_{fs}^{\frac{N-n-1}{N-1}}$$

is multiplied, in Eq. 2.10 by the constant

$$\sigma^{\frac{n}{N-1}}$$

and it can be shown, [68], that multiplying a two-parameter Weibull variate by a constant yields another two-parameter Weibull variate with the same shape parameter and  $\alpha$  scale parameter multiplied by that same constant. So the final Weibull parameters after multiplying by

$$\sigma^{\frac{n}{N-1}}$$

are:

$$\alpha_{final} = \frac{\alpha(N-1)}{N-n-1} \quad \beta_{final} = \sigma^{\frac{n}{N-1}} \beta^{\frac{N-n-1}{N-1}} \quad (2.16)$$

Therefore, if  $\alpha$  and  $\beta$  are the shape and scale parameters of the two-parameter Weibull distribution describing the static strength  $\sigma_{fs}$  of a composite structure, applying  $n$  cycles of maximum stress  $\sigma$  to that structure will

result in a residual strength  $\sigma_r$  which is also two-parameter Weibull distributed with shape and scale parameters given by Eq. 2.16.

One important conclusion can be drawn from the first of Eq. 2.16. The quantity multiplying the original shape parameter  $\alpha$  on the right hand side is always greater than 1. This implies that the new shape parameter, after  $n$  cycles, is greater than the original shape parameter, i.e. the shape parameter increases with fatigue cycles. An increasing shape parameter implies reduction in experimental scatter, therefore, the present model predicts that the scatter of the residual strength will decrease with cycles.

There is not sufficient data in the open literature to clearly support or refute this conclusion of decreasing scatter with increasing cycles even though results by Young and Jones [69] clearly demonstrate that for  $[45]_{2s}$  Graphite/Epoxy laminates. There are two qualitative arguments supporting the conclusion: One, it is well known, for example in specimens with holes tested in uniaxial tension or compression, that after fatigue cycling, the damage created in some specimens reduces notch sensitivity and the residual strength is higher than the static strength before cycling. This means that the effect of flaws present in regions of high stresses is less pronounced and since scatter is directly related to the presence of flaws, reduced sensitivity to flaws implies lower scatter. Two, specimens in a population with low strength will fail early during fatigue cycling leaving the stronger specimens in the population. Thus, the resulting population will be characterized by a narrower probability density distribution which is consistent with lower scatter. This is shown schematically in Figure 2.4 where, for emphasis, a non-zero endurance limit  $\sigma_E$  is included. During cycling, at a given load  $\sigma$ , specimens with strength less than  $\sigma$  fail early and the remaining form a population whose low strength must asymptotically reach  $\sigma_E$ . If the strength got lower than  $\sigma_E$  there would be specimens that would fail when  $\sigma < \sigma_E$ , contradicting the fact that  $\sigma_E$  is the endurance limit. At the same time, the high strength end of the population decreases with cycles because weaker fibers in specimens in the high strength end of the population fail but the failure stress is calculated using the original cross-section thus giving a lower strength. As a result, the residual strength population gets narrower with increasing cycles, implying reduced scatter. It should be pointed out that there is some experimental evidence that this conclusion of decreasing scatter of residual strength is not true in all cases [70].

This predicted effect of reduced experimental scatter of residual strength with increasing cycles becomes significant as the number of cycles  $n$  approaches the cycles to failure  $N$  corresponding to the applied stress  $\sigma$ . This can be seen by rearranging the first of Eq. 2.16 to obtain:

$$\frac{\alpha_{final}}{\alpha} = \frac{1}{1 - \frac{n}{N-1}} \quad (2.17)$$

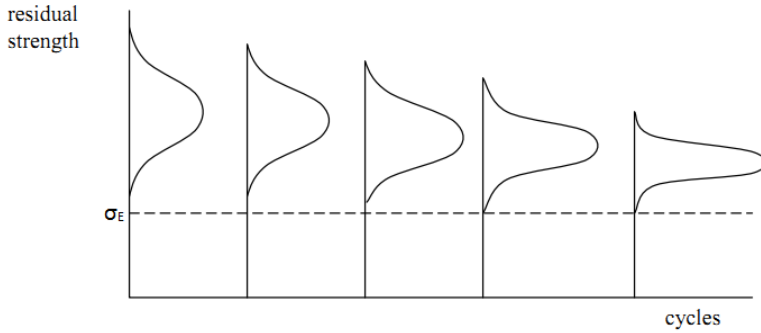


Figure 2.4: Evolution of residual strength probability density distribution with cycles when a constant cyclic stress  $\sigma$  ( $\sigma > \sigma_E$ ) is applied

The shape parameter after  $n$  cycles  $\alpha_{final}$  normalized by the shape parameter  $\alpha$  of the static strength population as given by Eq. 2.17 is plotted as a function of normalized fatigue cycles  $n/(N-1)$  in Figure 2.5. It can be seen from Figure 2.5 that, to double the shape parameter, i.e. decrease the CV by a factor of 2, the structure must be subjected to cycles corresponding to, approximately, 50% of its fatigue life.

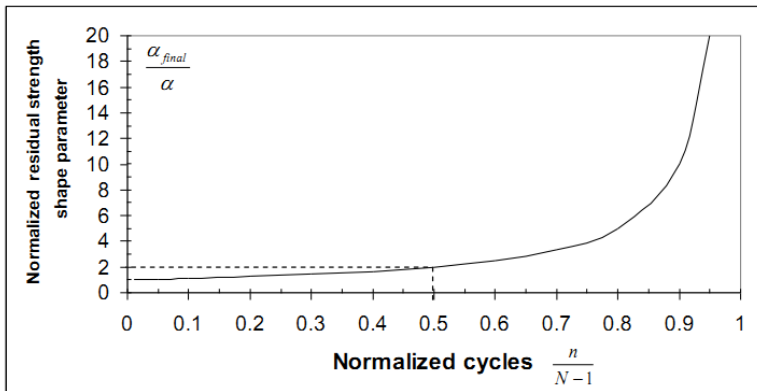


Figure 2.5: Change of shape parameter (scatter) of residual strength as a function of cycles

Given the shape and scale parameters from Eq. 2.16 and an applied maximum cyclic stress  $\sigma$ , the probability  $p$  that the strength of a given specimen is less than  $\sigma$  can be obtained from Eq. 2.12 with  $p(n) = F(\sigma)$ :

$$p(n) = 1 - e^{-\left(\frac{\sigma}{\beta_{new}}\right)^{\alpha_{new}}} \quad (2.18)$$

Substituting for  $\alpha_{new}$  and  $\beta_{new}$  from Eq. 2.16:

$$\begin{aligned}
 p(n) &= 1 - e^{-\left(\frac{\sigma}{\sigma \frac{n}{N-1} \beta \frac{N-n-1}{N-1}}\right)^{\frac{\alpha(N-1)}{N-n-1}}} \\
 &= 1 - e^{-\left(\frac{\frac{\alpha(N-1)}{\sigma \frac{n}{N-1} \frac{\alpha(N-1)}{N-n-1}}}{\sigma \frac{n}{N-1} \frac{\alpha(N-1)}{N-n-1}}\right) \left(\frac{1}{\beta}\right)^{\frac{\alpha(N-1)(N-n-1)}{(N-n-1)(N-1)}}} \\
 &= 1 - e^{-\left(\frac{\frac{\alpha(N-1)}{\sigma \frac{n}{N-1} \frac{\alpha(N-1)}{N-n-1}}}{\sigma \frac{n}{N-1} \frac{\alpha(N-1)}{N-n-1}}\right) \left(\frac{1}{\beta}\right)^{\alpha}} \\
 &= 1 - e^{-\left(\frac{\frac{\alpha(N-1)}{\sigma \frac{n}{N-1} \frac{\alpha(N-1)}{N-n-1}}}{\sigma \frac{n}{N-1} \frac{\alpha(N-1)}{N-n-1}}\right) \left(\frac{1}{\beta}\right)^{\alpha}} \\
 &= 1 - e^{-\left(\frac{\sigma}{\beta}\right)^{\alpha}}
 \end{aligned} \tag{2.19}$$

Note also that the value of  $p$  before cycling when  $X = \sigma$  can be obtained from Eq. 2.12 as:

$$p(n) = 1 - e^{-\left(\frac{\sigma}{\beta}\right)^{\alpha}} \tag{2.20}$$

Comparing Eqs. 2.19 and 2.20 it is obvious that the probability of failure  $p(n)$  after  $n$  cycles is the same as the probability of failure  $p$  before cyclic loading started. That is, the surviving population of specimens after cyclic loading at stress  $\sigma$  has a residual strength distribution in which the probability  $p$  that the strength of any given specimen is less than  $\sigma$  is constant. For conciseness,  $p$  will be referred to as the cycle-by-cycle probability of failure. The value of  $p$  does not change with cyclic loading, and is equal to its static value from the static strength population. This is a direct result of the residual strength assumption of Eq. 2.2 and the assumption that the static strength follows a two-parameter Weibull distribution.

At first glance, the conclusion that  $p$  is constant might appear to be limiting and unrealistic given the discussion in Chapter 1 about the different types of damage and their evolution during cyclic loading. One would expect that as damage evolves,  $p$  will change and, in general, it does. However, examples where this conclusion of constant  $p$  is supported by experimental evidence and analysis can easily be found.

The first such example is the case of a  $[0_m/90_n/0_m]$  laminate under tension-tension loading. The applied load is along the fibers in the  $0^\circ$  plies. Even if the applied load is relatively low, there will be a number of load repetitions after which matrix cracks will appear in the  $90^\circ$  plies. The first such matrix crack is shown in Figure 2.6 and extends along the full width of the laminate, perpendicular to the surface of Figure 2.6, through the thickness of the  $90^\circ$

layer. The matrix cracks in such a laminate are confined to the  $90^\circ$  plies because the  $0^\circ$  plies act as crack stoppers. Upon further cycling, more cracks will appear in the  $90^\circ$  plies and the crack density will increase [71]. For a large number of cycles, the only discernible difference at this scale of a few ply thicknesses, is the creation of more cracks in the  $90^\circ$  plies. Considering how load is transferred from one end of the laminate to the next, it is obvious that in the vicinity of a matrix crack, and because the crack surface is unloaded, the axial load in the  $90^\circ$  plies must shear itself to the adjacent  $0^\circ$  plies. This means that interlaminar shear and normal stresses develop near the matrix cracks (for a detailed solution of this problem see section 6.2.2). These interlaminar stresses die out very quickly and the matrix cracks must be very close to each other for interaction to occur. Therefore, for quite a large number of cycles, the crack density increases but in the vicinity of individual cracks the stress field does not change. This is shown in 2.7.

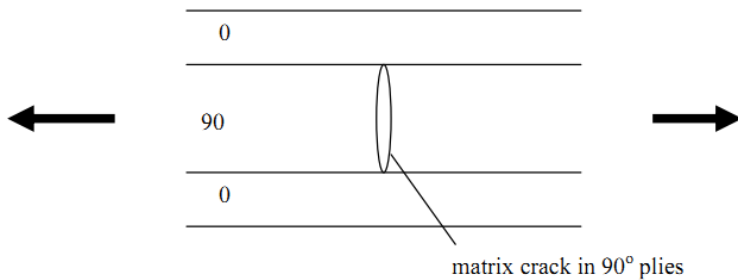


Figure 2.6:  $[0_m / 90_n / 0_m]$  laminate with matrix crack in  $90^\circ$  plies

So as long as adjacent matrix cracks are not too close and the stress field from one affects that from another, the critical stresses, in the  $0^\circ$  ply, since all the axial load is in the  $0^\circ$  ply, both in terms of magnitude and shape do not change. As a result, the residual strength of the laminate as predicted using any stress-based failure criterion does not change with cycles. This conclusion will be valid for the entire population of specimens tested under tension-tension fatigue. Therefore, for a large number of cycles, the residual strength population of specimens such as the one shown in Figure 2.7 will remain unaffected. This means that, for a given applied load  $\sigma$ , the cycle-by-cycle probability of failure  $p$  will remain constant.

Another example where the cycle-by-cycle probability of failure remains constant with cycles, is that of a laminate loaded in tension and developing an edge delamination. The situation is shown schematically in Figure 2.8.

Due to the fact that interlaminar stresses develop at the free edges of the laminate shown in Figure 2.8, delaminations of length  $a$  are created along

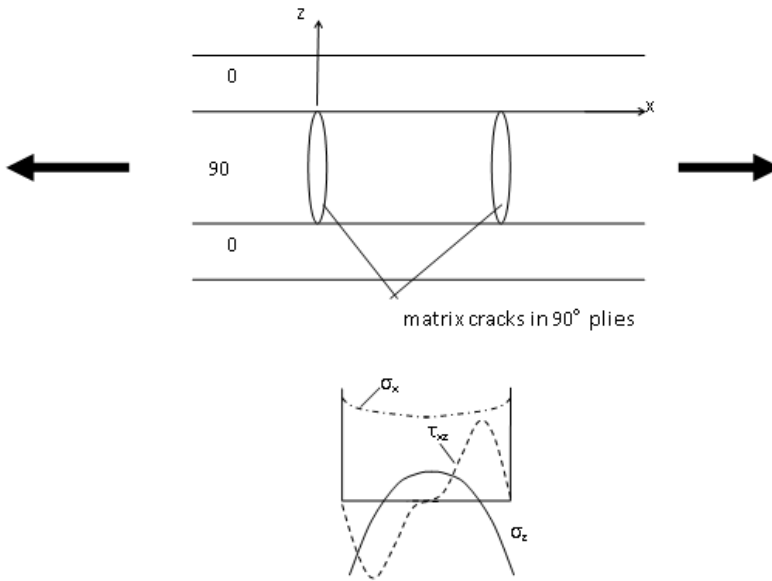


Figure 2.7: Stresses in the  $0^\circ$  ply between two successive matrix cracks

the entire edge of the laminate (at symmetric ply interfaces on both edges of the laminate). The static problem has been solved by O'Brien in [72] where he showed that the applied strain  $\epsilon$  is related to the energy release  $G$ , the laminate axial stiffness  $E_{LAM}$ , the axial stiffnesses  $E_i$  of the sub-laminates created by the delaminations, and the corresponding thicknesses  $h$  (laminate) and  $t_i$  (sublaminates) through the relation:

$$G = \frac{1}{2}\epsilon^2 h \left( E_{LAM} - \frac{\sum_{i=1}^n E_i t_i}{h} \right) \quad (2.21)$$

O'Brien [72] found excellent agreement of Eq. 2.21 with test results. Note that using strain instead of stress does not change anything in the model. What is really significant for the present discussion is that the delamination size does not appear in Eq. 2.21. This suggests that, even if, under repeated loading the delamination grows, towards the center of the laminate in Figure 2.8, the energy release rate will still be given by Eq. 2.21. As a result, one can expect that, even though the delamination grows under repeated loading, the cycle-by-cycle probability of failure  $p$ , directly related to  $G$  in this case, will remain relatively constant.

The two examples mentioned above are not meant to be proofs but strong indicators that under certain circumstances it will be possible to have constant cycle-by-cycle probability of failure  $p$ . In fact, in the present model it will, for the time being, be assumed that given a starting condition of a

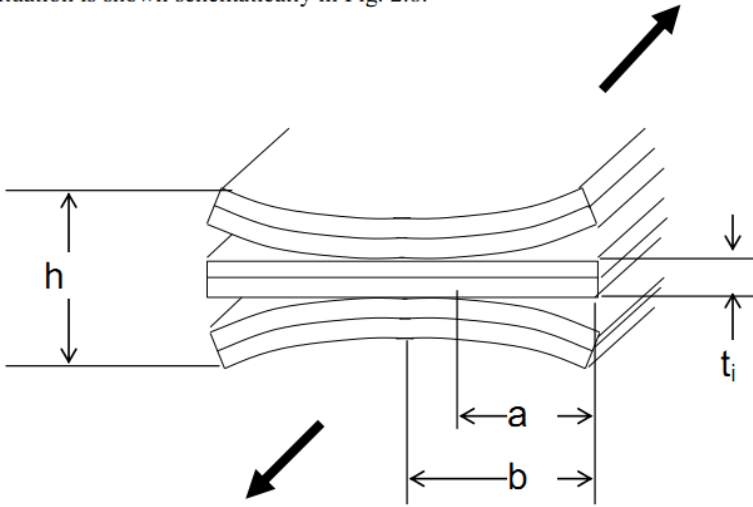


Figure 2.8: Edge delaminations developing in a laminate under tensile loading

composite structure, the probability of failure  $p$  will stay constant with cycles until a significant change in damage occurs (matrix cracks transitioning to delaminations, or delaminations leading to fiber breakage, etc.). In a sense, a constant value of  $p$  implies that (a) the current damage state is increasing without interaction or creation of a different type of damage, for example more matrix cracks are created without interacting with each other, or (b) damage mechanisms at lower scales than the ones examined are occurring and until they coalesce to form damage in the scale of interest (for example micro-voids coalesce to form matrix cracks or delaminations) they have no effect on the value of  $p$ .

It should be noted that a constant value of  $p$  does not mean that the residual strength is constant. The residual strength will always decrease according to Eq. 2.21. It is expected that this assumption of piecewise constant value of  $p$  as a function of cycles, will not always be sufficiently accurate. The range of applicability of this assumption will be investigated in more detail later in sections 2.3 and 6.1.

### 2.2.2 Determination of cycles to failure

The analytical framework that can be used to determine the cycles to failure  $N$  under constant amplitude loading has now been established. If  $p$  is the (constant) probability of failure during a cycle given an applied stress  $\sigma$ , then the probability  $P_i$  that there has been “failure” between cycle 1 and cycle  $i$  can be determined as the product of the probability of failure  $p$  during any

cycle and the probability that there has been no failure during any of the other  $i - 1$  cycles (the reason for the quotes for the word failure will be discussed later on in this section):

$$P_i = p(1 - p)^{i-1} \quad (2.22)$$

then the probability of failure  $P$  anywhere between 1 and  $N$  cycles is the sum of all probabilities  $P_i$  given by Eq. 2.22:

$$P = \sum_{i=1}^N P_i = \sum_{i=1}^N p(1 - p)^{i-1} \quad (2.23)$$

From a mathematical perspective, Eq. 2.23 gives the probability that there has been one (and only one) failure between 1 and  $N$  cycles. For the case of constant  $p$ , which is the case examined here, the summation in Eq. 2.23 can be simplified to:

$$P = Np(1 - p)^{N-1} \text{ for constant } p \quad (2.24)$$

Eq. 2.24 relates the probability  $P$  that the structure has failed anywhere between 1 and  $N$  cycles to the cycle-by-cycle probability of failure  $p$ . It is important to emphasize that  $P$  is not the probability of failure after  $N$  cycles but the probability that the structure failed at some point between cycles 1 and  $N$ . A plot of  $P$  as a function of  $N$  for an arbitrary value of  $p(= 1 \times 10^{-6})$  is shown in Figure 2.9.

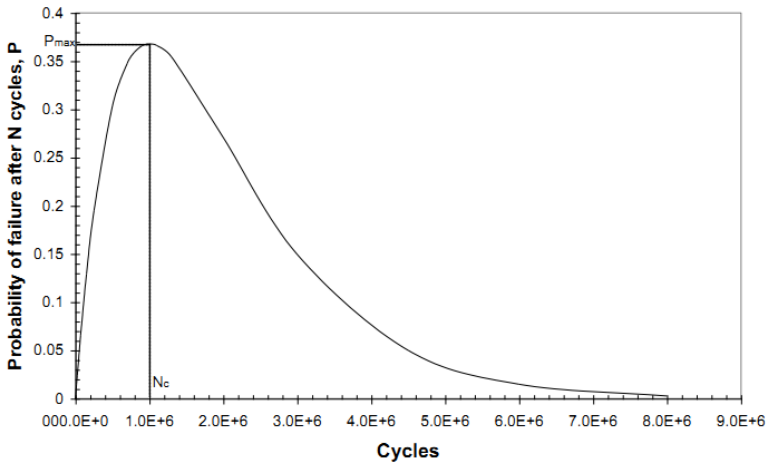


Figure 2.9: Probability that the structure failed between 1 and  $N$  cycles as a function of  $N$

As can be seen from Figure 2.9,  $P$  goes through a maximum as  $N$  increases and then decreases to zero. The number of cycles  $N_c$  at which  $P$  is maximum ( $P_{max}$ ) can be determined by differentiating Eq. 2.24 with respect to  $N_c$  and setting the result equal to zero. Then:

$$N_c = -\frac{1}{\ln(1-p)} \quad (2.25)$$

This relationship will form the basis for predicting the cycles to failure under constant amplitude  $\sigma$ . Before proceeding, however, a discussion on the derivation of Eq. 2.25 is in order.

The mathematical treatment from Eq. 2.22 to Eq. 2.25 used the word “failure” in rather broad terms and this is why it appears in quotes. Strictly speaking, Eq. 2.22 gives the probability that there has been one and only one failure between 1 and  $i$  cycles. However, for any structure, there can be no more than one failures, nor can one say that the structure can continue cycling after it has failed. This is a situation where a mathematical model can be applied to reality only with proper redefinition of terms. In the mathematical derivation the assumption is made that there is a probability  $p$  of an event happening. This event may happen more than once. For example, when tossing a fair coin,  $p = 0.5$ . Then,  $P$  from Eq. 2.22 could be the probability that after  $i$  tosses, heads has occurred once and only once. This is also the reason for the shape of the function  $P$  in Figure 2.9. There is a maximum and then  $P$  goes to zero because, for a sufficiently large number of tries (tosses), there would be a second time that heads occurred, and a third, etc.

If instead of occurrences of heads one used structural failure, there would be an inconsistency between the mathematical model and physical reality. Three explanations are provided to reconcile the two: One, in the physical model the structure is not allowed to fail but to get arbitrarily close to failure. So Eqs. 2.22-2.24 calculate the probability that the structure has gotten arbitrarily close to failure, but has not failed, once and only once between 1 and  $N$  cycles. Two, in a broader sense, and in agreement with damage modeling as already described, failure here denotes a change from one type of damage to another (matrix cracks transitioning to delamination for example). In such a case there is no problem with structural failure invalidating the mathematical model. Three, one can arbitrarily neglect the derivation from Eq. 2.22 to Eq. 2.24 and postulate that the cycles to failure are given by Eq. 2.25 without any proof or derivation.

Proceeding now with the implications of Eq. 2.25, it should be pointed out that the value of  $P_{max}$  corresponding to  $N_c$  can be found by substituting  $N = N_c$  in Eq. 2.24. For small values of  $p$ , i.e.  $p < 0.05$ , which covers most cases, it can be shown that:

$$P_{max} \cong \frac{1}{e}, p < 0.05 \quad (2.26)$$

This implies that the maximum value of  $P$  is relatively constant and independent of  $p$ , as long as  $p < 0.05$ , and equal to approximately 0.368 or 36.8%. The simplification of Eq. 2.25 that occurs when  $p$  is small, is also of some interest. If  $p$  is less than 0.05,  $N_c \approx 1/p$ .

Eq. 2.25 is the general expression of cycles to failure under constant amplitude with maximum stress  $\sigma$ . The dependence on  $\sigma$  is through  $p$  and Eqs. 2.19 or 2.20. For the special case where the static strength follows a two-parameter Weibull distribution, Eq. 2.19 can be used to substitute in Eq. 2.25 to obtain:

$$N_c = -\frac{1}{\ln(1-p)} = -\frac{1}{\ln\left(1 - \underbrace{\left(1 - e^{-\left(\frac{\sigma}{\beta}\right)^\alpha}\right)}_p\right)} \quad (2.27)$$

This can be further simplified to:

$$N_c = -\frac{1}{\ln\left(e^{-\left(\frac{\sigma}{\beta}\right)^\alpha}\right)} \quad (2.28)$$

which finally leads to:

$$N_c = \left(\frac{\beta}{\sigma}\right)^\alpha \quad (2.29)$$

or, solving in terms of stress  $\sigma$ , to recast in the form of an  $S - N$  curve (and dropping the subscript  $c$  from  $N_c$ ):

$$\sigma = \frac{\beta}{(N)^\frac{1}{\alpha}} \quad (2.30)$$

Eq. 2.30 gives the stress level that would be required for a structure to fail after  $N$  cycles where  $\alpha$  and  $\beta$  are the shape and scale parameters of the static strength distribution of the structure for the same type of loading, and failure mode, as during fatigue loading. Since  $\alpha$  and  $\beta$  are readily obtained from the statistical characterization of the static strength population, Eq. 2.30 has the great advantage of being a closed form expression that requires no curve fitting of fatigue data or the use of any model parameters that need to be determined by fatigue testing. This equation is only based on the residual strength model of Eq. 2.2 and the assumption that the static strength population follows a two-parameter Weibull distribution.

A minor correction to Eq. 2.30 may be necessary for low values of  $N$ . It can be seen from Eq. 2.30 that when  $N = 1$ , which coincides with a static strength test, the stress to cause failure is:

$$\sigma = \beta \quad (2.31)$$

This is a small inconsistency as the shape parameter  $\beta$ , as mentioned earlier, see discussion after Eq. 2.11, corresponds to the 63.2 percentile value and not the 50<sup>th</sup> percentile. Eq. 2.30 should recover the mean of the static strength population, 50<sup>th</sup> percentile, when  $N = 1$ . Using Eq. 2.30 as it is would give a small error for low values of  $N$ . For consistency, Eq. 2.30 can be corrected to read:

$$\sigma = \frac{X_m}{(N)^{\frac{1}{\alpha}}} \quad (2.32)$$

where  $X_m$  is the mean of the static strength population. A comparison of the predictions of Eqs. 2.30 and 2.32 is shown in Figure 2.10 for the same static strength population as that shown in Figs 2.2 and 2.3. The biggest difference (in stress) occurring for  $N = 1$  is, in this example, less than 5%.

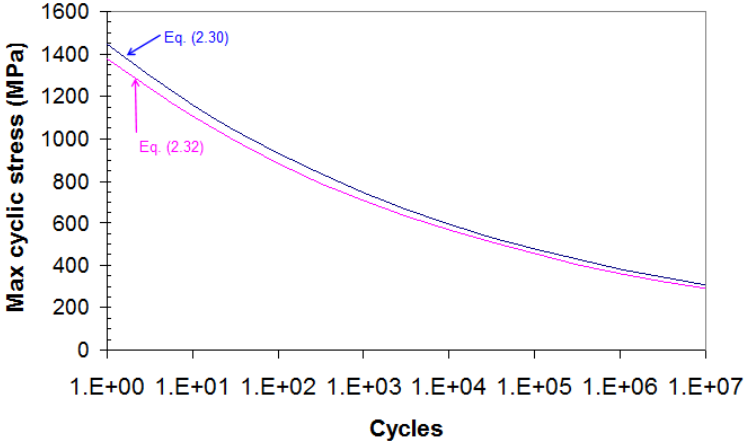


Figure 2.10: S-N curves predicted by Eqs 2.30 and 2.32

In the case where, instead of two-parameter Weibull, the static strength follows a normal distribution, the cycle-by-cycle probability of failure  $p$  is given by the well known expression for normal distribution:

$$p = \int_{-\infty}^{\sigma} \frac{1}{s\sqrt{2\pi}} e^{-\frac{(x-X_m)^2}{2s^2}} dx \quad (2.33)$$

where  $X_m$  and  $s$  are the mean and standard deviation respectively of the static strength population. Eq. 2.33 can be evaluated using canned software or tables of the standard normal distribution, or, to within 0.07%, the following equation can be used [73]:

$$p = 1 - 0.5[1 - [1 + (A + BZ_p)^C]^D + [1 + (A - BZ_p)^C]^D] \quad (2.34)$$

where

$$Z_p = \frac{|\sigma - X_m|}{s} \quad A = 0.644693 \quad B = 0.161984 \quad C = 4.874 \quad D = -6.158$$

Then, if the static strength population follows a normal distribution with mean  $X_m$  and standard deviation  $s$ , Eq. 2.34 can be used to obtain  $p$  which can then be substituted in Eq. 2.25 to obtain the cycles to failure. Note that, unlike the case of a two-parameter Weibull distribution where a concise closed-form  $S - N$  curve was derived, for a normal distribution the corresponding expression is more involved and requires combining Eqs. 2.25 and 2.34.

### 2.3 Effect of R Ratio

It has been implicitly assumed in the derivation of the previous two sections that the load excursion in each cycle starts from 0, goes to a maximum (or minimum) stress  $\sigma$  and returns again to 0 or starts from some negative value, goes to zero and then back to the same negative value. These correspond to the cases where

$$R = \frac{\sigma_{min}}{\sigma_{max}} = \frac{0}{\sigma_{max}} = 0 \quad \text{or} \quad \frac{\sigma_{min}}{\sigma_{max}} = \frac{\sigma_{min}}{0} = \infty \quad (2.35)$$

The case  $R = 0$  is shown in Figure 2.11. In this case, the cycle-by-cycle probability  $p$  is the ratio of the shaded area in Figure 2.11 to the total area under the strength distribution curve along the y axis.

If  $R$  is not equal to zero or infinity, the load excursion does not start and stop at zero and the cycle-by-cycle probability of failure  $p$  is smaller than the ratio of the areas in Figure 2.11. The structure must be credited for damage creation or accumulation corresponding to the load excursion going all the way down to zero. In a sense, this is analogous to calculating life expectancy values, which, at any time  $t_o$  in a persons life, are higher than the value when a person is born ( $t_o = 0$ ) since the person has survived up to that point ( $t_o$ ). Therefore, the solution must be modified when  $R \neq 0$  to account for the different load excursion. To do this accurately, test data in which specimens are tested statically loading from some non-zero value to failure would be needed but such data are not available. For the purposes of this work, relatively simple adjustments were made to the equations to account for the effect of  $R$  ratio.

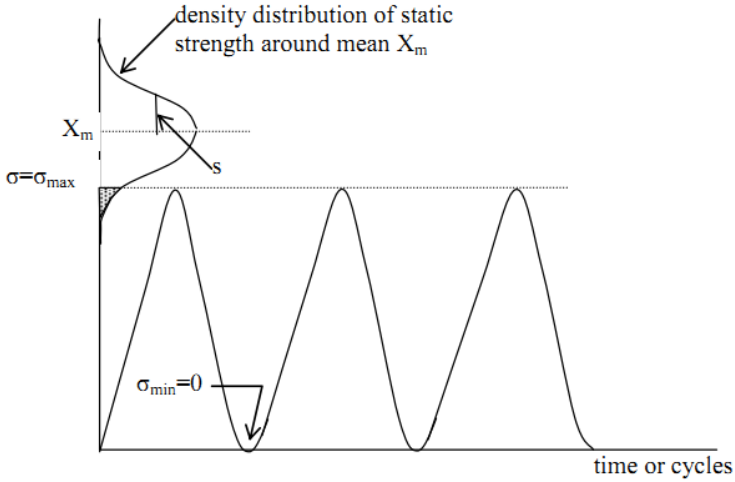


Figure 2.11: Cyclic loading for  $R = 0$

**2.3.1 Tension-tension ( $0 < R < 1$ ) or compression-compression ( $R > 1$ ) cases.**

The tension-tension ( $0 < R < 1$ ) and compression-compression ( $R > 1$ ) situation are shown in Figure 2.12. In this case, there is a loading region between 0 and the minimum load for tension-tension or 0 and the maximum load for compression-compression that is not exerted to the structure. This region has a probability of failure associated with it, however small, that must not be included in the value of  $p$  for the structure. This means that the value of  $p$  in this case is smaller than for the case where the load goes to zero.

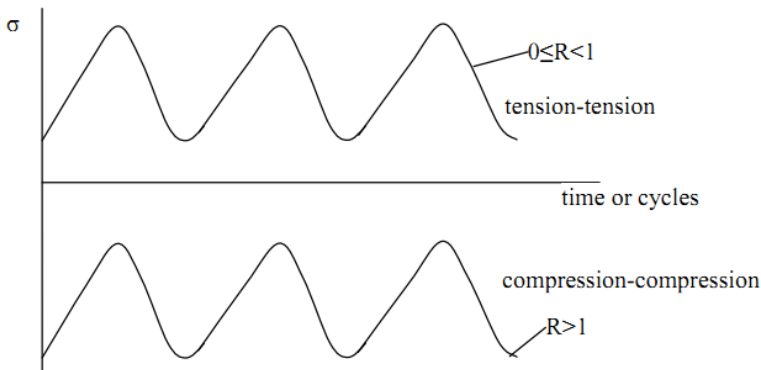


Figure 2.12: Cases where  $0 < R < 1$  or  $R > 1$

As a first approximation, the (known) probability distribution density when the maximum (or minimum) value equals zero ( $R = 0$  or  $R = 8$ ) is modified as follows:

Let  $x_1$  and  $x_2$  be the 1 percentile and 99 percentile values of the distribution when  $R = 0$  or  $R = \infty$ . In addition, without loss of generality, assume this is a normal distribution. If now the load excursion does not start from zero,  $x_1$  is moved to a new value  $x_1^*$  such that its distance from the mode (maximum value) of the original distribution is a fraction  $r$  times the original distance  $X_{mode} - x_1$ . Using normal distribution statistics, where the mode and the mean are the same ( $X_{mode} = X_m$ ) one can write:

$$\begin{aligned} x_1 &= X_m - r(2.326)s \\ x_2 &= X_m - (2.326)s \end{aligned} \quad (2.36)$$

where  $X_m$  is the mean (and mode) of the original distribution,  $s$  is the standard deviation of the original distribution, 2.326 is the one-sided tolerance limit factor for the 99<sup>th</sup> percentile value for normal distribution taken from Table 9.10.1 given in [73] and  $r$  is defined as:

$$\begin{aligned} r &= 1 - R \text{ for } 0 \leq R < 1 \\ r &= 1 - \frac{1}{R} \text{ for } R > 1 \end{aligned} \quad (2.37)$$

Note that when  $R = 0$  or  $R = \infty$  Eq. 2.37 gives  $r = 1$  and, thus, Eq. 2.36 gives back  $x_1$  which is the original 1 percentile of the original normal distribution. When  $r \neq 1$ , the first of Eqs 2.36 gives  $x_1 = x_1^*$ . Also, by construction, the quantity  $X_m - 2.326s$  is the 1 percentile value of a normal distribution with mean  $X_m$  and standard deviation  $s$  (Table 9.10.1 in [73]).

With this transformation of the 1 percentile value, note that the 99 percentile value remains unaffected, a new population is created 98% of which is contained between  $x_1^*$  and  $x_2$ . This population is approximated as a two-parameter Weibull distribution with mode equal to the mode or the original normal distribution (which equals the mean for a normal distribution) and 98% contained between  $x_1^*$  and  $x_2$ . The shape and scale parameters of this two-parameter Weibull distribution are obtained using Eq. 2.20, which gives:

$$e^{-\left(\frac{x_1}{\beta}\right)^\alpha} - e^{-\left(\frac{x_2}{\beta}\right)^\alpha} = 0.98 \quad (2.38)$$

and the equation for the mode of a Weibull distribution:

$$\beta \left(1 - \frac{1}{\alpha}\right)^{1/\alpha} = X_m \quad (2.39)$$

Eqs. 2.38 and 2.39 can be solved iteratively for  $\alpha$  and  $\beta$  which define the two-parameter Weibull distribution describing the strength of the structure when  $0 < R < 1$  or  $R > 1$ . The change from one statistical distribution to another is shown schematically in Figure 2.13.

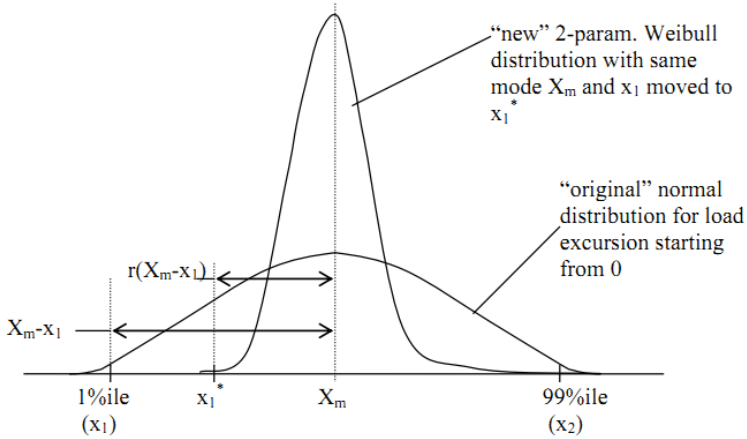


Figure 2.13: Modification of probability density distribution when  $R \neq 0$

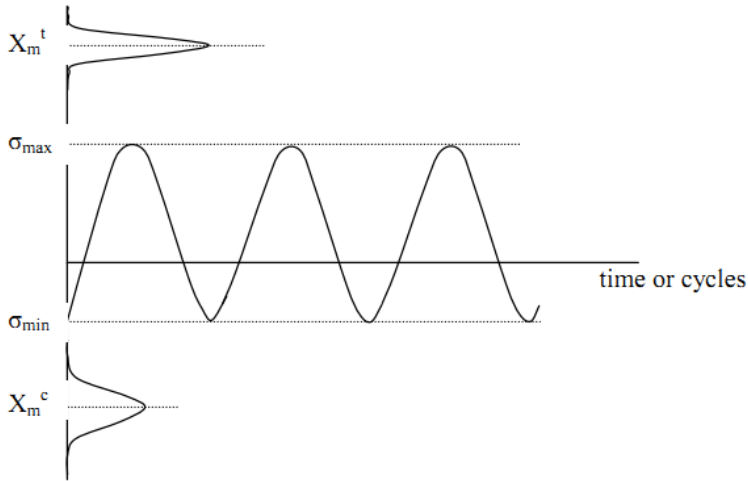
The procedure in this case is as follows:

1. given the static strength distribution, the 1 and 99 percentile points  $x_1$  and  $x_2$  are determined.
2. depending on the  $R$  value used,  $r$  is calculated from Eq. 2.37
3. the new  $x_1$  value ( $= x_1^*$ ) is determined from Eq. 2.36
4. the shape and scale parameters  $\alpha$  and  $\beta$  for a two-parameter Weibull distribution describing the modified strength population are determined by solving Eqs. 2.38 and 2.39.
5. the mean  $X_m$  of the modified strength population is determined using:

$$X_m = \beta \Gamma\left(1 + \frac{1}{\alpha}\right) \quad (2.40)$$

with  $\alpha$  and  $\beta$  as determined from step (4)

6. Eq. 2.32 is used to obtain cycles to failure with  $X_m$  from step (5) and  $\alpha$  from step (4)

Figure 2.14: Typical cyclic load for  $R < 0$ 

### 2.3.2 Tension-compression cases ( $R < 0$ )

The situation is shown in Figure 2.14. The maximum load is positive and the minimum load is negative.

The way to model this situation is to recognize that each cycle consists of two portions. One from 0 to the maximum (positive) load and back to zero and another from zero to the minimum (negative) load and back to zero. Each portion has its own probability of failure directly related to the static strength distribution for tension or compression. Representative strength distributions for tension and compression are shown along the y axis in Figure 2.14. Note that the corresponding mean values  $X_m^t$  and  $X_m^c$  respectively do not, usually, have the same magnitude. Nor are the corresponding standard deviations the same; this is why the bandwidths of the two distributions shown in Figure 2.14 are different. As a result, given a  $\sigma_{max}$  and a  $\sigma_{min}$  value, the cycle-by-cycle probabilities of failure during the tension portion of the cycle ( $p_T$ ) and the compression portion of the cycle ( $p_c$ ) are, in general different. This is a situation where the use of two different values of  $p$ ,  $p_T$  and  $p_C$  implicitly allows for two different types of damage to be included in the model one for tension and one for compression. For example, the tension could be dominated by matrix cracks and the compression could be dominated by kink band formation and fiber kinking. One type of damage could lead to failure during the tension portion of the cycle and the other during the compression portion.

The approach presented in section 2.2 must now be modified to account for the presence of two cycle-by-cycle probabilities of failure values  $p_T$  and  $p_C$ . The problem is formulated as follows.

Determine the probability of occurrence  $P$  of one failure after  $N$  trials each with probability  $p_T$  and  $N$  trials each with probability  $p_C$ . The derivation is analogous to that for Eqs. 2.23 and 2.24 and leads to the expression:

$$P = N(p_T + p_C - 2p_T p_C)(1 - p_T)^{(N-1)}(1 - p_C)^{(N-1)} \quad (2.41)$$

As before, the cycles to failure are determined by maximizing  $P$  in Eq. 2.41. Differentiating the right hand side of Eq. 2.41 with respect to  $N$  and setting the result equal to zero gives:

$$N = -\frac{1}{\ln(1 - p_T) + \ln(1 - p_C)} \quad (2.42)$$

Setting  $p_C$  equal to zero, results in a tension-tension case with  $R = 0$  as discussed in section 2.2. In such a case, Eq. 2.42 reduces to Eq. 2.25 as expected.

For the case where the static tension and compression strengths are described by two- parameter Weibull distributions, using Eq. 2.12 or 2.20 to substitute for  $p_T$  and  $p_C$  in Eq. 2.42 gives:

$$N = \frac{1}{\left(\frac{\sigma_{max}}{\beta_T}\right)^{\alpha_T} + \left(\frac{\sigma_{min}}{\beta_C}\right)^{\alpha_C}} \quad (2.43)$$

For the special case of fully-reversed loading ( $\sigma_{min} = \sigma_{max}$ , i.e.  $R = -1$ ), Eq. 2.43 simplifies to:

$$N = \frac{1}{\left(\frac{\sigma}{\beta_T}\right)^{\alpha_T} + \left(\frac{\sigma}{\beta_C}\right)^{\alpha_C}} \quad (2.44)$$

Eqs. 2.43 or 2.44 are analogous to Eq. 2.29 for the case  $R = 0$ . Due to their form, with, in general,  $a_T \neq a_C$  it is not possible to solve them in terms of  $\sigma$  as a function of  $N$  to recast them in a standard  $S - N$  curve form, however, they can easily be used to obtain  $S - N$  curves when  $R < 0$  by picking values for  $\sigma$  and solving for the corresponding cycles to failure  $N$ .

At this point, the basic model is complete. It relates fatigue life to residual strength through the cycle-by-cycle probability of failure. Other than the need to determine the statistical characteristics (mean and standard deviation for example) of the static strength distribution, it is a closed-form analytical model that requires no curve fitting of test data and does not depend on empirical or semi-empirical parameters. It is simple to use and, so far, requires no complex computational model to work. Comparisons of model predictions with test results in the next chapter will be used to identify its advantages and some of its shortcomings; the latter will require further improvements that will be introduced in chapter 6.



# 3

## *Comparison of analytical predictions with test results - implications*

In order to gauge the applicability and accuracy of the model in determining fatigue lives, its predictions are compared to test results in this chapter. These comparisons establish the accuracy of the model and help identify areas where the model needs improvements. Different parts of the model such as the prediction of residual strength and the prediction of cycles to failure are isolated and each is compared to test results. This helps in isolating areas where the analytical model may have difficulty in simulating the performance of composite structures under cyclic loading.

The predictions of residual strength are compared to test results in section 3.1. The predicted load or stress that would cause failure after a specified number of cycles under constant amplitude loading is compared to test results in section 3.2. Constant life diagrams constructed using the present model are compared to test results in section 3.3. Areas where the present model needs improvement as deduced from the results presented in the first three sections, are discussed in section 3.4. Conclusions are summarized in section 3.5.

### **3.1 Residual strength comparison**

The first aspect of the model was to determine the residual strength  $\sigma_r$  for a composite structure undergoing  $n$  cycles with maximum (or minimum) cyclic load  $\sigma$ . Test data obtained by Yang and Jones [69] for a  $[\pm 35]_2$ s Graphite/Epoxy laminate were used for comparison to model predictions. In these tests, both matrix cracks and fiber failures were present.

The test results were obtained for  $R = 0.1$  so the procedure described in section 2.3.1 was used to generate predictions. The resulting Weibull parameters for the static strength population were  $\alpha=23.28$  and  $\beta=431.1$  MPa with a mean strength  $\sigma_{fs}$  of 418.3 MPa obtained from Eq. 2.40. The following table can then be created:

The predictions of the model are in good agreement (within 8%) with test results in [69]. Unfortunately, very few data points were available at each cycle level to make more conclusive comparisons. This suggests that the proposed model for determining residual strength can be very useful in predicting fatigue lives of composite structures. It should be noted, however, that the analytical predictions obtained here were based on a constant cycle-by-cycle probability

Table 3.1: Comparison of residual strength predictions to test results

Applied cycle, n [69]	Applied stress $\sigma_{max}$ MPa [69]	N to failure under $\sigma_{max}$ (Eq. 2.32)	Predicted res. strength, MPa (Eq. 2.10)	Test res. strength MPa ( [69])	% Difference
1100	298.1	2663	363.7	392.3	-7.3
12100	268.3	30918	351.6	379	-7.2
137500	238.4	483964	356.5	363.7	-2.0
150000	232.9	833292	376.4	348.8	+7.9
900	290.7	4781	390.6	405.3	-3.6

of failure  $p$  which, as discussed in the previous chapter, will not necessarily be true for the entire fatigue life of the structure. Still, the accuracy of the predictions shows that this assumption does not limit the predictive capability of the method significantly.

### 3.2 Applied stress level to cause failure after N cycles (S-N curves)

With some confidence in the residual strength model established, one can proceed with predicting the cycles to failure for different cases and comparing predictions to test results. A wide variety of materials, loadings, and geometries will be used for comparison in order to better understand the limitations of the model.

It should be noted that wherever the published test data included more than one data point at the same load level, only the points corresponding to the minimum and maximum cycles at that load level are shown here for clarity. It is also important to note that, in many cases, the statistical information for the static strength data was not provided in the published papers used for comparison to analytical predictions. In such cases, the static strength data provided was assumed to cover a certain percentage of the population between 90 and 95%, depending on the number of data points. The actual percentage value was determined using Monte Carlo simulations for populations with the same mean as the available data and a range of standard deviations in the vicinity of the standard deviation of the test data. Then corresponding statistics for normal or two-parameter Weibull distributions were used to obtain the needed quantities, i.e. mean and standard deviation for normal distribution, shape and scale parameter for two-parameter Weibull.

One of the problems when comparing predictions to test data from fatigue tests is the quantification of the discrepancy between the two. It is possible to measure the error on stress  $\sigma$  for a given cycle level, or on life for a given

stress level. These two error estimates will be drastically different (less than 20% on stress level but a factor of 10 or more in some cases on life especially when the S-N curves are rather flat). In addition, this comparison requires a rigorous determination of the best fit curve to the test data which, in itself, can be an elaborate approach involving some degree of uncertainty [62]. For this reason, no quantitative measure of the discrepancy between analytical predictions and test results is given. Other than a qualitative assessment, it is left to the reader to form his/her own opinion.

The predictions of the present model are compared to test results for uni-directional AS4/3501-6 Graphite/Epoxy under cyclic loading with  $R=0$  in Figure 3.1. Normal distribution for the static strength and Eq. 2.25 were used in this case.

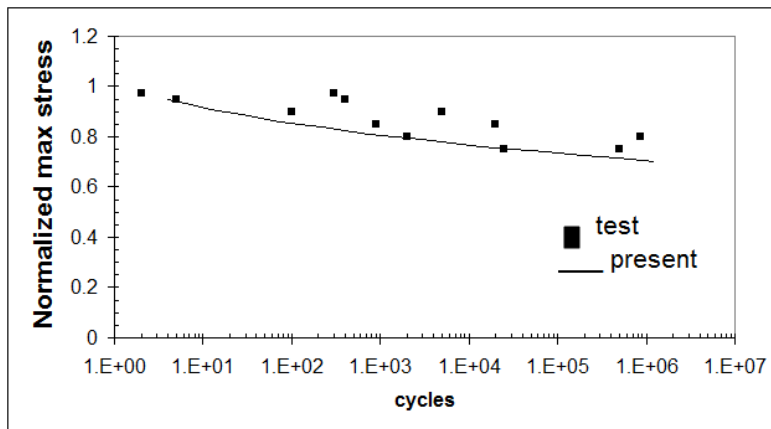


Figure 3.1: Analysis versus test for uni-directional AS4/3501-6 ( $R=0$ ). Test results are taken from [74]

While the predictions are in good agreement with test results, it is obvious from Figure 3.1 that the analytical model consistently under-predicts the test results. There are several reasons for this discrepancy. First, the statistics of the static strength distribution are not given in the reference and were estimated as described earlier. More importantly, the cycle-by-cycle probability  $p$  was assumed to be constant, however, as the weaker fibers in the laminate fail and load is redistributed,  $p$  will change. This effect is accounted for in the modified version of the model presented in section 6.2.1 where this case will be revisited.

To examine the validity of the model when  $R \neq 0$  two additional cases shown in Figures 3.2 and 3.3 are used. Comparisons for tension-tension fatigue for two positive  $R$  values ( $R=0.1$  and  $R=0.5$ ) are shown in Figure 3.2. This is a case of a  $[(\pm 45/0_2)_2]_s$  T800/5245 bismaleimide (BMI) laminate using the test

results obtained from [75]. No clear description of the types of damage created during test was provided in the reference. The predictions are obtained using the methodology of section 2.3.1. Excellent agreement between analytical predictions and test results is observed.

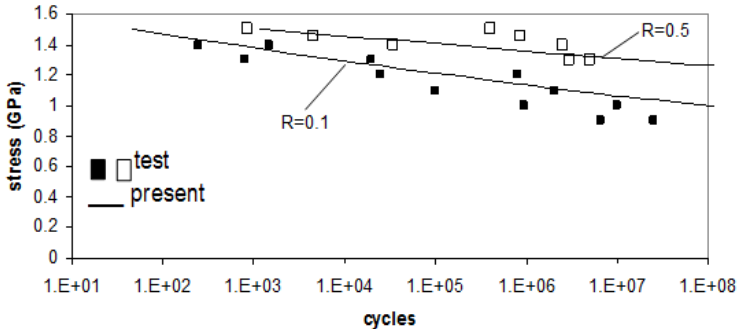


Figure 3.2: Analysis versus test for  $[(\pm 45/0_2)_2]_s$  T800/5245 ( $R=0.1$  and  $R=0.5$ ). The test results are obtained from [75]

The case of fully-reversed loading ( $R=-1$ ) for the same material is shown in Figure 3.3. Here the methodology described in section 2.3.2 was used. Again very good agreement is observed between the results and analytical predictions. To complete the range of typical  $R$  values, a compression-compression case ( $R=10$ ) with same laminate as in Figures 3.2 and 3.3 is shown in Figure 3.4. The agreement between predictions and test results shown in Figure 3.4 is not as good as that found in the previous cases. The predictions are conservative. There are a couple of explanations for this discrepancy.

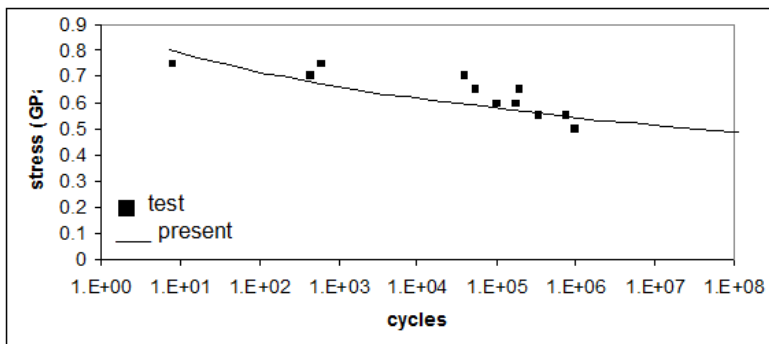


Figure 3.3: Analysis versus test for  $[(\pm 45/0_2)_2]_s$  T800/5245 ( $R=-1$ ). The test results are obtained from [75]

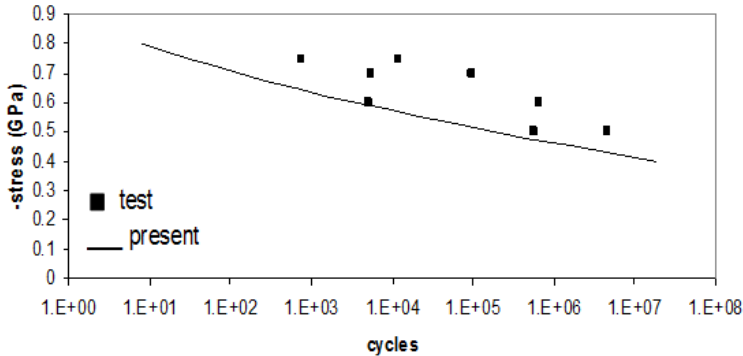


Figure 3.4: Analysis versus test for  $[(\pm 45/0_2)_2]_s$  T800/5245 ( $R=10$ ). The test results are obtained from [75]

The main reason is the assumption made of constant cycle-by-cycle probability of failure  $p$ , for the present laminate, breaks down as soon as kink-bands due to fiber micro-buckling occur. At this point, there is a jump in the value of  $p$  to a new value which will stay roughly constant until the next type of damage (e.g. delaminations) appears. Another reason is that it is difficult to obtain accurate information for the statistics of the static strength distribution of the laminate used in tests.

A case where the static strength is described more accurately using a two-parameter Weibull distribution is shown in Figure 3.5. This is a  $[0_2/\pm 45/0_2/\pm 45/90]_s$  BMI laminate at  $R=-1$  using test data obtained from Maier et al [76]. During the tests, transverse cracks developed in the 90 and 45 degree plies followed by delaminations. What is interesting in this case, from the perspective of the analytical model, is that the difference in static strengths in tension and compression is significant with the tension strength having a higher magnitude than the compression strength. As a result, the value of  $p$  during the tension part of the cycle  $p_T$  is negligible compared to the value of  $p$  during the compression part of the cycle  $p_C$ . The life predictions then can be generated either using Eq. 2.44 or Eq. 2.32 using only information from the compression part of the cycle. The latter approach was used here. Good agreement between tests and analytical predictions is observed.

A more complicated loading case of combined tension-torsion for woven glass fabric is shown in Figure 3.6. The magnitude of maximum tension and torsion loads was the same and  $R=0$ . As might be expected, this case stretches the “abilities” of the model. The complexity of the loading leads to the creation of different types of damage. A single constant value of the cycle-by-cycle probability of failure  $p$  is not sufficient to capture the behavior. The predicted

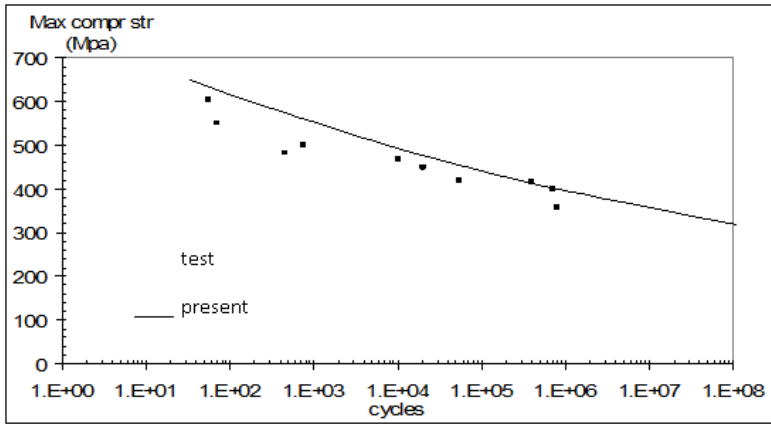


Figure 3.5: Analysis versus test for  $[0_2/\pm 45/0_2/\pm 45/90]_s$  Celion 6000/ H795E BMI ( $R=-1$ ). The test results are obtained from [76]

curve has a different slope than the test results but, after  $10^5$  cycles, the predictions are reasonable. This suggests that the damage has coalesced to a single major type of damage, which is captured well by a single  $p$  value. Unfortunately the authors of [77] did not give any description of the type of damage and how it evolved with cycles.

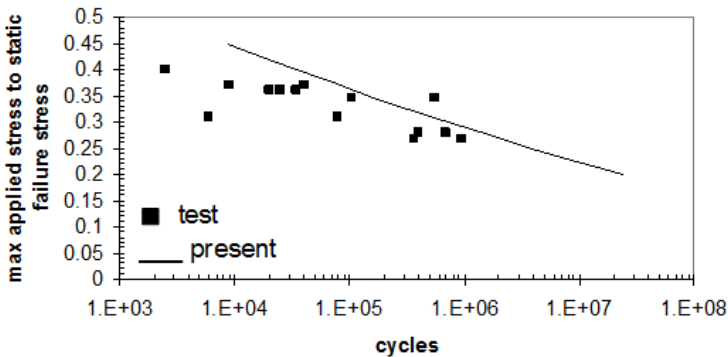


Figure 3.6: Tension-Torsion case (tension=torsion and  $R=0$ ) for woven glass fabric. The test results are obtained from [77]

So far, the test results have not included delaminations, other than as a by-product of coalescence of other types of damage such as matrix cracks. To examine how well the model performs when delaminations are the main type of damage created, three cases are shown in Figures 3.7 - 3.9. In all cases the

onset of delamination load is plotted as a function of cycles.

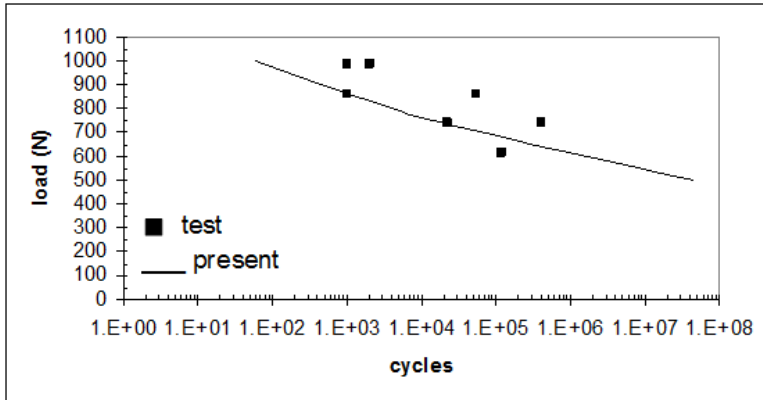


Figure 3.7: Onset of delamination load for skin/stiffener pull-off configuration ( $R=0.1$ , material: IM6/3501-6). The test results are obtained from [78]

The case of a stiffener flange with layup  $[45/90/-45/0/90]_s$  co-cured on a skin with layup  $[90/45/0_2/ - 45/45/ - 45/90]_s$  both made with IM6/3501-6 Graphite Epoxy is shown in Figure 3.7. The damage observed during testing was matrix cracks followed by delaminations. Note that only three data points were available for the static strength case. They were assumed to cover 90% of the entire population which was assumed to follow normal distribution. Good agreement is observed between the analysis and the test results.

The case of onset of edge delamination in a thermoplastic laminate with layup  $[35_2/ - 35_2/0_2/90_2]_s$  is shown in Figure 3.8. Here, the energy release rate  $G$  is used as the loading parameter. The material is AS4/PEEK where the resin is thermoplastic. The dominant failure mode during the tests was edge delamination. The predictions are slightly unconservative but follow the trend of the test data very well.

The last onset of delamination case is shown in Figure 3.9. This is the case of quasi-isotropic glass/epoxy. Edge delamination was again the damage observed during the tests. The predictions were obtained following the procedure in section 2.3.1. Good agreement between test results and analytical predictions is observed but the analytical curve has different slope from that of the test data.

The last comparison in this section involves a more complex structure. This is a bolted joint with T300/914 material and layup:  $[0_2/ \pm 45/0_2/ \pm 45/90]_s$  base plate with  $[0_2/45/9/ - 45/90]_s$  doublers. Loading was tension-compression with  $R=-1.66$ . The test data were obtained from Gerharz et al [81]. A combination of bearing failure, matrix cracks, and delaminations

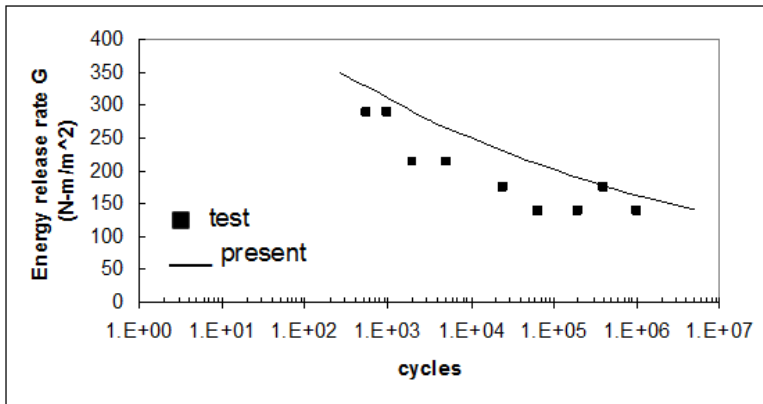


Figure 3.8: Onset of edge delamination for  $[35_2 / -35_2 / 0_2 / 90_2]_s$  AS4/PEEK ( $R=0.1$ ). The test results are obtained from [79]

were observed during tests. The comparison between theory and test is shown in Figure 3.10. The methodology in section 2.3.2 was used to obtain the analytical predictions. This is, again, a case where a constant cycle-by-cycle probability of failure  $p$  is not sufficient to capture the complexity of the types of damage created throughout the fatigue life. The analytical curve has a different slope, which matches the test results more closely at low cycles but is unconservative at high cycles.

### 3.3 Goodman diagrams

One disadvantage of S-N curves is that they are specific to a given  $R$  value. There is no way to use the S-N curve obtained for one  $R$  value to determine the corresponding S-N curve for another  $R$  value. Thus, given that most applications in practice are exposed to a variety of  $R$  values, the use of S-N curves can be limited. One method that can be used to account for different  $R$  values is to use constant life or Goodman diagrams.

Goodman diagrams are very useful in structural design because they provide lines of constant fatigue life for different combinations of steady and vibratory loads that relate directly to different  $R$  values. The term Goodman diagram is used here in a broader sense than in metals where clear regions of crack initiation, stable crack growth, and unstable crack growth are defined. In a composite several types of damage, matrix cracks, delaminations, fiber kink bands, cracks etc., may be present and interacting. This means that a Goodman diagram for a composite structure gives the cycles to failure for a given a combination of steady and vibratory loads, but does not give any information about the state of damage and damage evolution during cycling.

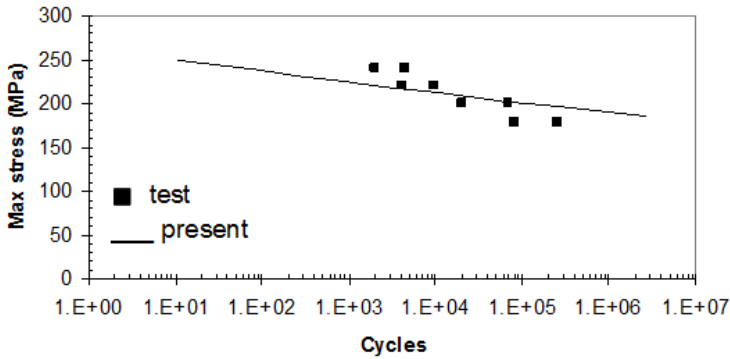


Figure 3.9: Onset of delamination for quasi-isotropic glass/epoxy ( $R=0.1$ ). The test results are obtained from [80]

Generating Goodman diagrams in practice requires a large amount of testing covering a wide range of  $R$  ratios and cycles. The method presented in chapter 2 can be used to generate the Goodman diagram for a given composite application without resorting to any fatigue testing. A brief description of how this is done is given below.

The steady and vibratory loads in a fatigue test are defined as

$$\sigma_{st} = \frac{1+R}{2}\sigma_{max} = \frac{1+R}{2R}\sigma_{min} \quad \sigma_{vib} = \frac{1-R}{2}\sigma_{max} = \frac{1-R}{2R}\sigma_{min} \quad (3.1)$$

with  $R = \sigma_{min}/\sigma_{max}$

The approach is easier to follow using an example. An open hole specimen is chosen here. The mean Open Hole Tension (OHT) strength is assumed to be equal to 410 MPa and the Open Hole Compression (OHC) strength to 331 MPa. These are typical values for intermediate modulus toughened Graphite/Epoxy material. For consistency, the statistical distribution for the static strength (even for  $R=0$  cases) is assumed here to be a two-parameter Weibull distribution.

This choice of two-parameter Weibull distributions introduces a small complication. Statistical information pertaining to test data in the open literature is typically presented in terms of a mean value and a coefficient of variation (CV) which is the ratio of the standard deviation divided by the mean. For a two-parameter Weibull distribution, a relation between mean and CV and the Weibull shape and scale parameters is needed. The scale parameter  $\beta$  is related to the mean of the distribution through Eq. 2.40. It is the relation between the CV and the shape parameter  $\alpha$  that

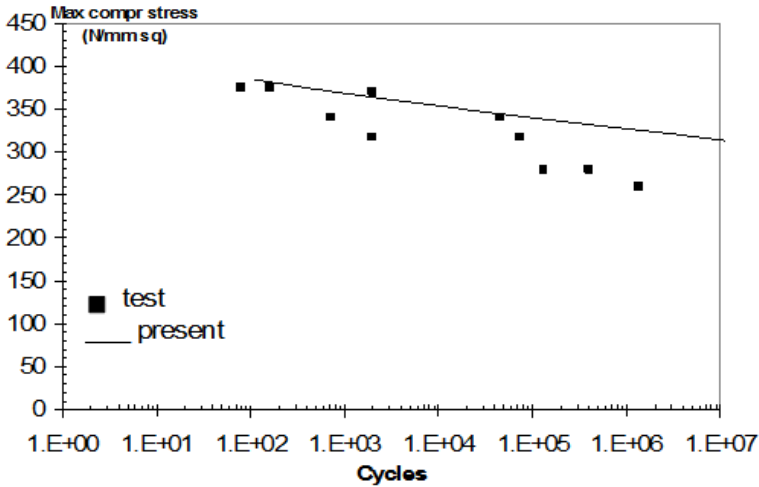


Figure 3.10: Tension-Compression ( $R=-1.66$ ) failure of T300/914 bolted joints. The test results are obtained from [81]

requires a little extra work. This was first introduced in section 2.2. Several authors have developed rigorous relations between CV and the Weibull shape parameter. For example, Sheikh et al [82] have developed a rather complicated expression between CV and the Weibull shape parameter that requires iterations. They also note that, for most CV values, the plot of shape parameter versus  $1/CV$  is a straight line. This was verified here by taking various standard normal distributions with different CV values and determining the “equivalent” two-parameter Weibull distribution that would match the 1 and 99 percentile values for the two populations using Eqs 2.12 and 2.33. For each of the equivalent two-parameter Weibull distributions, the corresponding shape parameter was calculated. A plot of the results is shown in Figure 3.11. The points in Figure 3.11 define a straight line (goodness of fit  $R^2 = 1$ ) the equation of which is

$$\alpha = -0.9686 + 124.78 \frac{1}{CV} \quad (3.2)$$

with CV expressed as a percentage. Note that the negative constant in Eq. 3.2 is an artifact of the curve-fitting procedure and will affect the results significantly only for very large CV values.

In order to proceed, the scatter (shape parameter or CV) for the OHT and OHC mean values is needed. This would depend on the specific material and stacking sequence selected. Instead of fixing material and stacking sequence, representative values are used to generate a generic Goodman diagram.

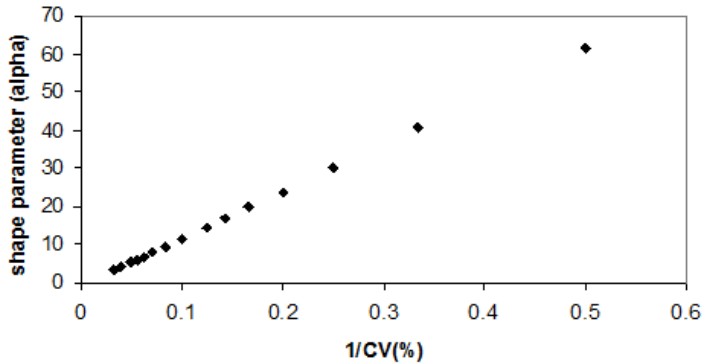


Figure 3.11: Relationship between Weibull shape parameter and Coefficient of Variation (CV)

Whitehead et al [83] examined thousands of data points for typical composite structures and, after pooling the data, determined that strength follows a two parameter Weibull distribution. This distribution has a shape parameter which, itself, follows another two-parameter Weibull distribution with modal value of 20 and mean value 23.2.

One can now use either the modal value or the mean value to substitute for  $\alpha$  in Eq. 3.2 to obtain the corresponding CV value. For conservatism, which results in a larger CV, the modal value is used. Then, solving for CV gives a value of 6%. Using Eqs. 2.39 and 2.40 and the mode of 20 and mean of 23.2, one can solve for the shape and scale parameters of the distribution describing the shape parameter of all the data examined in [83]. The equations to be solved are:

$$20 = \beta \left(1 - \frac{1}{\alpha}\right)^{\frac{1}{\alpha}} \quad (3.3)$$

$$23.1 = \beta \Gamma\left(\frac{1}{\alpha} + 1\right) \quad (3.4)$$

Solving these two equations for  $\alpha$  and  $\beta$  gives  $\alpha=2.22$  and  $\beta=26.2$ . These values can now be used in Eq. 2.12 to determine the percentile corresponding to the CV value of 6%. It is found that a modal value of 20 corresponds to  $p \approx 0.42$ . This means that a CV value of 6% is greater than or equal to 42% of the cases examined in reference [83]. In what follows, it was decided to add a degree of conservatism by increasing the CV for OHT from 6% to 7% and the CV for OHC from 6% to 10%. Using a greater CV value for OHC than OHT is consistent with the fact that compression tests typically have greater CV values than tension tests [83].

Using the CV values established above, the Goodman diagram can now be constructed using the following steps. An R value and a value N for the cycles to failure are selected. Then, Eqs 2.32 or 2.43, with appropriate adjustments for the value of R, are used to calculate the maximum or minimum stress to cause failure after N cycles. These results are then combined with Eq. 3.1 to determine the corresponding steady and vibratory loads. The cycle levels selected were,  $N = 10^{16}$  (assumed to represent infinite life),  $10^{10}$ ,  $10^8$ ,  $10^7$ , and  $10^6$ . Repeating the process for different R values will give different constant life curves. The resulting Goodman diagram is shown in Figure 3.12.

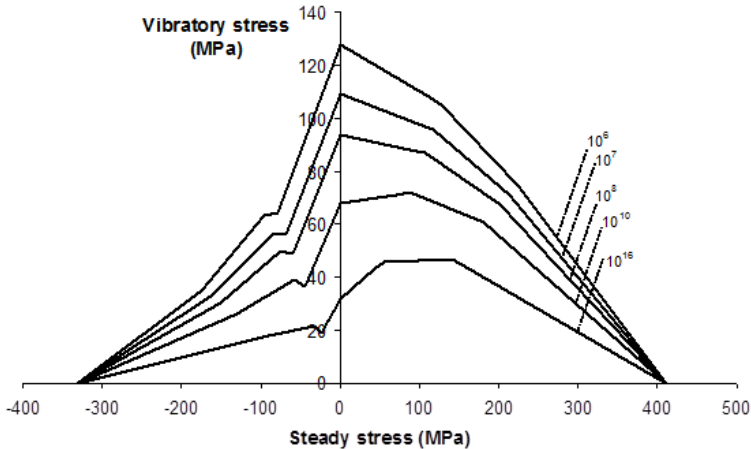


Figure 3.12: Typical Goodman diagram for open hole specimens ( $CV_{ten} = 7\%$ ,  $CV_{comp} = 10\%$ )

Usually, to construct a Goodman diagram, limited test data are used to obtain a few points on the Goodman diagram which are then connected with straight lines (see also [50]). The present method, which does not require any fatigue testing, allows the detailed and accurate construction of such a diagram to any desired level of detail. The curves shown in Figure 3.12 are not smooth because a finite number of R values were used to create them and straight line segments were used to interpolate in-between. It is interesting to note that the curves for positive steady stress (right hand side of the plot) are concave while the curves for negative steady stress (left hand side of the plot) are convex. Analytical derivations of Goodman diagrams with a very similar shape have also been developed by Schaff and Davidson [32], and Vassilopoulos et al [50]. Experimental evidence of such shapes has been reported by Gerharz et al [81] and Vassilopoulos et al [50] for notched and unnotched laminates.

As already mentioned, the Goodman diagram provides an overview of the fatigue life for different R values. Thus, comparing a Goodman diagram

created using the method presented here to test results will give a better overview of the accuracy of the method for a variety of  $R$  values. This comparison is shown in Figure 3.13 where test results from Gathercole et al [75] on T800/5245 BMI material are compared to predictions obtained using the present method. All stress values are normalized to the static tension strength. Note that in generating the predictions in Figure 3.13 actual CV values from the static test results in [75] were used and not the conservative values used for Figure 3.12.

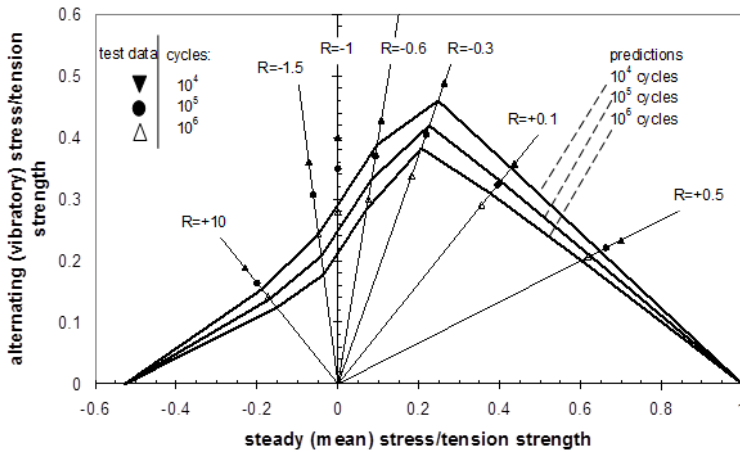


Figure 3.13: Predicted Goodman diagram versus test results from [75]

It can be seen from Figure 3.13 that for positive steady loads there is reasonable agreement between the analytical predictions and the test results. For negative steady loads, however, there is an appreciable discrepancy and the predictions are always conservative, i.e. lower than the test results. This suggests that the present method has trouble capturing the effect of damage on fatigue life when compressive loads are involved ( $R < 0$ ). As mentioned earlier, this is a limitation of using a constant cycle-by-cycle probability of failure  $p$ . In compression, small scale damage such as fiber micro-buckling combines with matrix cracking and fiber-matrix disbands to create damage on larger scales. This suggests that the value of  $p$  changes as the different types of damage are created and coalesce. Such multiple interacting damage types are not as common during tension-dominated loading, ( $0 < R < 1$ ), and using a single  $p$  value in such cases gives reasonable predictions.

### 3.4 Evaluation-shortcomings of the method as presented so far

The basic model presented in chapter 2 was compared to test results in this chapter covering predictions for residual strength, cycles to failure under constant amplitude loading for different R values, and Goodman diagrams. The comparisons presented in sections 3.1-3.3 showed that the agreement of the analytical predictions with test results, when based on a constant cycle-by-cycle probability of failure  $p$ , ranges from excellent to poor. More complex structures and/or loadings create multiple types of damage during cycling which result in a variable value of  $p$  and this must be accounted for in the analytical model. A method to do that will be presented later in chapter 6.

Nevertheless, the main advantages of the model presented so far should not be underestimated. The ability to generate approximate S-N curves without any fatigue data is of paramount importance in industry as it will help speed up the design process. Having to wait for fatigue test results in order to determine whether good static designs will have the required performance under fatigue loading can cause major delays and can carry significant cost penalties in a program. It was shown that reasonable to excellent predictions can be obtained, even with a constant value of  $p$ , for a variety of resins, thermosets, thermoplastics, BMIs, fibers (graphite, glass), in-plane and out-of-plane loading conditions, and laminates from uni-directional to quasi-isotropic and anything in-between. The power of the model lies in the fact that it is purely analytical and all the variables are either known from static tests or from other considerations. There is no need for curve-fitting of fatigue data, extra fatigue tests to characterize properties, or for other empirical or semi-empirical models to generate model variables. This makes the model very promising for general use in particular when the modifications presented in chapter 6 to model damage accumulation and interaction better are used.

Some important characteristics of the analytical model presented here should also be discussed. The first is the sensitivity of the model predictions to the scatter of residual strength. As can be seen in the general equation, Eq. 2.25, the cycles to failure depend on the cycle-by-cycle probability of failure  $p$ . This, in turn depends on the scatter of the residual strength. For the case where the residual strength follows a Weibull distribution this can be seen directly from Eqs. 2.29 or 2.32 where the shape parameter appears in the exponent in the right hand side. As mentioned in section 2.2, the shape parameter is inversely proportional to the scatter (the higher the value of  $\alpha$  the lower the scatter). As a result, the larger the scatter of residual strength, the lower will be the number of cycles to failure for a given cyclic load.

This means small differences in the determination of scatter, measured by  $\alpha$  in a Weibull distribution or standard deviation  $s$  or CV for a normal distribution, translate to big changes in the predicted cycles to failure. For

example, for  $R=0$ , a 10% increase in the standard deviation  $s$  can decrease the fatigue life by a factor of 5-10 (depending on the case). Thus, accurate characterization of the static strength or, after cycling, the residual strength population, is important for getting accurate predictions of cycles to failure.

The second characteristic, which indirectly relates to the point just made about the scatter, is the need for accurate characterization of the type of statistical distribution followed by the static or residual strength. There are rigorous methods for characterizing the statistical distribution of strength data described in detail in [84]. The discussion in the previous chapter was confined to normal and two-parameter Weibull distributions because these two cover the vast majority of distributions encountered in practice. If a different distribution is more appropriate, the approach to determine  $p$  is modified accordingly. Note however, that Eq. 2.25 is still valid.

One example of the effect of the statistical distribution on the prediction of cycles to failure is shown in Figure 3.14. This is the same case as in Figure 3.5 but now, instead of a two-parameter Weibull distribution that was used to generate the results in Figure 3.5, a normal distribution is also used. Clearly, the normal distribution gives erroneous predictions in this case.

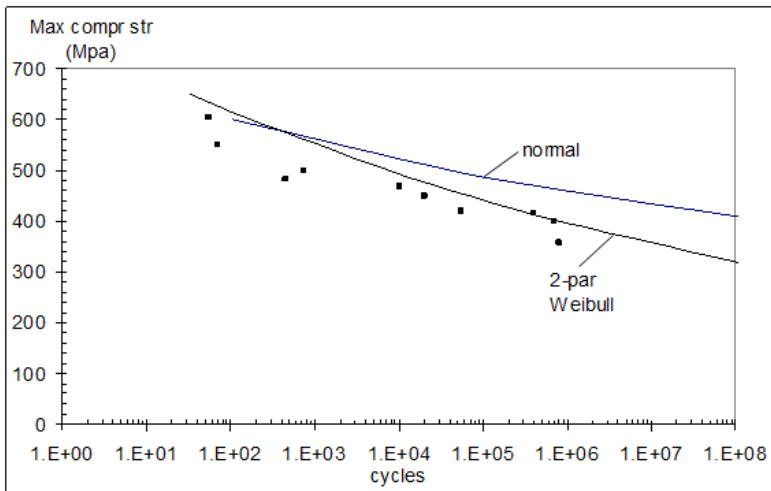


Figure 3.14: Effect of type of statistical distribution on theoretical predictions for  $[0_2/\pm 45/0_2/\pm 45/90]_s$  Celion 6000/ H795E BMI ( $R=-1$ )

The third characteristic is the assumption that there is no endurance or fatigue limit. Unlike ferrous materials, composite materials do not clearly show an endurance limit. It should be noted that the method presented does allow for the existence of endurance limit through Eq. 2.8. However, because there is no hard evidence of the existence of endurance limit, it was decided to

set it equal to zero. This assumption can be modified as necessary by keeping a non-zero  $\sigma_E$  value in Eq. 2.8 and then following the same procedure as given in chapter 2. As already mentioned the presence of an endurance limit, if it exists, (see [64, 66] for indications to the contrary) will have an effect mostly for high cycle fatigue

It should be pointed out that the numerics of the model presented may reproduce an artificial endurance limit depending on the type of software used to calculate the value of the cycle-by-cycle probability of failure  $p$ . If the applied load is low enough given the static strength distribution, the value of  $p$  will be so small (e.g.  $p < 10^{-17}$  in excel spreadsheets) that it will be treated as equal to zero and will give an infinite life. This would suggest that the stress level corresponding to that low  $p$  value behaves as an endurance limit. There is, however, no reason to believe that this numerical problem reflects a physical fact. Note also that this numerical problem manifests in life predictions greater than  $10^{17}$  cycles which is way beyond any situation found in practice and thus is of no particular immediate concern.

### 3.5 Summary

The simplest form of an analytical model that can be used to predict the cycles to failure of a composite structure under constant amplitude cyclic loading was presented in this chapter. It is the simplest form because it assumes that the cycle-by-cycle probability of failure of the structure is constant. Comparisons with test results showed that the model predictions range from excellent to poor. The main cause for the discrepancies between analytical predictions and test results was identified as the fact that the model in its present form does not account accurately in all cases for the way in which damage evolves in a composite structure. This suggests that better modeling of damage creation and evolution during cyclic loading must be incorporated in the model. This will result in a variable cycle-by-cycle probability of failure. Steps towards generalizing the present model are taken in Chapter 6.

# 4

## *Applications of the proposed model to establish reliability-based design curves and omission levels and reduced number of test cycles*

The model presented in the previous two chapters can be used to provide useful answers to two application-related questions with which typical composite programs in industry are faced. These are the following:

- determination of the required number of test cycles to achieve a given reliability
- determination of omission level during a test program

As also mentioned in previous chapters, the derivations and results presented in this chapter are consistent with one damage state dominating the fatigue performance and having no major interactions with or transitions to other damage states. A method to determine the number of test cycles required to achieve a specific reliability value is shown in section 4.1. The method to determine omission levels for fatigue tests of composite components is presented and is compared to test results in section 4.2. An approach to derive an exchange rule for reduced test cycles equivalent to the required service life cycles is presented in section 4.3. A summary of the chapter is provided in section 4.4.

### **4.1 Determination of number of lifetimes testing for B-basis reliability**

As mentioned in chapter 1, composites have flatter  $S - N$  curves than metals. While this is a significant advantage over metals because the strength reduction for a given number of cycles is less than the corresponding value for metals, it carries a significant penalty with it. Flatter  $S - N$  curves require a much larger number of tests in order to obtain a specific design curve, with a specific reliability.

For example, for secondary structure, the failure of which does not lead to loss of the aircraft, or for redundant structure ( which has redundant load paths) the loads of which, upon failure, can be taken by adjacent structure without compromising the performance of the adjacent structure, the design curve is a B-Basis reliability curve. A B-Basis value is, by definition, the 10 percentile of a statistical distribution such as the strength of a specimen [85].

This can be generalized to a B-Basis curve to imply the design curve which is below at least 90% of the test data of the fatigue test. A typical situation is shown in Figure 4.1 where the test data from Figure 3.1, taken, in turn, from [74], are shown. Recall that, for clarity, only the low and high data points are shown in Figure 4.1 at each load level.

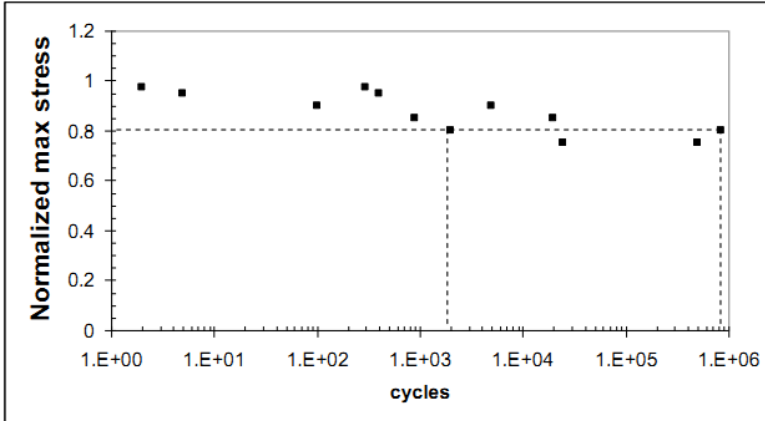


Figure 4.1: Fatigue tests on uni-directional AS4/3501-6 Graphite/Epoxy Scatter of fatigue tests.

It is easy to see from Figure 4.1 that, even at the same load level (max stress value on the y axis) the corresponding cycles to failure can easily cover three decades. For example, when the normalized maximum stress equals 0.8, the cycles to failure ranged from less than 2000 cycles to almost a million cycles, i.e., three orders of magnitude. This means that the mean curve fitted to the data in Figure 4.1 cannot be used for design since there will be a 50% probability that the actual structure will have a lower life than the mean curve for any given applied maximum stress. A statistically significant design curve must be determined that will be lower than almost all the test data, thus guaranteeing that the actual structure will have life longer than the one indicated by the design curve. The term statistically significant means that the design curve has a specific reliability value associated with it. Typical reliability values used in practice are B-Basis (90% reliability) as mentioned above for redundant or secondary structure and A-Basis (99% reliability) for primary structure, failure of which leads to loss of the aircraft.

There are rigorous methods for determining design fatigue curves with specific reliability, for example in [83] or [62]. These methods all require that a sufficient number of tests be done across several load levels. This adds to the cost and duration of the test program. Following these methods, a B-Basis design curve can be determined as shown in Figure 4.2.

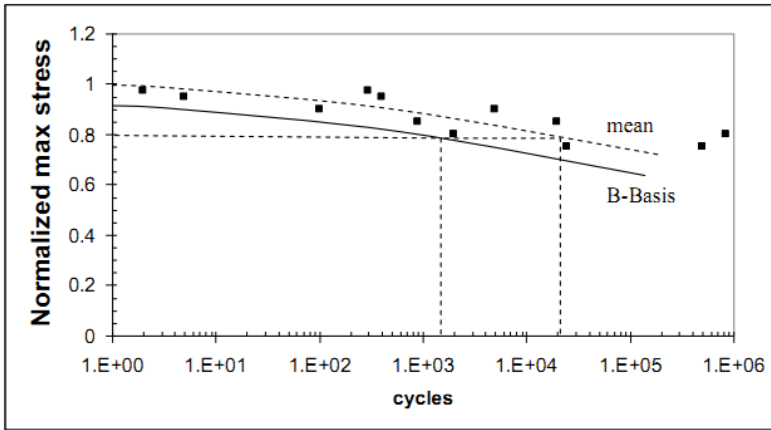


Figure 4.2: Mean and B-Basis curves for the data in Figure 4.1

The continuous line in Figure 4.2 is the B-Basis curve obtained by statistical analysis that determines at each cycle level the applied normalized maximum stress which is lower than 90% of the test data. The dashed line is the mean curve. What is of primary interest here is the relation of the B-Basis life compared to the mean life for a given stress level. One such example is shown in Figure 4.2 when the applied maximum stress is 80% of the static strength (normalized max stress=0.8 as shown by the horizontal dashed line in the Figure). Reading off the x-axis the cycles to failure that correspond to the intersections of the 0.8 normalized maximum stress line with the B-Basis and Mean curves, one gets approximately 1600 cycles for the B-Basis cycles to failure or life and 21000 cycles for the mean life. The ratio of these two values, mean/B-Basis life, is 13.4. This implies that if a single specimen or structure is used in a test program to verify that the structure has adequate life, then it should be tested to 13.4 times the service life in order to demonstrate B-Basis reliability. Rigorous statistical analysis of thousands of data points in reference [83] has shown that, for typical graphite/epoxy materials, this ratio of mean to B-Basis life is 13.6. This is a direct result of the flatness of S-N curves for composites and is a major problem in composite programs with fatigue sensitive parts because it requires a very large number of cycles to demonstrate the required reliability. Reduced test times where the applied loads are increased by a load enhancement factor are also possible [83] but the structure is running the risk of failing early because of the increased applied loads.

It is clear from this discussion that, for a given application, a large number of tests is necessary to obtain design fatigue curves. Simply using published values for the mean to B-Basis life ratio is not acceptable, unless the exact

same layups, materials and loads are used as in the references. An alternative methodology in which the analytical model presented in previous chapters is used without the need for fatigue tests is presented here.

The life prediction in the present model was obtained by determining when the probability  $P$  that there has been a (single) failure in a certain range of cycles is maximized. The expression for  $P$ , Eq. 2.24 was derived in section 2.2. It is now assumed that this expression for  $P$ , also describes the percentile values of  $N$ . That is,  $P = 0.1$  corresponds to a life  $N_B$  that is lower than 90% of the tests done at a given load level. There is no proof that this is valid but the fact that there is one-to-one correspondence between the probability  $P$  of one failure between 1 and  $N$  cycles and the cycles to failure, makes this a plausible assumption worth investigating.

For a B-Basis life prediction,  $P$  is set equal to 0.1, so the B-Basis design curve is lower than 90% of the test data. Rearranging Eq. 2.24:

$$\frac{0.1}{p} = N_B(1 - p)^{N_B - 1} \quad (4.1)$$

where  $N_B$  denotes the number of cycles corresponding to the B-Basis life (and  $P = 0.1$ ).

For a given  $p$  value, Eq. 4.1 can be solved iteratively for  $N_B$ . This can be done for different values of  $p$  and the first two columns of Table 4.1 are obtained. Now the mean cycles to failure  $N_m$  must be obtained for the same values of  $p$ . This would correspond to the mean value of  $P$ . It was shown in Eq. 2.25 that the modal value of  $P$  (the maximum value) is given by:

$$N_B = -\frac{1}{\ln(1 - p)} \quad (4.2)$$

The value of  $N$  that corresponds to the mean or average of  $P$  is by definition the first moment of the function given by the integral of the variable  $N$  times the function divided by the integral of the function. According to the correspondence established between  $P$  and  $N$ , this value  $N_m$  is the mean life:

$$N_m = \frac{\int_0^{\text{inf}} N(Np(1 - p)^{N-1})dN}{\int_0^{\text{inf}} (Np(1 - p)^{N-1})dN} \quad (4.3)$$

The integrals can be evaluated in closed form (after successive use of L'Hospital's rule for the upper limit). The result is:

$$N_m = \frac{-\frac{p}{1-p} \frac{2}{(\ln(1-p))^3}}{-\frac{p}{1-p} \frac{(-1)}{(\ln(1-p))^2}} = -\frac{2}{\ln(1 - p)} \quad (4.4)$$

Comparing the result for  $N_m$  to Eq. 2.25 it can be seen that the mean value of  $N$  is twice the modal value. Thus, the third and fourth columns in Table 4.1

Table 4.1: B-Basis, modal, and mean cycles to failure for various  $p$  values

Cycle-by-cycle probability of failure $p$	B-Basis cycles to failure $N_B$	Cycles to max value of $P N_c$ (Eq. 2.25)	Mean cycles $N_m$ (Eq. 4.4)
1.0E-7	1120000	1.00E+07	2.00E+07
1.0E-6	112000	1.00E+06	2.00E+06
1.0E-5	11200	1.00E+05	2.00E+05
1.0E-4	1120	1.00E+04	2.00E+04
1.0E-3	112	1.00E+03	2.00E+03
1.0E-2	11.1	1.00E+02	2.00E+02
0.1	1	9.49E+00	1.90E+01
0.4	1.64E-01	1.96E+00	3.92E+00

can be completed using Eqs. 2.25 and 4.4 respectively. Now the ratio of the mean life  $N_m$  to the 10 percentile (B-Basis) life  $N_B$  can be easily calculated and is shown in Table 4.2. For comparison purposes, the ratio of the modal life  $N_c$  is also shown in Table 4.2.

The results in Table 4.2 are plotted in Figure 4.3. It can be seen that over a very wide range of  $p$  values ( $p < 0.1$ ) the two ratios of mean and modal lives to B-Basis life are essentially constant. This means that unless the applied load is very high, which would correspond to  $p > 0.1$ , the ratios are constant. So with the exception of very low cycle fatigue cases, the mean/B-Basis and modal/B-Basis ratios are constant.

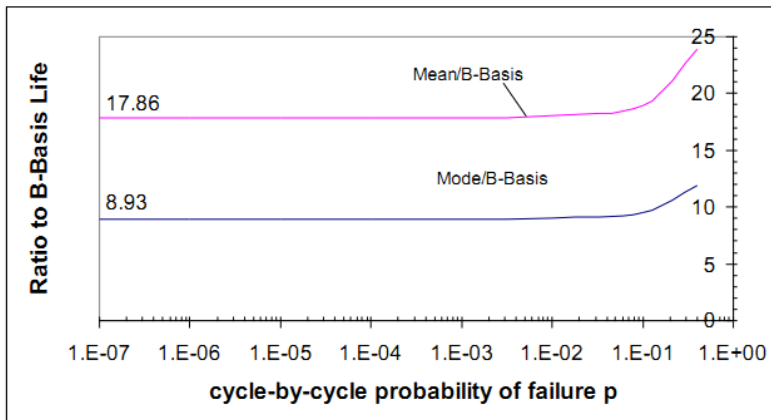


Figure 4.3: Ratios of Mean and Modal lives to B-Basis life as a function of  $p$

This means that these ratios can be used in test programs to determine by

Table 4.2: Ratio of Mean to B-Basis and Modal to B-Basis lives

Cycle-by-cycle probability of failure $p$	Modal to B-Basis life $N_c/N_B$	Mean to B-Basis life $N_m/N_B$
1.0E-7	8.93	17.86
1.0E-6	8.93	17.86
1.0E-5	8.93	17.86
1.0E-4	8.93	17.86
1.0E-3	8.93	17.86
1.0E-2	9.01	18.02
0.1	9.49	18.98
0.4	11.9	23.87

how much the service life testing of a single specimen should be increased to demonstrate B-Basis life reliability. If one uses the Mean/B-Basis life ratio, the factor is 17.86, i.e. 17.86 lives are equivalent to one service life with B-Basis reliability. If the Mode/B-Basis ratio is used, the factor is 8.93. These two ratios compare favorably with the value of 13.4 generated from two data points in Figure 4.2. What is interesting, is that the average of the two ratios, 13.4 is very close to the value of 13.6 determined in [83] after statistical analysis of thousands of data points.

More work is needed in this area to determine whether it should be one of these two ratios or their average that should be used to determine the design (B-Basis) life curve in relation to the average curve. It should be noted that the approach in previous chapters has been to use the modal value to obtain cycles to failure so, for consistency, the ratio 8.93 should be used. However, using the mean instead of the modal value is also possible, increasing predicted lives by a factor of 2 which is barely discernible as a difference in an  $S - N$  plot, and should be investigated further.

## 4.2 Determination of omission levels in test programs

A typical fatigue test program contains a large number of cycles per service lifetime. Given the requirement of demonstrating specific reliability (B-Basis or A-Basis) with the test program, the service lifetime can be multiplied by at least a factor of 9 (Modal to B-Basis reliability calculated in the previous section) to create the required number of cycles for the test program. As was mentioned in the previous section, to avoid such a large number of cycles, combinations of lower multiples of service lives, for example 2 instead of 9, and increased applied loads, through a load enhancement factor in the range

of 1.13 to 1.18 according to [83], are possible. Even so, non-rotating parts and parts not exposed to rotor wake or vibration excitation can have as many as 500000 cycles per lifetime (for 20-30 years service life), which is a large number of cycles. At the other extreme, rotors, and high frequency vibrating parts may undergo billions of cycles per service life. At no more than a few Hz loading rate or, more appropriately for full-scale test articles at less than one Hz, testing to 500000 cycles would take anywhere from 46 hrs (approx. 2 days) to 277 hrs (11.5 days). This assumes continuous round the clock shifts without stopping the test for inspection, maintenance, etc.

It is obvious that the number of test cycles can be so high that the test duration and cost can be prohibitive. For this reason, methods to reduce test duration, without reaching unconservative conclusions or compromising the reliability of the test data, are always in high demand. One such method is based on the determination of an omission level. The omission level is the load level corresponding to a number of cycles that is comfortably higher than the number of cycles expected in service. Any load in the spectrum below the omission level would cause failure only after that high number of cycles is reached. It can, therefore, be truncated out of the spectrum. This reduces drastically the number of cycles that need to be applied in a test program.

The omission level is a function of the number of cycles expected in service and the extra margin applied to them for safety. For non-rotating parts whose service life requirement is less than 500000 cycles, one million cycles is a target life that gives a comfortable margin. For parts with higher service life requirements, the target life is accordingly increased. For rotating parts, depending on the rotational speed, the target life can be more than  $10^7$  or  $10^8$  cycles.

The approach would then involve testing representative laminates or structural details from the structure at different R values that cover the entire spectrum and determining for each laminate, loading, and R value combination the load level that will cause failure at one million cycles. Load levels below the omission level are eliminated from the test spectrum of sub-components and full-scale tests. Clearly, this approach, even though it helps reduce the duration of the full scale and component tests, is quite expensive and time consuming.

The model presented in previous chapters can be used to determine analytically the omission level. In order to be able to apply the results across different materials and layups, the omission level will be determined as a fraction of the static strength. In addition, to incorporate damage tolerance, the reference static strength may include the effect of damage so the omission level is determined as a ratio of the load to reach one million cycles divided by the static strength in the presence of damage (barely visible impact damage, open hole, delamination, etc.).

The omission level will also depend on the value of  $R$ . Usually a large number of  $R$  values are present in a test spectrum. For this reason, the most conservative omission level is determined and used across all  $R$  values. It is possible, of course, to use  $R$  value- specific omission levels to minimize the number of test cycles.

The omission level determined here analytically will depend on the scatter of the residual strength. This happens because the cycles to failure for a given load depend on the scatter of the residual strength as demonstrated in chapter 2. Instead of calculating different omission levels for different values of scatter, conservative values can be used to obtain a single value that will cover all, or most, cases. In what follows, the same conservative  $CV$  values as in section 3.3 will be used: for tension  $CV_{ten} = 7\%$  and for compression  $CV_{com} = 10\%$ .

The procedure is the following.

1. A value of  $R$  in the range  $-10 \leq R \leq 10$  (which covers most cases in practice) is selected.
2. The value of  $p$ , or  $p_T$  and  $p_C$  in Eqs. 2.25 or 2.42 is determined that yields cycles to failure  $N$  equal to one million cycles
3. The value of  $p$  is translated to a normalized maximum and/or minimum cyclic stress using Eqs. 2.32, 2.34, 2.43
4. The procedure is repeated for other  $R$  values

Certain characteristics of the resulting omission curve can be anticipated by considering the equations developed in chapter 2. For high negative  $R$  values ( $R < -2$ ), the tension part of the cycle is small. The corresponding  $p_T$  value would be negligible compared to the  $p_C$  value. Thus the  $p_c$  value dominates the prediction. Then, Eq. 2.43 simplifies to:

$$N = \frac{1}{\left(\frac{\sigma_{min}}{\beta_C}\right)^{\alpha_C}} \quad (4.5)$$

In this equation, the parameter  $\alpha_C$  can be determined by using the assumption that  $CV_{com} = 10\%$  to substitute in Eq. 3.2.  $N$  is set equal to 1 million. Then, the ratio  $\sigma_{min}/\beta$  or  $\sigma_{min}/X_m$ , see analogy between Eqs. 2.30 and 2.32, can be determined. This ratio is uniquely defined independent of the value of  $R$  because the tension part of the cycle has a negligible effect on the right hand side of Eq. 4.5. As a result, the omission curve is expected to be a horizontal line for  $R < -2$ . This means that the omission level is constant with  $R$  for large negative  $R$  values.

Similarly, for large positive  $R$  values ( $R > 5$ ) the compression part of the cycle will have a negligible effect and Eq. 2.43 simplifies to:

$$N = \frac{1}{\left(\frac{\sigma_{max}}{\beta_T}\right)^{\alpha_r}} \quad (4.6)$$

Again,  $\alpha_T$  can be determined from  $CV_{ten} = 7\%$  and Eq 3.2. With  $N = 1$  million, the ratio of maximum stress to mean static strength  $\sigma_{max}/X_m$  can be obtained as a constant value independent of  $R$ . Thus, the omission curve is expected to be constant for high positive  $R$  values.

For  $R$  values in the intermediate range,  $-2 < R < 5$ , both the tension and compression portion of the cycles will have significant contributions. The omission curve is, therefore, expected to be a strong function of  $R$  in this range.

The analytically predicted omission curve obtained by the procedure described above is shown in Figure 4.4. In addition to the analytical curve shown as a continuous line, test data obtained from a wide range of publications is also shown in Figure 4.4 as individual points [10, 18, 19, 34, 74–76, 78, 79, 81, 86–95]. The test data cover 72 different material/geometry/damage/loading configurations. The materials include various thermoset and thermoplastic materials, graphite, glass, and even boron fibers, undamaged and damaged with holes, delaminations or impact, and both thin and thick laminates are included ranging from simple coupons to bolted joints.

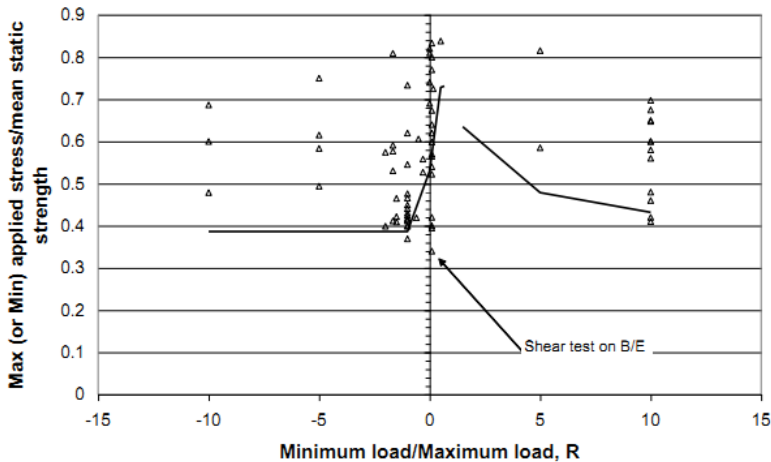


Figure 4.4: Omission level for one million cycles. Test results and analytical prediction

The test data in Figure 4.4 cover a range of omission values for each  $R$  value. This is because of the variety of materials, layup, loading, and damage levels used. This also makes it imperative that a conservative omission level that

covers all these cases without being too conservative be developed. As can be seen from Figure 4.4, the analytical prediction, based on the two conservative  $CV$  values of 7% in OHT and 10% in OHC, envelops the test data very well. Only 3-4 data points fall just outside the envelope with the worst case a shear test on Boron/Epoxy [92] for which the omission level is 0.34 (34%). An analytically predicted conservative omission level valid for all  $R$  values would be 0.38 (38%) which is only 10% higher than the worst outlier, the Boron/Epoxy case just mentioned. It is suspected that the shear tests that generated this outlier had scatter greater than the  $CV$  value of 10% assumed here. Of course, instead of using a single omission level of 0.38 across all  $R$  values it is possible to follow the curve shown in Figure 4.4, which, especially for positive  $R$ , values would give significant reductions in test times by using omission levels higher than 0.38 wherever appropriate.

It should also be emphasized that the shape of the predicted curve in Figure 4.4 is a function of the  $CV$  values used and the relative magnitudes of tension and compression strength. A different selection would lead to a different curve shape. It is expected that the case presented in Figure 4.4 is conservative for most cases.

The results of Figure 4.4 are important because they provide analytical and experimental evidence that an omission level between 34-38% of the mean static strength, including damage where appropriate, is sufficient for the great majority of composite structures to reach at least one million cycles. Similar curves can be constructed for other cycle levels. Unfortunately, beyond one million cycles, available test data are scarce. The fact that the present method worked well for test results for one million cycles gives confidence in the method and suggests that it can be used to determine omission levels for different life requirements even when the available test data are limited. It should be noted that these predictions are in line with results presented in reference [96] (sections 6.3.4.1, 7.6.5 and 7.9.1) with the present method being more conservative (34-38% versus 40-50% in [96]).

### 4.3 An exchange rule for reduced equivalent number of cycles

In a typical application, a number of load cycles representing a desired number of lifetimes for the structure must be applied to demonstrate or verify the structural adequacy of the design. Usually, the number of cycles to be applied is quite high and the test duration can be very long. For dynamic components (propellers, blades, rotating engine parts) the number of cycles can be more than  $10^8$  and for fuselage and wing components it can be as high as  $10^6$  cycles. It is often desirable to devise test programs of reduced duration to lower cost and shorten the time to market.

Eq. 2.9 can provide the means to define test programs of reduced duration.

A one-to-one correspondence between different combinations of load levels and applied number of cycles can be created where the residual strength remains constant. This can be used as an exchange rule that maps the desired number of test cycles to a reduced number of cycles that can be used for shorter duration of the test program.

Using Eq. 2.9, the number of cycles  $n_2$  for which an applied maximum stress  $\sigma_2$  will cause the same residual strength as a maximum stress  $\sigma_1$  applied for  $n_1$  cycles, must satisfy the following relationship:

$$\sigma_r = \sigma_{fs} \left( \frac{\sigma_1}{\sigma_{fs}} \right)^{\frac{n_1}{N_1-1}} = \sigma_{fs} \left( \frac{\sigma_2}{\sigma_{fs}} \right)^{\frac{n_2}{N_2-1}} \quad (4.7)$$

which can be simplified and rearranged to read:

$$n_2 = \frac{N_2 - 1}{N_1 - 1} \frac{\ln \sigma_1 - \ln \sigma_{fs}}{\ln \sigma_2 - \ln \sigma_{fs}} n_1 \quad (4.8)$$

and using Eq. 2.32 with  $X_m = \sigma_{fs}$ :

$$n_2 = \frac{\left( \frac{\sigma_{fs}}{\sigma_2} \right)^\alpha - 1}{\left( \frac{\sigma_{fs}}{\sigma_1} \right)^\alpha - 1} \frac{\ln \sigma_1 - \ln \sigma_{fs}}{\ln \sigma_2 - \ln \sigma_{fs}} n_1 \quad (4.9)$$

This equation relates the number of cycles  $n_2$  for which maximum stress  $\sigma_2$  must be applied to result in the same residual strength and thus, by assumption, damage state, as a number of cycles  $n_1$  with applied maximum stress  $\sigma_1$ . Usually, this equation will be applied when  $n_1$  is large and a reduced number  $n_2$  is sought for to shorten the test duration. For sufficiently large  $n_1$  and  $n_2$ , the corresponding cycles to failure  $N_1$  and  $N_2$  are even larger and thus the stress ratios raised to the exponent  $\alpha$  in the right hand side, are equal to  $N_2$  or  $N_1$  respectively and are much larger than 1, see also Eq. 2.32. Therefore, Eq. 4.9 can be rewritten:

$$n_2 = \left( \frac{\sigma_1}{\sigma_2} \right)^\alpha \frac{\ln \sigma_1 - \ln \sigma_{fs}}{\ln \sigma_2 - \ln \sigma_{fs}} n_1 \quad (4.10)$$

valid for  $N_1, N_2 \gg 1$ .

Eq. 4.10 or its equivalent:

$$n_2 = \left( \frac{\sigma_1}{\sigma_2} \right)^\alpha \frac{\ln \left( \frac{\sigma_1}{\sigma_{fs}} \right)}{\ln \left( \frac{\sigma_2}{\sigma_{fs}} \right)} n_1 \quad (4.11)$$

can be used to obtain a plot that shows how  $n_2/n_1$  varies as a function of  $\sigma_1$  and  $\sigma_2$ . As an example, assume the ratio of the applied load  $\sigma_1$  to the static strength  $\sigma_{fs}$  to vary in the range 0.4-0.85 and the allowable load increase  $\sigma_2/\sigma_1$  to vary between 1.05 and 1.23.

$$\frac{\sigma_1}{\sigma_{fs}} = 0.4 - 0.85 \tag{4.12}$$

$$\frac{\sigma_1}{\sigma_2} = \lambda, \lambda < 1 \tag{4.13}$$

and  $\alpha = 20$ , which is a value typical of the scatter of most composites [83].

Results are shown in Figure 4.5. Even for a load increase as little as 5% ( $\sigma_2/\sigma_1 = 1.05$ ) the number of test cycles is reduced to 50% of its original value (for  $\sigma_1/\sigma_{fs} = 0.85$ ) or 40% (for  $\sigma_1/\sigma_{fs} = 0.40$ ). A 15% increase in loads ( $\sigma_2/\sigma_1 = 1.15$ ) reduces the number of cycles to 17% of its original value for  $\sigma_1/\sigma_{fs} = 0.85$  and 7% of its original value for  $\sigma_1/\sigma_{fs} = 0.40$ . It should be noted that for  $\sigma_1/\sigma_{fs}$  values greater than 0.75 Eq. 4.9 should be used instead of 4.10 for increased accuracy.

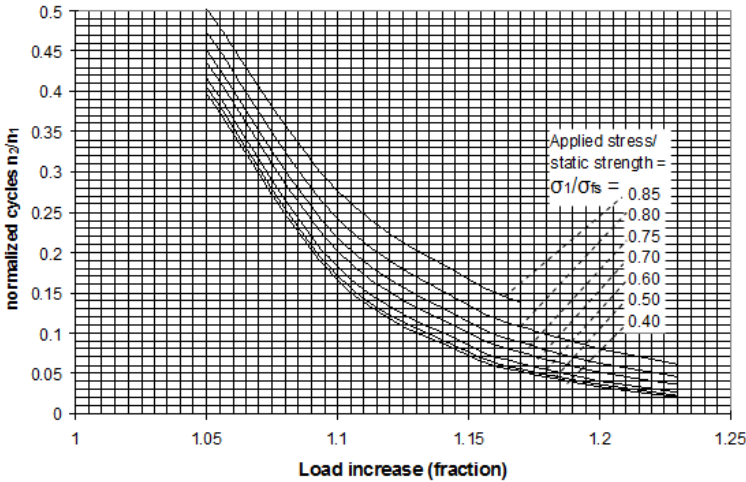


Figure 4.5: Reduction in number of test cycles as a function of increase in applied load

While such drastic reductions in the number of test cycles are very welcome in a test program, it is important to keep in mind that additional load enhancement factors, on the order of 1.15 for typical composites [83] must be applied in order to demonstrate B-Basis reliability when the test duration is, for example, equal to two service lives (one full-scale specimen). Therefore it is unlikely that one will be able to operate towards the right of Figure 4.5 with  $\sigma_2/\sigma_1 > 1.15$  because the combined load increase would be greater than  $1.15 * 1.15 = 1.323$  and the structure may not be capable of withstanding these loads. Judicious choice of the load increase to reduce the number of test

cycles and the load increase to demonstrate the required reliability would give an economical test duration with manageable risk due to the increase in the applied loads.

The results presented in this section are based on three key assumptions: (a) the residual strength of the structure follows a two-parameter Weibull distribution, (b) the failure mode during fatigue cycling is the same as during static testing and (c) the residual strength is sufficient to describe the damage state of the structure. The first assumption can easily be relaxed and other distributions can be used. The second implies that the cycle-by-cycle probability of failure does not change. The third neglects the fact that two different damage states can lead to the same residual strength. These assumptions are revisited and discussed in more detail in chapter 6. In addition, the numerical results in Figure 4.5 make use of the assumption of a Weibull shape parameter  $\alpha = 20$  which, even though representative of most composites used in aerospace industry, is not specific to a material and loading case.

#### 4.4 Summary

The analytical model for predicting the cycles to failure developed in previous chapters was used in this chapter to determine the number of test cycles that correspond to a specific reliability value. It was shown that the number of test cycles should be between 9 and 18 times the number of required service life cycles. In a second application, the model was used to determine the load level that will lead to a life of at least one million cycles. All cyclic loads below this omission level can be removed or truncated out of the test spectrum if no more than one million cycles are required. It was found that the omission level varies with R-ratio but a conservative value that covers all R-ratios is 38% of the static ultimate strength when damage is present in the structure. The same methodology can be used to determine omission levels corresponding to life requirements different than the one million cycles used here as an example. In addition, a simple exchange rule that can be used to replace a certain number of test cycles by an equivalent reduced number of cycles, but at a higher applied load, was presented.



# 5

## *Extension of the analytical model to situations with spectrum loading*

The method presented in chapters 2 and 4 was focused exclusively on constant amplitude loading. In this chapter, the method is extended to include spectrum loading. As in previous chapters, the formulation assumes one dominant damage state is present in the structure with no interaction with or transition to another damage state. Typical airframe structures are mostly under spectrum loading and not constant amplitude. Thus, extending the method to encompass spectrum loading makes the model developed here more widely applicable. A schematic example of a spectrum loading situation is shown in Figure 5.1.

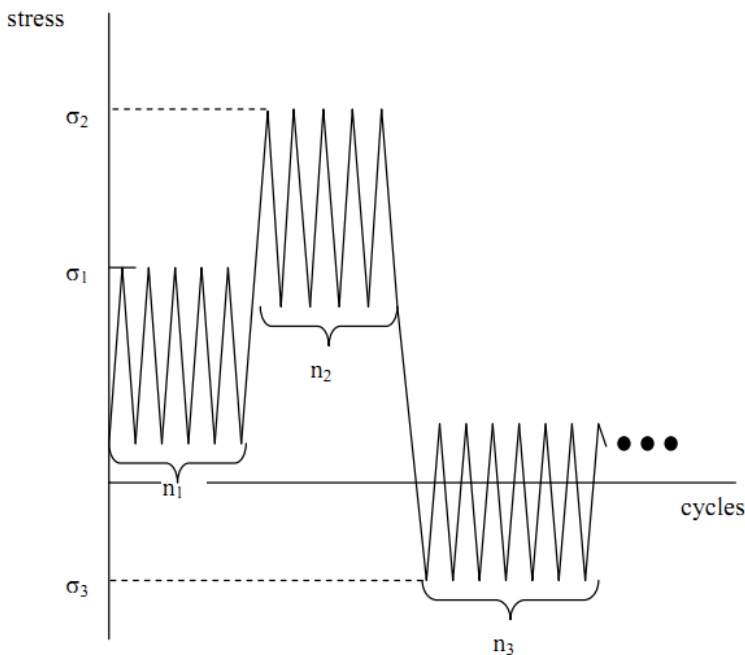


Figure 5.1: Schematic of loading spectrum as a function of cycles

In the past, many methods have been proposed to predict the performance of composite structures under spectrum loading. These are usually based

on a model for the residual strength or the loss of stiffness as a function of cycles. One of the early efforts with moderate success was that proposed by Broutman and Sahu [97]. It is based on a linear model of residual strength. Modifications to include non-linearity have been introduced by many researchers [e.g. [98], [99], [100], [101], [32] ]. Linear and non-linear cumulative damage models were compared to experimental data by Adam et al in [101]. Weibull statistics and a wear-out model were proposed by Kedward and Beaumont [33] within the context of aircraft certification. Philippidis and Vassilopoulos [34] used a tensor-based fatigue criterion which required several fatigue strength parameters obtained through curve fitting fatigue test data for basic laminates. In addition to strength-based models, stiffness-based models used to track damage creation and growth have been proposed [ [26], [102]].

All these models, except the linear ones, require some parameters to be predetermined. These can either be arbitrary parameters such as exponents in the model, or parameters related to static or fatigue strength of basic laminates or laminate constituents such as the fiber/matrix interphase [ [26], [102]]. Usually these models show good to excellent agreement with test results but the use of semi-empirical or curve-fitted parameters limits their applicability and ease of use. In addition, extending the models to cases that are drastically different than those used to obtain the model parameters may not be valid.

## 5.1 Model development

The model is developed based on the assumption that the static strength follows a two- parameter Weibull distribution. This, as was shown in section 2.2, leads to a two- parameter Weibull distribution for the residual strength after  $n$  cycles. The assumption of a two-parameter Weibull distribution is made here to simplify the derivation and obtain closed form expressions. Other assumptions such as normal distribution are also possible. The procedure for different distributions is the same but the resulting transcendental equations may require iterations to solve for the number of cycles to failure.

### 5.1.1 Residual strength as a function of applied load segments

To understand the model better, it is easier to consider first a case where only two load segments are considered,  $n_1$  cycles at maximum (or minimum) stress  $\sigma_1$  and  $n_2$  cycles at  $\sigma_2$  (see for example Figure 5.1). Let  $N_1$  the number of cycles to failure if  $\sigma_1$  were applied alone, and  $N_2$  the cycles to failure if  $\sigma_2$  were applied alone.

The approach is based on tracking the state of residual strength of the structure and determining the equivalent number of cycles under one type of loading that will lead to the same residual strength as a given number of cycles under the other type of loading. This is shown in Figure 5.2. Suppose that ,

$n_1$  cycles at  $\sigma_1$  are applied first followed by  $n_2$  cycles at  $\sigma_2$ . Then, after the first  $n_1$  cycles, the residual strength  $\sigma_{r1}$  is given by Eq. 2.10 with appropriate subscripts for the present case:

$$\sigma_{r1} = \sigma_1^{\frac{n_1}{N_1-1}} \sigma_{fs}^{\frac{N_1-n_1-1}{N_1-1}} \quad (5.1)$$

The question is how many cycles  $N_{2u}$  at  $\sigma_2$  are required to reach the same residual strength  $\sigma_{r1}$  if one starts with loading  $\sigma_2$  instead of  $\sigma_1$ . This can be determined by substituting  $\sigma_2$  instead of  $\sigma_1$ ,  $N_2$  instead of  $N_1$  and  $N_{2u}$  instead of  $n_1$  in the right hand side of Eq. 5.1 to obtain:

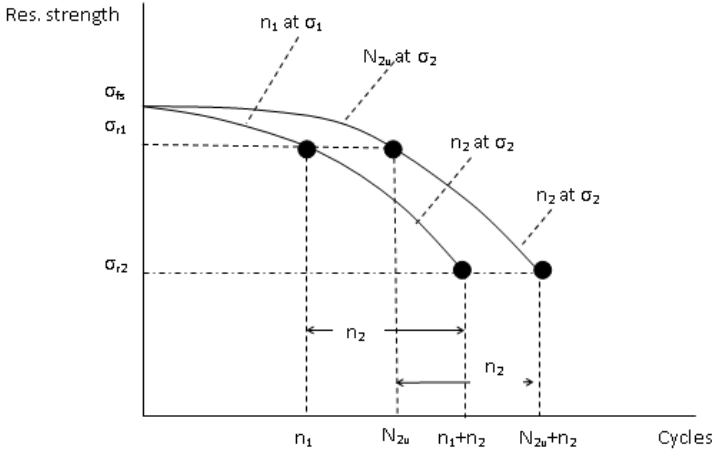


Figure 5.2: Combinations of cycles and loads giving the same residual strength at the end of two load segments

$$\sigma_{r1} = \sigma_2^{\frac{N_{2u}}{N_2-1}} \sigma_{fs}^{\frac{N_2-N_{2u}-1}{N_2-1}} \quad (5.2)$$

Eq. 5.2 can be solved for  $N_{2u}$  using Eq. 2.32 which is rewritten here in terms of the cycles to failure:

$$N = \left( \frac{X_m}{\sigma} \right)^\alpha \quad (5.3)$$

Thus, combining Eqs. 5.2 and 5.3 and solving for  $N_{2u}$  gives:

$$N_{2u} = (N_2 - 1) \frac{\ln \sigma_{r1} - \ln \sigma_{fs}}{\ln \sigma_2 - \ln \sigma_{fs}} = (N_2 - 1) \frac{\ln \frac{\sigma_{r1}}{\sigma_{fs}}}{\ln \frac{\sigma_2}{\sigma_{fs}}} \quad (5.4)$$

Note that while Eqs. 5.1 and 5.2 are general, within the assumptions of the residual strength model given in section 2.1, Eq. 5.3 also requires that

the strength be described by a two parameter Weibull distribution. In what follows, it is assumed that the static strength follows a two-parameter Weibull distribution.

Using now Eqs. 2.10 2.30, and 2.32 to substitute in Eq. 5.4 and rearranging,

$$N_{2u} = \frac{N_2 - 1}{N_1 - 1} n_1 \frac{\ln N_1}{\ln N_2} \quad (5.5)$$

Eq. 5.5 gives the number of cycles  $N_{2u}$  for which the second load case with applied cyclic stress  $\sigma_2$  must be applied to result in a residual strength  $\sigma_{r1}$ , which is the same residual strength that would result if  $n_1$  cycles were applied with applied cyclic stress  $\sigma_1$ . This means that the  $n_1$  cycles at  $\sigma_1$  that started the spectrum loading can be replaced by  $N_{2u}$  cycles at  $\sigma_2$  and, from a residual strength perspective there will be no difference in the resulting condition of the structure. It is now easy to apply the second load segment of the spectrum which was  $n_2$  cycles at  $\sigma_2$  because it is the same load level as the  $N_{2u}$  cycles. Therefore,  $n_1$  cycles at  $\sigma_1$  followed by  $n_2$  cycles at  $\sigma_2$  is the same as  $N_{2u} + n_2$  cycles at  $\sigma_2$ . This means that the residual  $\sigma_{r2}$  strength at the end of the two segments ( $n_1$  cycles at  $\sigma_1$  followed by  $n_2$  cycles at  $\sigma_2$ ) can easily be obtained using Eq. 2.10 with applied load  $\sigma_2$  for  $N_{2u} + n_2$  cycles. The result is:

$$\sigma_{r2} = \sigma_2^{\frac{n_2 + N_{2u}}{N_2 - 1}} \sigma_{fs}^{\frac{N_2 - (n_2 + N_{2u}) - 1}{N_2 - 1}} \quad (5.6)$$

which, using Eq. 5.5 and rearranging leads to:

$$\sigma_{r2} = \sigma_2^{\frac{n_2}{N_2 - 1} + \frac{n_1}{N_1 - 1} \frac{\ln N_1}{\ln N_2}} \sigma_{fs}^{1 - \left( \frac{n_2}{N_2 - 1} + \frac{n_1}{N_1 - 1} \frac{\ln N_1}{\ln N_2} \right)} \quad (5.7)$$

Eq. 5.7 gives the residual strength if  $n_1$  cycles at  $\sigma_1$  were applied first followed by  $n_2$  cycles at  $\sigma_2$ . If the order of loading were reversed,  $n_2$  cycles at  $\sigma_2$  were applied first followed by  $n_1$  cycles at  $\sigma_1$ , the residual strength  $\sigma_{r2}^*$  is obtained from Eq. 5.7 by interchanging indices:

$$\sigma_{r2}^* = \sigma_1^{\frac{n_1}{N_1 - 1} + \frac{n_2}{N_2 - 1} \frac{\ln N_2}{\ln N_1}} \sigma_{fs}^{1 - \left( \frac{n_1}{N_1 - 1} + \frac{n_2}{N_2 - 1} \frac{\ln N_2}{\ln N_1} \right)} \quad (5.8)$$

The first important conclusion that can be drawn, is that the right hand sides of Eqs. 5.7 and 5.8 are equal. This can be shown by rearranging, bringing the fractions under a common denominator and using Eq. 5.3 to relate applied stresses to cycles to failure. This result can easily be generalized to any number of applied load segments and means that the residual strength does not change when the order of applied loads changes. This does not mean that the number of cycles (or load segments) to failure does not change with a change in the order in which the load segments are applied. This will be demonstrated later. Only the residual strength is independent of the order of load application. The

fact that the residual strength is not a function of the order in which loads are applied is a result of the residual strength model that was used (section 2.1) and the assumption that the static strength follows a two-parameter Weibull distribution.

Assuming now that there were three load segments instead of two, applied in the order  $n_1$  (at  $\sigma_1$ ),  $n_2$  (at  $\sigma_2$ ), and  $n_3$  (at  $\sigma_3$ ), the number of cycles  $N_{3u}$  used up from the cycles to failure  $N_3$  after the first two segments are applied and right before the third segment starts, can be determined in a similar fashion to Eqs. 5.4 or 5.5:

$$N_{3u} = (N_3 - 1) \left[ \frac{n_1}{N_1 - 1} \frac{\ln N_1}{\ln N_3} + \frac{n_2}{N_2 - 1} \frac{\ln N_2}{\ln N_3} \right] \quad (5.9)$$

Eq. 5.9 gives the number of cycles that, if only  $\sigma_3$  were acting, would result in the same residual strength as the case where  $n_1$  cycles at  $\sigma_1$  were applied followed by  $n_2$  cycles at  $\sigma_2$ . Thus, to determine the residual strength after  $n_1$  cycles at  $\sigma_1$ ,  $n_2$  cycles at  $\sigma_2$  and  $n_3$  cycles at  $\sigma_3$ , it suffices to determine  $N_{3u}$  (at  $\sigma_3$ ) followed by  $n_3$  again at  $\sigma_3$ . As a result, spectrum loading with three different load segments becomes equivalent to constant amplitude loading ( $N_{3u} + n_3$  cycles at  $\sigma_3$ ). Then, Eq. 2.10 can be applied again to obtain the residual strength at the end of the third load segment as:

$$\sigma_{r3} = \sigma_3^{\frac{n_3 + N_{3u}}{N_3 - 1}} \sigma_{fs}^{\frac{N_3 - (n_3 + N_{3u}) - 1}{N_3 - 1}} \quad (5.10)$$

By induction, the general expression for the cycles  $N_{mu}$  that give the same residual strength after  $m - 1$  load segments at constant amplitude  $\sigma_m$ , can be shown to be:

$$N_{mu} = \frac{N_m - 1}{\ln N_m} \left[ \sum_{i=1}^{m-1} \frac{n_i}{N_i - 1} \ln N_i \right] \quad (5.11)$$

and, finally, the residual strength after  $m$  load segments is found to be:

$$\sigma_{rm} = \sigma_m^{\frac{n_m + N_{mu}}{N_m - 1}} \sigma_{fs}^{\frac{N_m - (n_m + N_{mu}) - 1}{N_m - 1}} \quad (5.12)$$

### 5.1.2 Cumulative damage law

At this point, Eq. 2.12 can be used to determine how many cycles at  $\sigma_m$  would cause failure after  $m - 1$  load segments. If, for a pristine structure,  $N_m$  cycles cause failure at applied stress  $\sigma_m$ , and  $N_{mu}$  cycles given by Eq 5.11 have already been used during the first  $m - 1$  load segments, there are  $n_m$  cycles to failure given by:

$$n_m = N_m - N_{mu} \quad (5.13)$$

Using now Eq. 5.11 to substitute in Eq. 5.13,

$$\frac{1}{\ln N_m} \left[ \frac{n_m}{N_m} \ln N_m + \frac{N_m - 1}{N_m} \sum_{i=1}^{m-1} \frac{n_i}{N_i - 1} \ln N_i \right] = 1 \quad (5.14)$$

Eq. 5.14 provides the condition for failure when  $m$  different load segments, each with cycles to failure  $N_i$ , are applied to the structure. This, therefore, is analogous to Miner's rule used for metals. A simplification of Eq. 5.14 can be obtained if  $N_m - 1$  can be set equal to  $N_m$ . This can be done when  $N_m > 20$ . To see what  $N_m > 20$  means in terms of applied load, Eq. 5.3 is solved for  $\sigma/X_m$ . For a typical Graphite/Epoxy material, tension-dominated properties have  $\alpha = 16.86$  ( $CV = 7\%$ ). Then, rearranging Eq. 5.3:

$$\frac{\sigma}{X_m} = \left( \frac{1}{N} \right)^{1/\alpha} \quad (5.15)$$

and setting  $N = 20$  and  $\alpha = 16.86$  gives  $\sigma/X_m = 0.837$ . That is, if the applied load is less than 83.7% of the mean strength, the term  $N_m - 1$  in Eq. 5.14 can be approximated by  $N_m$ . Eq. 5.14 is then simplified to:

$$\frac{1}{\ln N_m} \sum_{i=1}^m \frac{n_i}{N_i} \ln N_i = 1 \quad (5.16)$$

This expression should be compared to Miner's rule:

$$\sum_{i=1}^m \frac{n_i}{N_i} = 1 \quad (5.17)$$

to see how the two expressions differ.

First, the form of the equations is significantly different with Eq (5.16) involving logarithms of the cycles to failure and, in the case of Eq. 5.14 not being linear in  $n_i/N_i$ . The second difference is that, in Miner's rule, the order in which the load segments are applied makes no difference. In the present model, however, changing the order changes the answer.

This can be seen easily if the two load segment case is considered. According to Miner's rule, Eq. 5.17, if  $n_1$  cycles are applied with cyclic stress  $\sigma_1$ , then, the number of cycles  $n_2$  to failure under load  $\sigma_2$  is given by

$$n_2 = \left( 1 - \frac{n_1}{N_1} \right) N_2 \quad (5.18)$$

If now the order is reversed and  $(1 - n_1/N_1)N_2$  cycles at level  $\sigma_2$  are applied, the number of cycles to failure under  $\sigma_1$  is:

$$\text{cycles to failure} = \left( 1 - \frac{\left( 1 - \frac{n_1}{N_1} \right) N_2}{N_2} \right) N_1 = n_1 \quad (5.19)$$

and the order of load application makes no difference.

On the other hand, according to the present model, after  $n_1$  at  $\sigma_1$ , Eq. 5.16 gives

$$n_2 = N_2 \left( 1 - \frac{n_1 \ln N_1}{N_1 \ln N_2} \right) \quad (5.20)$$

If the order is reversed and  $n_2$  cycles given by eq. 5.20 are applied at stress  $\sigma_2$ , the subsequent number of cycles to failure under  $\sigma_1$  is given by:

$$\text{cycles to failure} = N_1 \left( 1 - \frac{N_2 \left( 1 - \frac{n_1 \ln N_1}{N_1 \ln N_2} \right) \ln N_2}{N_2 \ln N_1} \right) = N_1 \left( 1 - \frac{\ln N_2}{\ln N_1} \right) + n_1 \quad (5.21)$$

which does not equal  $n_1$  except for the unlikely situation where  $N_1=N_2$ ., Therefore, according to the present model, changing the order of load application changes the answer. There is strong experimental evidence that changing the order of load application changes the cycles to failure [97], The present model, predicting different cycles to failure when the order of load application changes, is expected to be more versatile than the conventional Miner's rule.

It should be emphasized again that one should not be confused here with the order of load application affecting the cycles to failure given the earlier statement in the discussion following Eqs. 5.7 and 5.8 that the residual strength is not affected by changing the order of load application. Cycles to failure will change when the order is changed but the residual strength will not.

The third difference between the expression for cumulative damage derived here, Eq. 5.16, and the classic Miner's rule is that the summation of  $n_i/N_i$  may be greater than, equal to, or lower than 1, depending on the situation. In the classic Miner's rule, that summation always equals 1.

Again, for simplicity, this will be demonstrated for the two load segment case. Solving Eq. 5.16 for  $n_2/N_2$  gives:

$$\frac{n_2}{N_2} = 1 - \frac{n_1 \ln N_1}{N_1 \ln N_2} \quad (5.22)$$

while solving Eq. 5.17 for  $n_2/N_2$  gives:

$$\frac{n_2}{N_2} = 1 - \frac{n_1}{N_1} \quad (5.23)$$

It can be seen from equations 5.22 and 5.23 that while the plot of  $n_2/N_2$  versus  $n_1/N_1$  is a line of slope -1 in the case of Eq. 5.23, linear Miner's rule, the slope of the curve for the present model given by Eq. 5.22 can be less than -1 or greater than -1 depending on the value of the ratio  $(\ln(N_1)/\ln(N_2))$ . This is shown schematically in Figure 5.3.

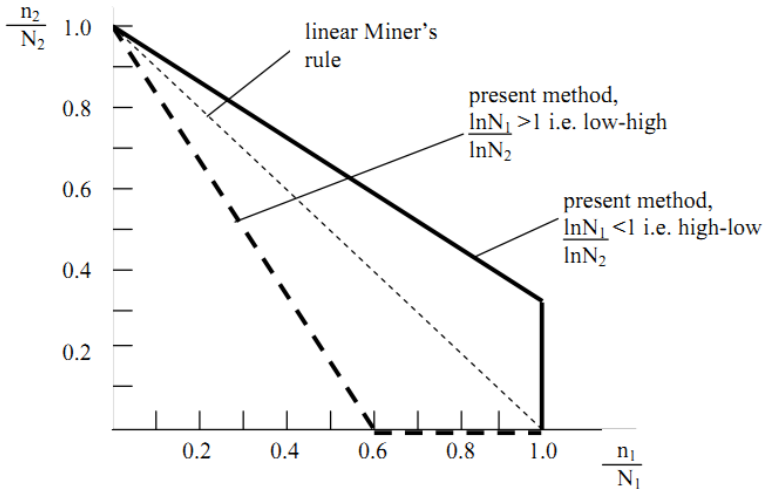


Figure 5.3: Comparison of present method to (linear) Miner's rule predictions (two load segment case)

As can be seen from Figure 5.3, the present method predicts that for high-low load sequences the summation  $n_1/N_1 + n_2/N_2$  is always greater than 1 and for low-high load sequences it is always less than 1. This can be seen by referring to Eq. 5.22. In a high-low sequence, the high loads are applied first. This means that the cycles to failure  $N_1$  corresponding to these high loads will be lower than the cycles to failure  $N_2$  corresponding to the low loads. Therefore,  $\ln(N_1)/\ln(N_2) < 1$  and the magnitude of the (negative) slope of the curve in Figure 5.3 will be less than 1. Then, the curve will lie above the Miner's rule curve, which has slope -1. Conversely, in a low-high sequence,  $N_1 > N_2$  and the magnitude of the slope will be greater than 1. The resulting curve is below the Miner's rule curve. It should be noted that by cyclically exchanging  $n_1, N_1$  with  $n_2, N_2$ , a symmetric plot of that in Figure 5.2 is obtained with respect to a line dissecting the right angle at the origin to two equal angles. Then, for example, the dashed line would extend from 0.6 on the

y axis to 1.0 on the x axis and the bold line would start from approximately, the point (0.35,1) and extend to the point (1.0,0.)

This result is supported, to some extent, by the test results obtained by Broutman and Sahu [97] where the authors report that 10 out of 12 low-high cases had Miner's sum less than 1 and six out of 12 high-low cases had sum greater than 1. Similar but less definitive test results are reported by Wahl [103].

### 5.1.3 Implications of the spectrum loading model

Two important aspects of Eq. 5.22 and the corresponding curve shapes in Fig. 5.3 should be discussed here. The first relates to the fact that, under certain circumstances, it is impossible to apply any of the cycles of the second load segment. For example, for the low-high case, the curve terminates at  $n_1/N_1 = 0.6$  and continues horizontally to  $n_1/N_1 = 1$ . The reason for this is that, when ( $n_1 = 0.6N_1$ ) cycles are applied, the residual strength of the structure has dropped to the applied stress  $\sigma_2$  of the second load segment. Thus, during application for the first cycle of the second load segment, the structure will fail. Of course, the value 0.6 here is just an example and the actual value will depend on the applied loads and cycles to failure for each load segment.

At the other extreme of fatigue behavior, for the high-low case, the curve terminates at  $n_1/N_1 = 1$  and  $n_2/N_2 \cong 0.35$  and drops vertically to meet the x axis in Figure 5.3. This simply means that if  $n_1 = N_1$  the structure fails after application of the first load segment and there is no way to apply even a single cycle of the second load segment. For the specific example of Figure 5.3, this is true for  $n_2/N_2 = 0.35$ . If  $n_2/N_2 > 0.35$ , say 0.4, the only way to apply both load segments is if  $n_1/N_1 \cong 0.9$ . Again, the values 0.35, 0.4, and 0.9 are used here to illustrate an example and are not generic. The actual values will depend on the applied loads and cycles to failure for each load segment.

The second important aspect, a direct consequence of Eq. 5.22 and the fact that the residual strength at the end of  $m$  segments is independent of the order in which these  $m$  segments are applied, is that the number of cycles to failure during the  $m^{th}$  segment, after  $m - 1$  segments are applied, does not change if the last segment does not change. That is, if the  $m - 1$  segments are reordered, as long as the  $m^{th}$  segment does not change so its applied stress remains  $\sigma_m$ , the cycles to failure during this  $m^{th}$  segment does not change. Only if the last segment is replaced by another segment in the series, do the cycles to failure  $N_m$  change.

To demonstrate this, a minimum of three load segments are necessary:  $n_1$  at  $\sigma_1$ ,  $n_2$  at  $\sigma_2$  and a third load segment at  $\sigma_3$ .

If the order of applied loads is as stated, then Eq. 5.9, repeated below for convenience, gives the number of cycles  $N_{3u}$  that have been used up from a

life of  $N_3$  cycles if only  $\sigma_3$  were applied, after  $n_1$  at  $\sigma_1$  and  $n_2$  at  $\sigma_2$  have been applied.

$$N_{3u} = (N_3 - 1) \left[ \frac{n_1}{N_1 - 1} \frac{\ln N_1}{\ln N_3} + \frac{n_2}{N_2 - 1} \frac{\ln N_2}{\ln N_3} \right] \quad (5.24)$$

In this case, the number of cycles to failure when the application of  $\sigma_3$  starts is:

$$(\text{cycles to failure})_{\sigma_3} = N_3 - N_{3u} \quad (5.25)$$

If the order of the first two segments is reversed, the right hand side of Eq. 5.9 does not change. This is due to the fact that the two terms in brackets are interchanged as the indices 1 and 2 are interchanged. Thus, the result of Eq. 5.25 remains unaffected. If, however, the last load segment is changed from  $\sigma_3$  being the applied load to any of the other two ( $\sigma_1$  or  $\sigma_2$ ), then the denominators involving the logarithm of  $N_3$  in the right hand side change. This changes  $N_{3u}$  which, in turn, changes the result of Eq. 5.25.

It should be pointed out that this result, that the cycles to failure during the  $m^{\text{th}}$  segment are not affected by the order in which the previous load segments are applied, is again a result of the assumptions made in the present model. If these assumptions do not hold, this result will not be valid. An example where this result is probably not valid is given in section 5.2.3 and a method that can be used to modify the model for improved predictions is presented in chapter 6.

#### 5.1.4 Number of block repetitions to cause failure

The conclusions drawn in section 5.1.3 can be used to obtain a relatively simple expression for the number of blocks to failure for a given spectrum loading. Typically, the loading segments are combined in repeating blocks to create the applied test loads. An example is shown in Figure 5.4. Suppose that  $m$  loading segments are combined in some loading sequence that makes up a single block and that this block is repeated until the structure fails. The number of repetitions of test blocks  $M_{fail}$  to cause failure must be determined.

It was shown, in section 5.1.1, that the residual strength is independent of load sequence. Then, if  $m$  load segments are combined in a block which is repeated  $M$  times, the residual strength at the end of  $M$  blocks is the same as a situation where a single block is applied within which each loading segment is repeated  $M$  times. That is, a single block where the cycles  $n_i$  of segment  $i$  are repeated  $M$  times gives the same residual strength as  $M$  blocks where each segment  $i$  has  $n_i$  cycles. Using Eq. 5.11 the number of cycles  $N_{mu}(M)$  that have been used up, from a total of  $N_m$  cycles at constant  $\sigma_m$ , when  $m$  segments repeat  $M$  times is given by:

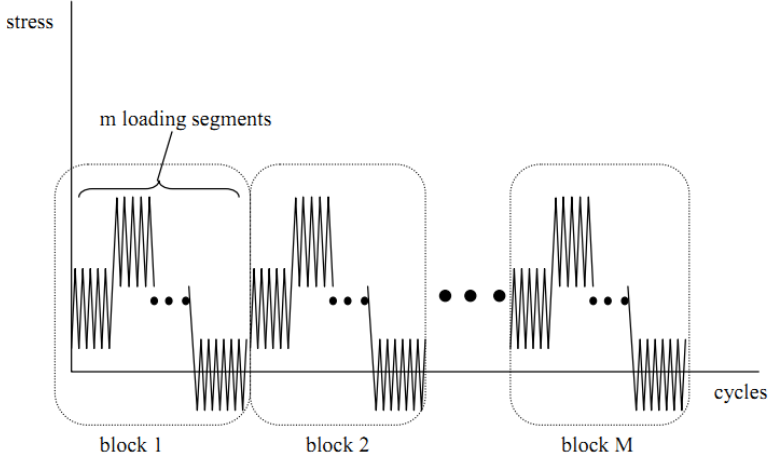


Figure 5.4: Schematic of repeating blocks making up a spectrum

$$N_{mu}(M) = \frac{N_m - 1}{\ln N_m} \left[ \sum_{i=1}^{m-1} \frac{M n_i}{N_i - 1} \ln N_i \right] = M \frac{N_m - 1}{\ln N_m} \left[ \sum_{i=1}^{m-1} \frac{n_i}{N_i - 1} \ln N_i \right] \quad (5.26)$$

The residual strength after  $M$  blocks is given by Eq. 5.12 with  $N_{mu}$  given by Eq. 5.26. Failure occurs when the residual strength equals the applied stress at any given time. Using Eq. 5.26 to substitute in Eq. 5.11 and setting successively the residual strength equal to the applied stress of each segment, different predictions for the blocks to failure  $M_{fail}$  can be obtained. Each prediction corresponds to the number of blocks at which the residual strength equals the applied load for one of the load segments. The lowest value of  $M_{fail}$  is the sought-for number of blocks to failure. For example, assuming  $\sigma_{rm} = \sigma_{max}$  ( $\sigma_{max}$  is the highest stress across all load segments) the following relation is obtained:

$$M \frac{N_m - 1}{\ln N_m} \left[ \sum_{i=1}^{m-1} \frac{n_i}{N_i - 1} \ln N_i \right] = (N_m - 1) \frac{\ln \sigma_{max} - \ln \sigma_{fs}}{\ln \sigma_m - \ln \sigma_{fs}} - n_m \quad (5.27)$$

Letting:

$$K_m = \sum_{i=1}^m \frac{n_i}{N_i} \ln N_i \quad (5.28)$$

and using Eq. 5.3 to express stresses in terms of cycles to failure, one can solve for the number of blocks to failure  $M_{fail}$ :

$$M_{fail} = \frac{1}{K_m} (\ln N_{min} - \frac{n_m}{N_m - 1} \ln N_m) \quad (5.29)$$

where  $N_{min}$  is the number of cycles to failure corresponding to  $\sigma_{max}$ :

$$N_{min} = \left( \frac{\sigma_{fs}}{\sigma_{max}} \right)^\alpha \quad (5.30)$$

and  $N_m, n_m$  are the cycles to failure and applied cycles for the last segment in the block, segment  $m$ . The value of  $M_{fail}$  in eq. 5.29 will either be the blocks to failure or one less if  $\sigma_{max}$  is reached after the corresponding segment in the block has been completed. In this case, failure will occur the next time the applied load equals  $\sigma_{max}$  which will be during the next block. Note that while the basic form of Eq. 5.29 does not change,  $N_{min}$  will have to be replaced by the number of cycles to failure corresponding to the applied stress  $\sigma$  to which the residual strength after  $(m)M_{fail}$  segments is set equal to.

## 5.2 Comparison with test results and discussion

The analytical results presented in the previous sections of this chapter are compared here to test results available in the open literature. Two sets of comparisons are made. The first is when only two load segments are applied and the second when four load segments are applied. Conclusions are drawn after both sets of results are presented.

### 5.2.1 Two-load segment case: test versus analytical predictions

The two load segment case is based on test results obtained on fiberglass by Broutman and Sahu [97]. Before comparing directly spectrum loading results, it is instructive to compare the building blocks of the present model, the cycles to failure under constant amplitude loading and the residual strength to test results of [97]. This helps identify specific strengths and weaknesses of the model and, in cases of discrepancies with test results for spectrum loading, might point to problem areas in the model building blocks.

First, because the static strength data in [97] are relatively limited, the static strength information in that reference was used to create a two-parameter Weibull distribution to describe it. This was done by matching the mean value and setting the 10 percentile value of the Weibull distribution equal to the lowest static strength value in the tests. Setting the 10 percentile value of the distribution equal to the lowest value in the static strength tests is justified because, as mentioned in section 3.3, a typical CV value is 6%. The mean static strength in [97] was 65 ksi (448.1 MPa) and the low value was 60 ksi (413.6 MPa). Using normal distribution statistics it can be shown that

the 60 ksi value of the low strength corresponds to the 9.99 percentile of the strength distribution.

Using Eqs. 2.12 and 2.40, the corresponding two-parameter Weibull distribution was found to have shape and scale parameters  $\alpha = 20.01$  and  $\beta = 67.14$  respectively. Since the fatigue tests were done at  $R = 0.05$ , the correction mentioned in section 2.3.1 was also applied but was shown to have a negligible effect compared to using  $R = 0$ . Then, the predicted  $S - N$  curve was obtained using Eq. 2.32 and is compared to test results from [97] in Figure 5.5.

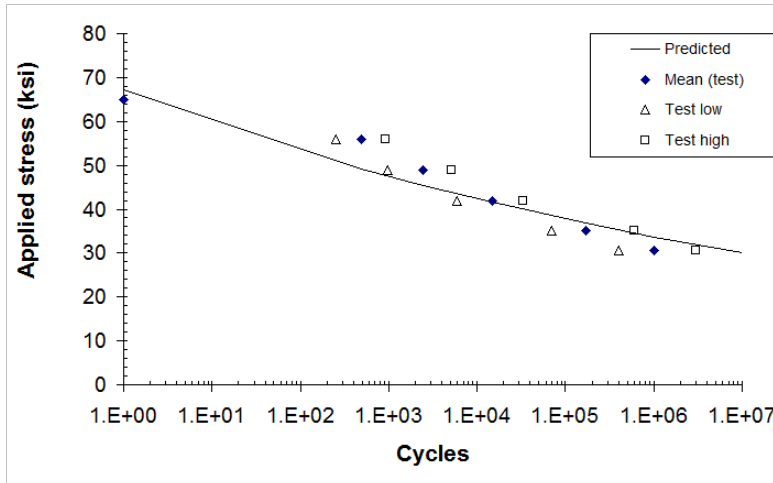


Figure 5.5: S-N curve for E-glass/epoxy (test results from [97])

It can be seen that the prediction from the present model is in very good agreement with test results for lives greater than 1000 cycles even though the slope of the predicted curve is different than that of the test data. For lower lives ( $< 1000$ ) the predictions are conservative, i.e., below the test data. The test results suggest an  $S - N$  curve that is nearly horizontal up to about 100 cycles then dropping gradually with a slope slightly higher than the slope of the predicted curve.

For the residual strength, Broutman and Sahu [97] tested specimens at different stress levels (at least three specimens per level) then stopped the tests at prescribed fractions of the fatigue life and tested the specimens to failure (residual strength test). The stress levels are shown in Table 5.1. The percentage of static strength to which the applied stress level corresponds is also given in Table 5.1.

Comparisons of the analytical predictions from Eq. 2.10 to test results are given in Figures 5.6 - 5.9. The test data, only the high and low are shown in the figures, are limited so it is hard to make conclusive comparisons. Discrepancies

Table 5.1: Cases for residual strength comparison (from [97])

Case	Stress Level (ksi / MPa)	% static strength
1	56/386	86.1
2	49/338	75.4
3	43/296	66.1
4	35/241	53.8

in Figures 5.7 and 5.9 for  $n/N \cong 0.2$  may be due to the lack of test data or inaccuracies in the analytical model. The model as used here does not differentiate matrix cracking from fiber failure. Both mechanisms are present in cross-ply laminates, the specimens used here. More accurate modeling, accounting for matrix cracks, fiber failures, and the resulting changes in the cycle by cycle probability of failure  $p$ , is presented in chapter 6. Despite this discrepancy, the predictions are in good agreement with the test results available. It should be noted that the prediction is not a straight line. The parameters of the graph and the scale are such that it appears so. In general, it is a curve convex to the origin.

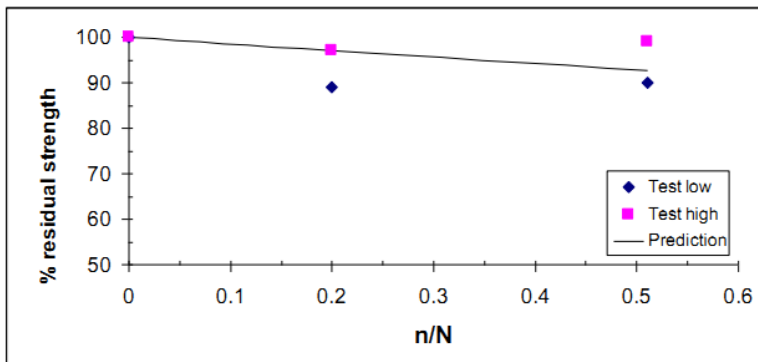


Figure 5.6: Residual strength: Analysis versus test (Case 1)

The test data from [97], summarized in Table 5.2 were used to compare predictions to test results when two load segments are applied. The test procedure was as follows. First, the load in column 2 of Table 5.2 was applied for the number of cycles shown in column 3 of the same Table. Then, the load shown in column 3 was applied until failure. The goal is to predict the cycles to failure when load segment 2 is applied and compare to the test results given in [97].

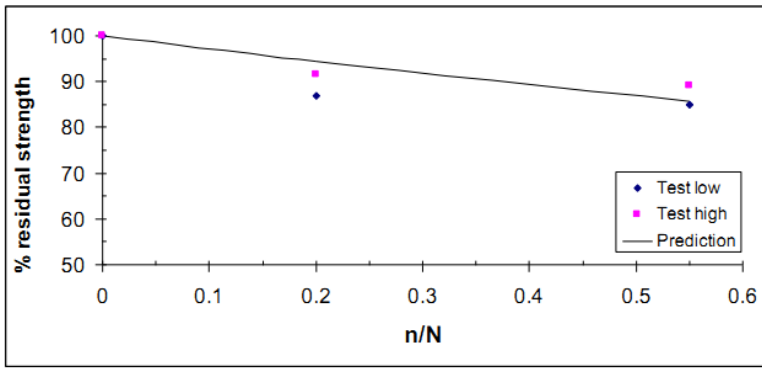


Figure 5.7: Residual strength: Analysis versus test (Case 2)

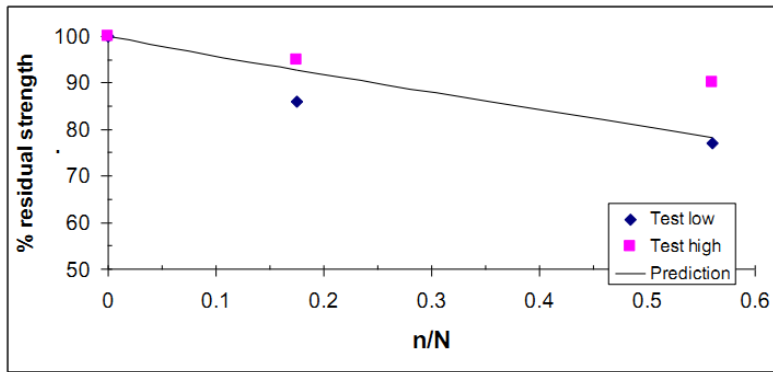


Figure 5.8: Residual strength: Analysis versus test (Case 3)

Due to the large scatter in test results shown in [97], comparing the cycles to failure during load segment 2 to the test result requires some care. Since the static strength  $\sigma_{fs}$  was assumed to follow a two-parameter Weibull distribution, it can be shown, based on Eq. 2.29, and on arguments presented in section 2.2, that  $N_1$  and  $N_2$  also follow two-parameter Weibull distributions. However,  $\ln N_1$  and  $\ln N_2$ , which are both present in Eq. 5.20, do not. They both are extreme value distributions. It is very difficult to determine the type of distribution that  $n_2$  follows on the basis of the right hand side of Eq. 5.20. Instead, a different approach was selected. First, a random number generator was used to select 100  $\sigma_{fs}$  values from the two-parameter Weibull distribution that was constructed to represent the static strength of the data given in [97]. The shape and scale parameters were as presented earlier ( $\alpha = 20.01$  and  $\beta = 67.14$ ). The random number generator was based on an equation of the form (see for example ref [104]):

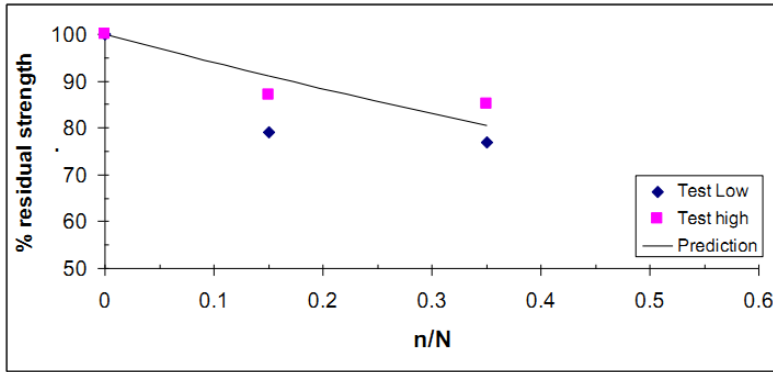


Figure 5.9: Residual strength: Analysis versus test (Case 4)

$$\sigma_{fs} = [-\beta^\alpha \ln(1 - x)]^{(1/\alpha)} \quad (5.31)$$

where  $x$  is uniformly distributed between 0 and 1 ( $\alpha = 20.01$  and  $\beta = 67.14$ ).

For each  $\sigma_{fs}$  value obtained from Eq. 5.31,  $N_1$  and  $N_2$  in Eq. 5.20 were determined by solving Eq. 2.32 for  $N$  (setting  $X_m = \sigma_{fs}$  and  $\sigma = \sigma_1$  or  $\sigma = \sigma_2$  from columns 2 and 4 in Table 5.2). Then, Eq. 5.20 was used with  $n_1$  taken from the third column of Table 5.2 to determine a corresponding  $n_2$  value. The procedure was repeated for all 100  $\sigma_{fs}$  values to generate 100  $n_2$  values. The resulting  $n_2$  population was checked to see if it followed two-parameter Weibull distribution using the Anderson-Darling test [105]. As expected from the form of Eq. 5.20, the test failed in all the cases given in Table 5.2. The  $n_2$  population was then checked for lognormality, again using the tests in ref [105]. The test was successful in all 22 cases of Table 5.2, i.e. the assumption that  $n_2$  follows lognormal distribution cannot be rejected. This is in agreement with the test results given in [97] where a lognormal distribution was found to describe the test data well. Therefore, the logmean, average of the logarithms of the data, value of the resulting  $n_2$  population was compared to the logmean value of the test data reported in [97]. The results are shown in Figure 5.10.

It should be noted that the scale of the y axis of Figure 5.10 is logarithmic. This was done to better fit all 22 cases in one graph. The agreement between predictions and test results is very good except for cases 3, 4, 5, 16, 18, 19, 20. In all these cases, the prediction is lower than the test result. Also, all but one of these cases involved the highest load of 56 ksi (386.1 MPa). And the remaining one (case 18) involved the second highest load of 49 ksi (337.8 MPa). This is consistent with the results of Figure 5.5, which showed that in the low cycle fatigue region (high applied stresses) the present method does not match the test results as well as it does in the high cycle fatigue region.

Table 5.2: Cases for spectrum loading comparison on fiberglass [97]

Case	Segment 1 stress (ksi/MPa)	Segment 1 cycles	Segment 2 stress (ksi/MPa)
1	35/241.3	50000	49/337.8
2	35/241.3	20000	49/337.8
3	49/337.8	1000	56/386.1
4	49/337.8	250	56/386.1
5	56/386.1	100	49/337.8
6	49/337.8	1000	42/289.5
7	49/337.8	1000	35/241.3
8	49/337.8	250	35/241.3
9	49/337.8	250	42/289.5
10	42/337.8	2000	35/241.3
11	56/386.1	250	35/241.3
12	56/386.1	250	42/289.5
13	56/386.1	100	42/289.5
14	42/289.5	10000	35/241.3
15	56/386.1	100	35/241.3
16	35/241.3	20000	56/386.1
17	42/289.5	10000	49/337.8
18	42/289.5	2000	49/337.8
19	42/289.5	2000	56/386.1
20	56/386.1	250	49/337.8
21	35/241.3	50000	42/289.5
22	35/241.3	20000	42/289.5

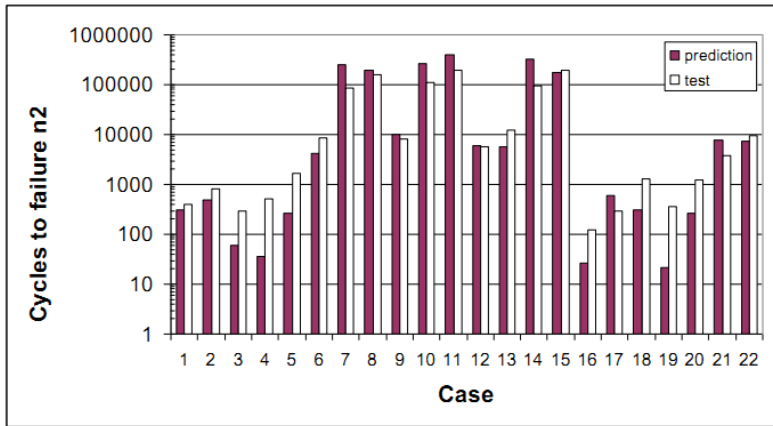


Figure 5.10: Comparison of predictions to test results from [97] for two-segment spectrum loading of cross-ply fiberglass laminates

And since the cycles to failure appear in Eq. 5.20, either as  $N_1$  or as  $N_2$ , it is believed that the discrepancy found for these cases is due to the discrepancy in the cycles to failure.

### 5.2.2 Four load segment case: test versus analytical predictions

Another set of comparisons of the analytical predictions from section 5.1 to test results is presented in this section for spectrum loading where each block contains four different load segments. The test results were obtained from the work of Adam et al [101] where a Bismaleimide (BMI) [(45/0<sub>2</sub>)<sub>2</sub>]<sub>s</sub> T800/5245 laminate was tested. A summary of the test cases is shown in Table 5.3.

Each case in Table 5.3 is made up of four segments described by the load sequence in the second column. For example, sequence 1/3/2/4 had the first, third, second, and fourth load segments applied in that order to make one loading block, and this loading block was repeated until failure. The load segments are described in the top half of Table 5.3 where load segment 1, for example, consisted of 231 cycles with maximum stress at 77.8% of the static failure strength. For all load segments, the R value was 0.1.

The analytical predictions were obtained using Eq. 5.29. They are compared to the test results from [101] in Figure 5.11. No detailed information was given in the reference about the type and sequence of damage created during the test. Bars in the Figure indicate the range of test results. It can be seen that the predictions are in very good agreement with the test results. Even though they are not very close to the average test result, they are well within the range of test results. It should also be noted that the predictions consist of only two different values, 4.94 and 4.73 blocks for all six cases given in Table

Table 5.3: Cases for spectrum loading comparison on Graphite/BMI material [101]

Load Level (% of static strength)	Number of cycles
(1) 77.8%	231
(2) 71.9%	4016
(3) 65.9%	29256
(4) 59.9%	162574
Test cases	
Case 1	Load sequence in each block
1	1/3/2/4
2	4/2/3/1
3	4/3/2/1
4	1/2/3/4
5	3/1/2/4
6	2/4/3/1

5.3. The reason is that cases 2,3, and 6 have the same last segment, segment 1, and cases 1, 4, and 5 have the same last segment, segment 4. As was shown in section 5.1.3, rearranging the load segments in a block leads to the same number of blocks to failure if the last segment in the block is unchanged. Even though the predictions are in good agreement with test results in Figure 5.11, using the present method is not always as successful. Two cases with larger discrepancies between analysis and test are the remaining spectrum loading cases in reference [101]. In the first case one of the segments of Table 5.3 is replaced by compressive load. In the second all load segments are compressive.

For the case where tension and compression cycles are mixed, the residual strength model described by Eqs. 2.2 and 2.10 does not explicitly account for the effect of load reversal. The damage and failure mechanisms are, typically, different in tension than in compression. Applying first tension and then compression in a loading sequence does not mean that the residual strength at the beginning of the compression segment will be given by that predicted at the end of the tension segment from Eq. 2.10. For example, if, after applying the tension loading, the residual tensile strength is 80% of the static tension strength, continuing on with compression loading does not mean that the residual strength in compression is also 80% of the compressive static strength. In this case, more detailed modeling of damage creation and evolution under the types of loading present in the sequence is necessary. As a simplifying compromise, it is proposed that two separate residual strength values, one for tension and one for compression, be determined and failure then

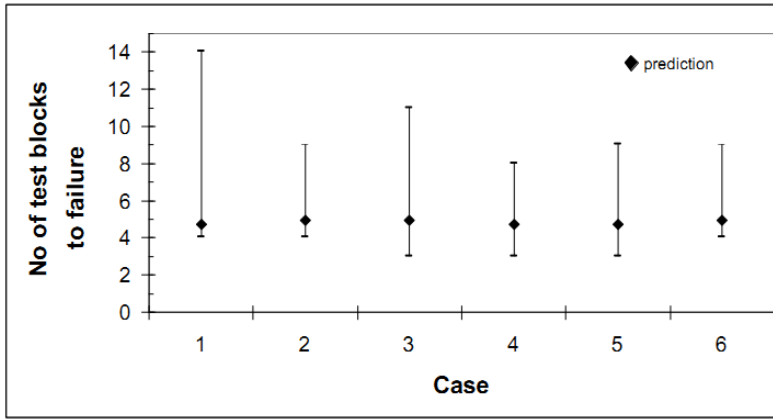


Figure 5.11: Spectrum loading predictions compared to test results from [101]

be assumed to occur when one of the two residual strength values reaches the corresponding applied cyclic tension or compression stress. For the particular case of combined tension and compression loading of reference [101], this approach predicts failure during the first block while the test results range from 1 to 5 blocks depending on the loading sequence. For the all-compression loading sequences presented in reference [101] the prediction is also failure in the first block with the test failures ranging from 1 to 39 blocks. While the test scatter is very large, the analysis model clearly needs to be improved. A method to incorporate such improvements is presented in chapter 6.

### 5.2.3 Discussion

One implication of the model presented that requires more careful evaluation is the fact that the cycles or blocks to failure do not change if the order of load application changes (provided the last load segment remains the same). A thought experiment that suggests inapplicability of this conclusion in general, is provided in the following.

Consider an all  $0^\circ$  laminate with a hole loaded first in tension-tension and then in compression-compression. The situation is shown in a hand-drawn schematic in Figure 5.12. During the tension-tension loading, longitudinal splits and delaminations develop at the edges of the hole and progress along the load direction (vertically in Figure 5.12). Test data for this situation was obtained by Badaliane and Dill [88]. This damage is confined in a narrow strip above and below the hole. If now the compression-compression loading is applied, the laminate acts as if it consists of two individual undamaged strips on either side of the hole with one failed strip in the middle the width of which equals the hole diameter. As a result, the damage state at the end

of the compression-compression cycling will consist of fiber splits mostly in the region above and below the hole and failed fibers, caused by fiber micro-buckling, forming cracks with brooming failure as shown in the right part of Figure 5.12.

If instead of tension followed by compression, the loading sequence were reversed, the damage state would be quite different. Loading a uni-directional laminate with a hole under compression-compression leads to the creation of delaminations and fiber breakage emanating from the hole, perpendicular to the loading direction. Test results for such a case have been obtained by Guynn et al [15] and are shown in a hand-drawn schematic in Figure 5.13. If at the end of the compression-compression loading the tension-tension loading is applied, the damage created, shown in the right of Figure 5.13 will be very different than that shown in the right if Figure 5.12. In Figure 5.13, it will consist of mostly fiber splits emanating from the delaminations and broken fibers that occurred during the tension- tension part of the loading.

The different types of damage shown at the end of the two load sequences on the right of Figs. 5.12 and 5.13 suggest very different cycle-by-cycle probabilities of failure. Then, even if the same type of loading is applied as a third load sequence to each of the end results in the two Figures, the cycles to failure are expected to be different. This is in disagreement with the analytical prediction that the cycles to failure do not change as long as the last, third in this case, load segment is the same. The reason is that the analytical model assumed that the cycle-by-cycle probability of failure  $p$  does not change.

The analytical conclusion would still be valid if  $p$  were relatively constant as was shown in comparing predictions with test results in Figure 5.11 in the previous section.

One last comment related to comparison of test results with analytical predictions is in order. When comparing predictions to experimental results from fatigue tests one should be careful in using the term good agreement between the two. Fatigue test data commonly have large scatter and several predictive models based on quite different assumptions may appear to be in equally good agreement with tests. Also, the test data may be limited and the predictions may not agree with test results not only because of drawbacks in the analytical model but also because of insufficient data. It is worth stressing that, although perfect accuracy was not been achieved for the validation case under examination, the proposed model represents a solid starting point which can be further improved.

Since the residual strength predictions, see Figures 5.6-5.9, are in good agreement with test results, it is believed that the first area where the model needs improvement is in the determination of cycles to failure under constant amplitude loading. The main issue is that the probability of failure during

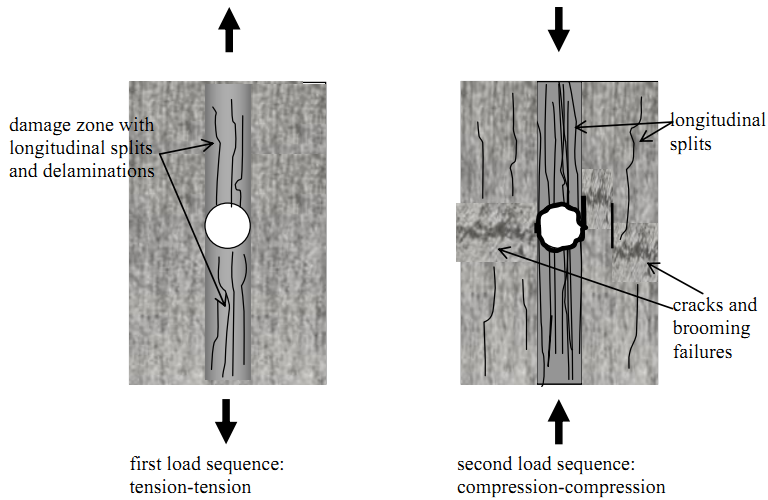


Figure 5.12: All  $0^\circ$  laminate with a hole: Damage creation when tension-tension is applied first followed by compression-compression

each cycle is constant as a consequence of the assumptions given in section 2.2. Improvements in this direction are proposed in chapter 6.

Despite the issues just mentioned, some of the obvious attractive aspects of the model should not be glossed over. The model leads to relatively simple closed form expressions for the cycles or blocks to failure under spectrum loading and requires no fatigue testing for calibration or determination of semi-empirical parameters. The predictions of the model for two-segment spectrum loading of fiberglass laminates were in good agreement with test results except in some low-cycle fatigue cases. The model was also found to be in very good agreement with test results from four-segment all-tension spectrum loading of Graphite/BMI.

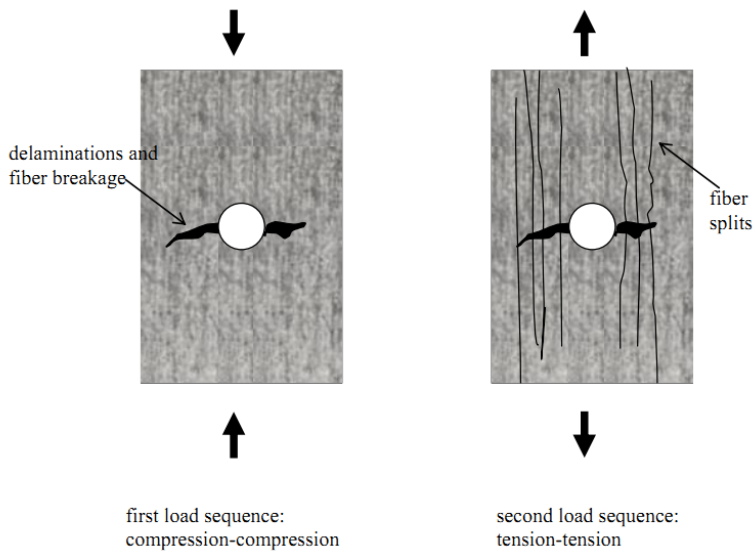


Figure 5.13: All  $0^\circ$  laminate with a hole: Damage creation when compression-compression is applied first followed by tension-tension



# 6

## *Enhancements to the analytical model for prediction of cycles to failure*

The comparison of the analytical predictions of the model to test results taken from the literature showed that the accuracy of the model ranged from poor to excellent depending on the loading case. While, overall, its ease of use, closed form expressions, and no dependence on empirical parameters make the model in its current form a useful tool for preliminary design, the discrepancies found between the model and test results in more complex structure which may exhibit multiple failure modes and in load cases that include compression suggest that further improvements are necessary. Improvements to the model developed in chapter 2 are presented in this chapter. The goal is to provide a framework within which more than one types of damage and their possible interactions can be included. As examples, fiber damage, matrix cracking, and, to a lesser extent, edge delaminations will be considered.

Specific reasons were presented for these discrepancies in the discussion presented in chapters 3, 4, and 5. The main reason for these discrepancies was the convenient simplification that the cycle-by-cycle probability of failure  $p$  was constant throughout the fatigue life. It was shown in section 2.2 that, under certain assumptions, the value of  $p$  is, indeed, constant. However, these assumptions hold true only as long as the damage that is present and failure mode do not change. That is, if the main type of damage is matrix cracks, as long as no other type of damage, such as delaminations, appears, the value of  $p$  will be, according to the analytical framework presented here, constant. As soon as, subsequently, different types of damage appear and/or the failure mode changes from the static failure mode,  $p$  will no longer be constant. This fact was recognized in chapters 3, 4, and 5 when some test results were presented but it was overlooked in order to see how far the simplifying assumption of constant  $p$  could go.

The assumption of constant  $p$  will be relaxed in this chapter and improved analytical predictions will be developed. The improvements will be demonstrated for two cases: (a) a uni-directional laminate under tension-tension loading where new results will be compared to results from chapter 3, and (b) a cross-ply laminate under tension-tension loading.

## 6.1 Description of improved model

Consider a composite laminate or structure under constant amplitude cyclic loading  $\sigma_a$ . The structure is divided into representative sections (such as plies and ply interfaces as appropriate) each of which is under its own load which is a function of the total applied load. For the  $i$ th section, the applied cyclic stress is  $\sigma(i)$ . The division into sections is done based on the types of damage and failure patterns expected during cyclic loading. These include matrix cracking, delaminations, fiber kinking, fiber splitting, etc. Note that these types of damage are not selected on the micromechanics scale (on the order of a few fiber diameters) or smaller where surface or internal cracks in the fibers or damage in the fiber/matrix interphase would have to be included. It is assumed that damage from the micro scale will have already evolved to the next scale level of damage represented by matrix cracks, delaminations, etc. It is possible to start modeling at lower scales but considerable test data and elaborate analytical modeling is needed. While this modeling at lower scales could and should be done, at this point it is not necessary to do so to convey the approach. Damage modeled at the level of matrix cracks and delaminations is sufficient to show how the model works and its accuracy suggests that, for most cases, this level may be sufficient. The accuracy of the approach, of course, depends on how representative the damage model is.

For each section into which the structure is divided, the stress at which the first type of damage occurs, whichever damage is appropriate for that section, is determined using a static analysis. As soon as damage is created in one section, any load redistribution from that section to other (adjacent) sections must be taken into account to update the applied loads in the various sections. Then, the model determines the stress at which the next type of damage occurs, in the same section, and so on, until final (static) failure of that section occurs. The same analysis is done for the remaining sections such that, for each section, the static stresses at which damage occurs are determined and the stress at which the section cannot carry any more load (failure stress) is also determined.

The applied stresses at which different sections develop various types of damage and eventually fail, form the basis of the improved fatigue model. For purposes of discussion, it is assumed that there is only one type of damage for section  $i$ , occurring when the applied static stress is  $\sigma_i(i)$ . It is also assumed that the failure stress for the  $i$ th section, the stress at which it can carry no more load, is  $\sigma_f(i)$ . Finally, it is assumed, for simplicity, that the structure consists of only two sections, section  $i$  and section  $j$ . Extending to more than two sections, each with more than one damage types, can be done relatively easily provided good analytical models for each damage type are available.

The situation just described is shown schematically in Figure 6.1. It is

assumed that the applied cyclic stress  $\sigma(i)$  is lower than  $\sigma_i(i)$  (the stress at which first damage occurs in section  $i$ ). Also, to be consistent with Figure 6.1, it is assumed that cyclic loading starts with the structure in a pristine (undamaged) condition. This assumption is not necessary for the analytical model to work but simplifies the discussion. During cycling at  $\sigma(i)$ , the residual strength of section  $i$  starts from the static strength  $\sigma_f(i)$  and decreases following the lower curve in Figure 6.1. During this process, and until the first damage in section  $i$  appears, the cycle-by-cycle probability of failure  $p_i$  for section  $i$  is assumed constant. This means that damage at a lower scale than the one accounted for in this model is occurring and is causing a decrease in the residual strength of section  $i$ . The type of damage occurring could be coalescence of micro-voids, matrix crazing, damage creation and growth in the fiber/matrix interphase, etc. The residual strength for section  $i$  can be predicted using Eq. 2.10. To use Eq. 2.10, it is necessary to know the cycles-to-failure  $N$  which are obtained through Eq. 2.25. As soon as the residual strength value equals  $\sigma_i(i)$ , the first damage (at the scale used in this analysis) appears. This corresponds to point A in Figure 6.1. Once the first damage is present, it is expected that the stiffness of section  $i$  will change (probably decrease), which, in turn, means that load will be redistributed from section  $i$  to section  $j$ . Then, due to the change in load in section  $i$  and the presence of damage there, the applied stress in section  $i$  will now be a different percentile of the residual strength of section  $i$ . Therefore,  $p_i$  given by Eq. 2.18 or 2.34 changes as does the slope of the residual strength curve for section  $i$ .

Using the new  $p_i$  a new cycles to failure for section  $i$  can be determined from Eq. 2.25 and used with Eq. 2.10 to determine the residual strength beyond point A. When it equals the applied stress  $\sigma(i)$ , at point B in Figure 6.1, section  $i$  fails.

At the same time, section  $j$  follows an analogous scenario to that of section  $i$  with  $\sigma(j)$  the stress acting on it. Its residual strength goes from  $\sigma_f(j)$  to  $\sigma_i(j)$  when the first damage appears in section  $j$ .

This is shown as point C in Figure 6.1. The new value of  $p_j$  is calculated for section  $j$  and load is redistributed, as necessary, from section  $j$  to section  $i$ . Equations 2.10 and 2.25 are used to track progress of the residual strength beyond point C. However, when  $n_A$  cycles are reached and damage appears in section  $i$ , any load redistributed onto section  $j$  must be accounted for. This may lead to changes in the applied stress and/or  $p_j$ , with corresponding change of the slope of the residual strength curve. This is shown schematically in Figure 6.1 as a second big slope change on the residual strength of section  $j$  occurring after  $n_A$  cycles. Upon further cycling, the residual strength of section  $j$  decreases until cycle level  $n_B$  is reached when, as already mentioned, section  $i$  fails. This means that the remaining load in section  $i$  is now transferred over to section  $j$  and the slope of the residual strength for section  $j$  changes again as

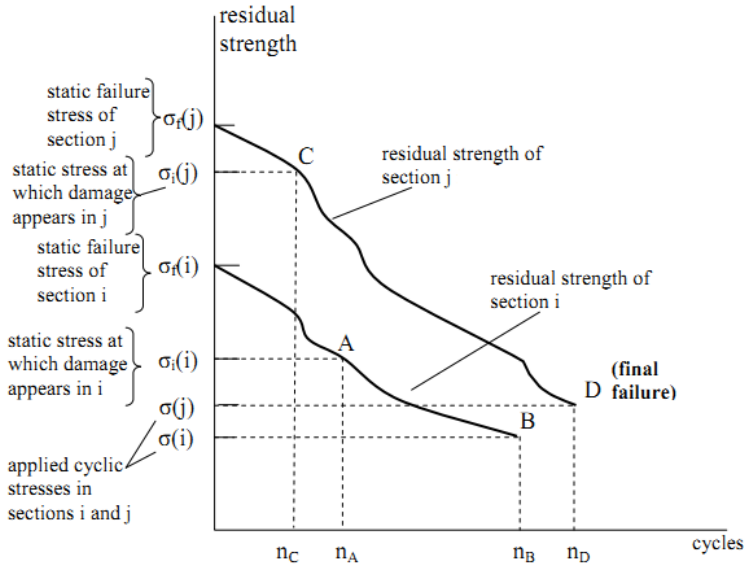


Figure 6.1: Example of damage tracking and interaction in a composite structure consisting of two sections,  $i$  and  $j$ . The residual strength of section  $i$  and  $j$  come from Eq. 2.11

shown in Figure 6.1. The cycle-by-cycle probability of failure  $p_j$  is recalculated and the cycles to failure  $N$ , with static strength the current residual strength of section  $j$ , are determined from Eq. 2.25. Using these to substitute in Eq. 2.10 gives the residual strength curve from this point forward. In the end after more cycling, the residual strength of section  $j$  becomes equal to its applied stress  $\sigma(j)$  and section  $j$  fails. This happens at point D in Figure 6.1, after  $n_D$  cycles. Since section  $i$  has failed already after  $n_B$  cycles, this point defines complete failure of the structure. Therefore, the applied stress  $\sigma_a$  on the entire structure and the cycles to failure  $n_D$  define one point on the S-N curve,  $(n_D, \sigma_a)$ , for this structure and this type of loading. Repeating the procedure for other  $\sigma_a$  values will give the complete S-N curve.

The description of interaction between different parts of the structure as damage occurs, given above, was one of several possibilities in order to bring out the basic features. The sequencing of which section is damaged first and which fails first can vary depending on slopes of residual strength curves, load redistribution, etc. It should also be noted that a pristine structure was assumed at the beginning of the scenario just presented. This is not limiting as one can start anywhere in the fatigue life of a structure treating the residual strength at any point as the static strength to be used as input in Eq. 2.10 and

proceeding from that damage level onward. This, of course, requires knowledge of the damage state of the structure in question at that particular point in time. With respect to load redistribution, the approach just described implicitly accounts for load sharing between fibers or plies through the adjustment of the residual strength of each constituent of the structure every time a local failure event occurs. However, the mutual enhancing of failure modes that occurs, for example, when matrix cracks lead to delaminations, is not accounted for in the current form of the model.

It should be emphasized again that one important implicit assumption of the approach presented here is that there is a one-to-one correspondence between residual strength and damage. This was already discussed in section 2.1 but becomes even more important here where the model is modified. The implicit assumption is that if a certain type of damage results in a certain residual strength in a structure then, if, during cycling, that residual strength is reached, that specific type of damage will also occur. Even though some experimental evidence supporting this assumption can be found in the literature [e.g. [74]], this may not be always true and must be investigated further. It is possible that different damage types will have the same residual strength.

A rather extreme example where this assumption is violated would be an all  $0^\circ$  laminate under tension-tension cyclic loading compared to the same laminate under the same loading but also subjected to impact damage. In the first case, (blue curve in Figure 6.2) if the tension-tension cycles are repeated a sufficient number of times, some fibers will fail and their load will be redistributed to adjacent fibers. This causes a significant slope change in the residual strength curve. Suppose that after  $n_t$  cycles at maximum stress  $\sigma$  (with  $R = 0$ ), the residual strength is 65% of the static strength. Consider now the same laminate starting with the same static strength and undergoing the same cyclic loading but for a fraction  $n_i$  of the  $n_t$  cycles (red curve in Figure 6.2). Then, the laminate is impacted with sufficient energy to drop its residual (tensile) strength from the undamaged value  $\sigma_r$  to the value  $\sigma_{rt} = 0.65\sigma_{fs}$  that is the residual strength of the undamaged laminate after  $n_t$  cycles. Clearly, the damage states of the two laminates after  $n_t$  cycles without impact and  $n_i$  cycles with impact are different (more localized damage under the impact site in the second case) but their residual strengths are the same. This example is extreme in the sense that the damage in one case is not caused by fatigue loading but it does represent a real life scenario where different damage states may correspond to the same residual strength.

To summarize, the enhanced analysis model:

- divides the structure in sections each of which has its own applied cyclic load and cycle-by-cycle probability of failure  $p$

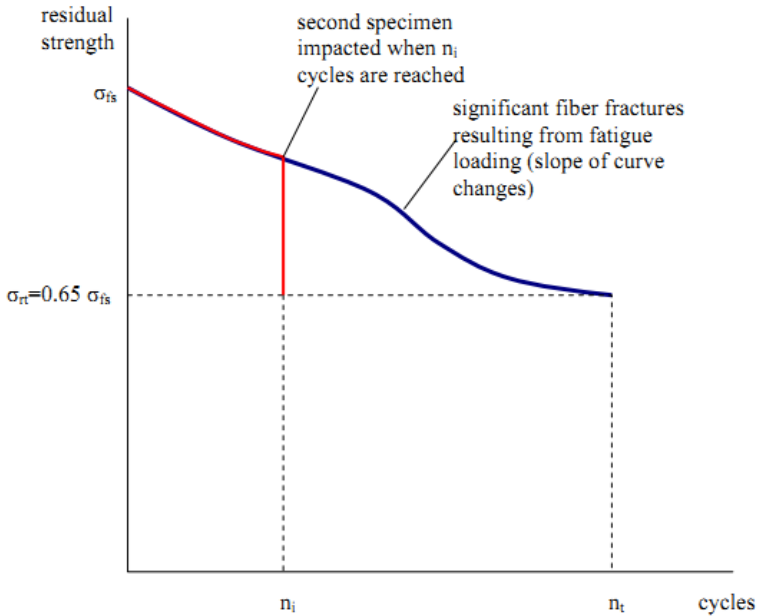


Figure 6.2: Different damage scenarios leading to the same residual strength when starting with identical specimens.

- assumes that  $p_i$  in section  $i$  is constant and proceeds with the calculations presented in chapters 2 and 4 until damage appears in section  $i$  that is different from that already present and/or load is redistributed to/from section  $i$  due to failure in adjacent sections
- calculates new value of  $p_i$  due to new damage creation and/or load redistribution
- continues cycling until residual strength in section  $i$  equals the applied stress in section  $i$ , at which point, section  $i$  fails
- redistributes the load of section  $i$  to adjacent sections and repeats the procedure until all sections fail

Two examples of how the enhanced model described in the previous section can be applied are presented in the next two sections. The first is a uni-directional laminate with all plies in the 0 direction loaded under tension-tension cyclic loading. The second is a cross-ply laminate under tension-tension cyclic loading. Both examples were selected to demonstrate different types of damage created during cyclic loading and how they can be modeled using the analysis framework presented here.

## 6.2 Application 1: uni-directional laminate under tension-tension loading

In a general laminate under tension-tension cyclic loading, different types of damage occur at different stages of the life. The R ratio, maximum load, and the stacking sequence have a significant effect on the damage scenario. A detailed description of the type of damage and its evolution was given by Charewicz and Daniel [11]. Damage first manifests as matrix cracks in plies with fibers not aligned with the loading. This is most pronounced in laminates with plies at  $90^\circ$  to the (dominant) load direction. As loading continues, the crack density in these plies increases and some branching to adjacent plies, which are not at  $90^\circ$  to the load direction, may occur. These cracks can then become longitudinal cracks or splits in plies with fibers aligned with the loading direction. When transverse and longitudinal cracks intersect at ply interfaces in a laminate delaminations are created. Delaminations may also appear at free edges of composite laminates due to the presence of interlaminar stresses. At later stages of cyclic loading, matrix cracks and delaminations act as stress risers that cause localized fiber failures which accumulate to lead to final laminate failure.

The simplest special case of such a situation is a uni-directional laminate with all the plies in the 0 direction. The loading is also in the 0 direction. Here the types of damage considered are multiple fiber failures causing load redistribution within the plies. In view of the discussion of the previous section where the laminate or structure is sub-divided into sections, it would appear that a uni-directional laminate consists of only one section. As will be shown below, however, it is still possible to divide it into different sections. Each section contains a number of fibers that have approximately the same strength. Different sections will have different strength values, and these strength values differentiate one section from another.

It is known from static tests (e.g. [106]) that the static strength of 0 plies may be lower than the value that would be predicted using the individual fiber and matrix strengths and a rule of mixtures. This can also be seen by checking several commercially available materials for which individual fiber strength and  $0^\circ$  ply strengths are reported. For example, for AS4/8552, reference [107] reports the fiber strength as 4433 MPa and the  $0^\circ$  ply strength, at 60% fiber volume, as 2205MPa. The rule of mixtures would give a  $0^\circ$  strength of at least  $0.6 \times 4433 = 2660$  MPa, not including a tiny contribution from the matrix. Several methods have been proposed to improve the prediction of a straight rule of mixtures equation [e.g. [108]]. Of interest in the present discussion are the reasons why the test value is often lower than the prediction. These are related to flaws in the laminate. The main flaws are surface flaws or cracks in fibers, inadequate bond between fibers and matrix, non-uniform distribution

of fibers in the matrix, variations in fiber diameter, and fiber misalignment. Related to some of these flaws, and their frequency of occurrence, is the fact that individual fiber strength is a function of fiber length [109]. In order to proceed, a model is needed that incorporates all these effects.

Due to the reasons just mentioned, fibers within each ply will have different strengths that, depending on the material, may cover a relatively wide range with mean fiber strength  $X_f$ . The sources of fiber strength variation are arbitrarily divided in two categories. The first category contains variations in fiber diameter, and fiber misalignment as the possible sources. The second contains flaws in the fibers or the fiber/matrix interphase. These two categories are treated as independent and can thus be considered separately. After the effect of each is quantified, they are combined to create a model of the strength of fibers in a uni-directional ply.

### 6.2.1 Effect of fiber diameter variation and fiber waviness on fiber strength

The variation in fiber diameter and the presence of waviness are considered first. For a fiber with sinusoidal waviness embedded in a ply, as shown in Figure 6.3, the governing equation for the displacement  $w$ , when a tensile load  $N_x$  is applied, can be obtained by treating the fiber as a beam surrounded by linear and torsional springs with stiffnesses representing the constraining effect of the material (matrix and fibers) surrounding the fiber. The governing equation can then be shown to be [110]:

$$E_f I_f \frac{d^4 w}{dx^4} - (\lambda^2 k_T + N_x) \frac{d^2 w}{dx^2} + k_L w = N_x \frac{d^2 w_i}{dx^2} \quad (6.1)$$

where  $E_f$  is the fiber stiffness,  $I_f$  is the fiber moment of inertia per unit of fiber width,  $k_T$  and  $k_L$  are torsional and linear spring stiffnesses provided by the material surrounding the fiber and  $w_i$  is the initial waviness of the fiber (prior to loading) given by:

$$w_i = A_o \sin \frac{\pi x}{L} \quad (6.2)$$

as shown in Figure 6.3.

The solution to Eq. 6.1 can be found by assuming that the wavy fiber and the surrounding material have a deformation that can be described by:

$$w = A \frac{z}{z_c} \sin \frac{\pi x}{L} \quad (6.3)$$

where  $z_c$  is the length over which the fiber waviness affects its surrounding material.

Then, in a manner analogous to Lee and Harris, [110], the torsional and linear spring stiffnesses of the surrounding material are found to be:

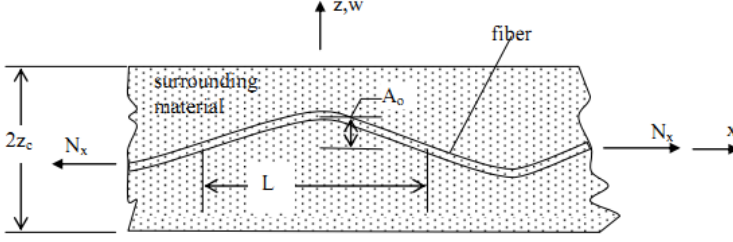


Figure 6.3: Wavy fiber in a uni-directional composite

$$k_T = 2(z_c - r_f)G_{xz} \quad (6.4)$$

$$k_L = \frac{2E_c}{z_c - r_f} \quad (6.5)$$

where the assumption that the original amplitude of the fiber waviness  $A_0$  is much smaller than  $z_c$  has been imposed. Note that  $r_f$  is the radius of the fiber, and  $G_{xz}$ ,  $E_c$  are the shear and Young's moduli of the surrounding material. If  $z_c$ , at this point unknown, turns out to be smaller than the average distance between fibers, then  $G_{xz}$  and  $E_c$  are matrix properties. Otherwise they are properties of the composite as a whole, i.e. fiber and matrix at the desired fiber volume.

The unknown distance  $z_c$  is determined in a manner analogous to the determination of the portion of the core that is effective in sandwich wrinkling (see, for example, [111]). By minimizing the total energy, (bending of fiber, shear and extensional energy of the surrounding material),  $z_c$  is found to be:

$$z_c = \frac{L}{\pi} \sqrt{\frac{3E_c}{G_{xz}}} \quad (6.6)$$

Based on the previous derivation, the geometry parameter  $\lambda$  defined as the ratio of the total structure under deformation divided by the portion of the material surrounding the fiber that undergoes deformation is given by

$$\lambda = \frac{z_c}{z_c - r_f} \quad (6.7)$$

The solution to Eq. 6.1 can now be completed using Eq. 6.3 with  $z = z_c$  to substitute for  $w$  and solving for  $A$ . The result is:

$$A = -\frac{A_0}{1 + \left(\frac{\pi}{L}\right)^2 \frac{E_f I_f}{N_x} + \frac{\lambda^2 k_T}{N_x} + \frac{k_L}{N_x} \left(\frac{L}{\pi}\right)^2} \quad (6.8)$$

with  $\lambda$ ,  $k_T$ , and  $k_L$  determined from Eqs 6.7, 6.4 and 6.5 respectively.

The effect of the waviness and fiber diameter variation on the fiber strength can now be assessed by determining the maximum stress in the fiber and examining how it varies as the waviness (defined by  $A_o$  and  $L$ ) and fiber radius  $r_f$  vary within typical ranges measured in practice. The maximum fiber stress in a wavy fiber is obtained by combining the axial stress with the maximum bending stress:

$$\sigma_w = \frac{Mr_f}{I_f} + \frac{N_x 2r_f}{\pi r_f^2} \quad (6.9)$$

where  $M$  is the bending moment in the fiber (per unit width) given by:

$$M = E_f I_f \frac{d^2 w}{dx^2} \quad (6.10)$$

Using the solution for  $w$  to substitute in Eq. 6.10 and, in turn, in Eq. 6.9, the maximum stress in the wavy fiber is found when the sine in Eq. 6.3 is maximized and is given by:

$$\sigma_{w,max} = \frac{E_f A_o r_f \left(\frac{\pi}{L}\right)^2}{1 + \left(\frac{\pi}{L}\right)^2 \frac{E_f I_f}{N_x} + \frac{\lambda^2 k_T}{N_x} + \frac{k_L}{N_x} \left(\frac{L}{\pi}\right)^2} + \frac{2N_x}{\pi r_f} \quad (6.11)$$

Fiber failure will occur when  $\sigma_{w,max}$  equals the tensile failure strength of the fiber. If  $A_o$ ,  $L$ , and  $r_f$  are now allowed to vary over their expected ranges corresponding to the composite system under investigation, the variation of the fiber strength due to waviness and fiber diameter variation can be obtained. This is done using a Monte Carlo simulation. It is assumed that  $A_o$ ,  $L$ , and  $r_f$  are each normally distributed with a mean and standard deviation obtained from tests. For example, for AS4 fiber in 3501-6 epoxy resin, the mean diameter is found to be 6.9 microns, with a standard deviation of 0.25 microns and  $L/(2r_f)$  and  $A_o/(2r_f)$  lie in the ranges 150-400 and 3-10 respectively ([109], [112], [113]). In the Monte Carlo simulation, a random number generator for a normally distributed variable is used three different times to obtain a value of  $r_f$ ,  $A_o$ , and  $L$ . These values are then substituted in Eq. 6.11. The process is repeated 1000 times to create 1000 values of the maximum bending stress in a wavy fiber. These values are used to obtain the coefficient of variation  $CV$  for the fiber strength population. The resulting  $CV$  value was 0.0642. It is important to note that this  $CV$  value was found to be very stable. Repeating the simulation 10 times yielded a  $CV$  value that varied after the fourth decimal (less than 0.1%). Changes by almost a factor of 2 on the waviness parameters  $A_o$  and  $L$  had a negligible effect to its value. There was a somewhat stronger dependence on the variation of the fiber diameter but, still, a 40% change in the fiber diameter caused less than a two percent change in the  $CV$  value.

### 6.2.2 Effect of flaws on fiber strength

The strength variation due to the presence of flaws in the fiber and the fiber/matrix interphase is now considered. It is well known that fiber strength depends strongly on fiber length [109]. Longer fibers have lower strength. The exact reason(s) for this are not clearly understood. It is believed that, in longer fibers, the probability of a larger flaw being present in the fiber is greater than in a short fiber and thus longer fibers will have lower strength. In the present model, it is assumed that an individual ply will contain fibers with strengths that cover the entire range of strength values from very low to very high. This should be expected as the number of fibers present in a ply is so large that the likelihood that fibers are present with any given strength value in the range is very high. However, the number of fibers with strength value within a specific range will vary. A very small number of fibers will have either very low or very high strength with larger quantities of fibers having strengths comparable to the mean value  $X_f$ . Therefore, the strength of the fibers in a ply is assumed to follow the shape of the cumulative distribution curve as shown in Figure 6.4. The y-axis denotes strength with  $X_f$  the mean strength corresponding to the 50<sup>th</sup> percentile of the strength distribution. The x axis denotes some measure of the number of fibers within each quantile. Wider bars indicate that a larger number of fibers fall in that strength range.

It is now assumed that all fibers have the same stiffness. Then, if a stress  $\sigma$  is applied to the fibers, all fibers with strength less than  $\sigma$ , (the diagonally shaded portion on the left of Figure 6.4) will fail. Now the load acting on the failed fibers is redistributed to the remaining fibers. If there is no resin, the load is equally distributed to all non-failed fibers. The presence of the resin, however, allows load to shear from failed fibers to adjacent fibers and fibers further away from a failed fiber will share a smaller fraction of the load to be redistributed than fibers closer to the failed fiber. On-going work by Qian [114] using detailed finite element models, has shown that in a typical uni-directional composite with fiber volume around 60%, the stress concentration in non-failed fibers in the immediate vicinity of a failed fiber ranges between 1.04 to less than 1.1 depending on the number of adjacent (non-failed) fibers and how they are arranged (2-D array or 3-D spatial distribution). There are several models for the stress concentration factor [e.g. [115], [116]] for 2-D arrays of fibers. In a 3-D situation, however, which is the case for a uni- directional ply, modeling becomes very complex and, so far, reliable solutions can only be obtained using finite element methods as in [114]. In what follows, the load acting on the failed fibers will be evenly re-distributed among the remaining fibers, neglecting the effect of the matrix. Improved models for the load re-distribution can be incorporated, if desired, without changing the basic approach.

If  $X_f$  is the mean strength of the fibers and  $s_f$  is the standard deviation describing the curve in Figure 6.4, the fraction of failed fibers when  $\sigma$  is applied

is given by:

$$f = cdf(\sigma, X_f, s_f) \quad (6.12)$$

where  $cdf$  denotes the cumulative distribution function evaluated at  $\sigma$ , for a normal distribution of mean  $X_f$  and standard deviation  $s_f$ . Then, distributing evenly the load of the failed fibers to the remaining fibers, the new applied stress (on the remaining fibers) is:

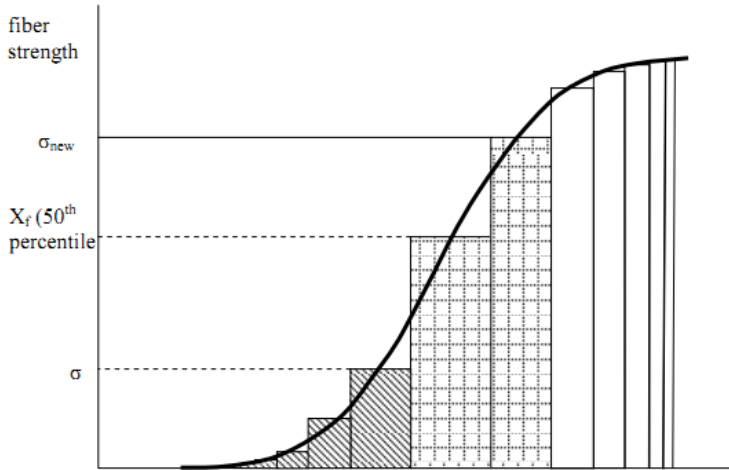


Figure 6.4: Schematic of strength of fibers in a uni-directional ply (width of each bar is proportional to number of fibers with strength in the corresponding range)

$$\sigma_{new} = \frac{\sigma}{1 - f} \quad (6.13)$$

which is shown (on the y axis) in Figure 6.4. Again, some fibers with strength less than  $\sigma_{new}$  will fail and are denoted by the checkered shading in Figure 6.4. The load is again re-distributed to the remaining fibers and the procedure is repeated until the process either converges to a value of  $f < 1$ , meaning that there is no failure and some fibers are still able to carry load, or it diverges and all fibers fail.

At this point, the mean fiber strength  $X_f$  and standard deviation  $\sigma_f$  are unknown. Note that these are not the conventional strength and standard deviation one would measure by testing individual fibers for two reasons: (a) fiber strength is a function of fiber length and (b) in the present model, the fiber strength in Figure 6.4 represents all possible values corresponding to flaws

of different severity and does not include the effect of waviness or variations in fiber diameter which were modeled separately earlier.

Information from static strength tests for uni-directional plies of the material of interest is used to determine  $X_f$  and  $\sigma_f$ . This information consists of an average strength  $X_p$  value for the entire ply and its corresponding standard deviation  $\sigma_p$ . Again, a Monte Carlo simulation was used. A random number generator was used to create 40 strength values for a normally distributed variable with mean  $X_p$  and standard deviation  $\sigma_p$ . To check convergence and stability, the process was repeated 10 times and showed that extreme  $X_p$  and  $\sigma_p$  values varied by less than 2% suggesting that a sample with more than 40 strength values would be needed if higher accuracy were deemed necessary. These 40  $X_p$  values represent strength values of a 0 ply. For each of these values, the nominal fiber strength  $X_{fi}$  is obtained by dividing it by the fiber volume fraction:

$$X_{fi} = \frac{X_{pi}}{v_f} \quad (6.14)$$

Then, Eqs. 6.12 and 6.13 are applied to this population. The fraction of failed fibers  $f_i$  for an applied fiber stress of  $X_{fi}$ , is given by (see also analogous Eq. 6.12)

$$f_i = cdf(X_{fi}, X_{fav}, s_i) \quad (6.15)$$

where the mean fiber strength  $X_{fav}$  is the experimentally measured average across all individual fiber tensile tests (all lengths) and  $s_i$  is an assumed standard deviation of fiber strengths for the specimen  $i$ . This means that first a series of individual fiber tests are done with different fiber lengths and the overall average fiber strength,  $X_{fav}$ , is determined experimentally. The new fiber stress  $X_{fnew}$  resulting from redistributing the load that was applied to the fraction  $f_i$  of fibers that failed is given by (see also analogous Eq. 6.13):

$$X_{fnew} = \frac{X_{fi}}{1 - f_i} \quad (6.16)$$

The fiber stress is updated as the load from failed fibers is redistributed to all unfailed fibers. This is done until all fibers fail or some that have not failed remain. In the latter case, the value of standard deviation  $\sigma_i$  used is increased and the procedure repeated until there is convergence or failure of all the fibers. The value of  $\sigma_i$  at which the specimen just fails is the sought-for standard deviation for the specimen in question. The process is repeated for all 40 specimens in the Monte Carlo simulation yielding 40 values of  $\sigma_i$ . The average value of  $\sigma_i$  across all 40 specimens is the standard deviation  $\sigma_f$  used to determine the shape of the curve in Figure 6.4. It represents the standard

deviation of the fibers in an average uni-directional specimen and reflects the fact that the presence of flaws causes nominally identical fibers (since they have no waviness and have all the same diameter) to fail at different strength values.

Since now the effect of flaws is represented by the shape of the curve in Figure 6.4, which is determined by the standard deviation  $\sigma_f$  just obtained, the mean strength for the fibers in the same population has to be the mean strength from individual fiber tests with the shortest fibers. This is done since, as already mentioned, short fibers tend to have less critical flaws and, therefore, the average strength for the shortest available fibers which are about 1 cm long, will be a reasonable approximation of the average strength of a flawless fiber. This is based on the fact that data, in [109] for example, show that the strength levels off at this range of fiber lengths (around 1 cm). More testing at even shorter fiber lengths and for different fibers is necessary to verify this trend.

The AS4 fiber in 3501-6 matrix is used again as an example. For 60% fiber volume, the average strength of a uni-directional ply of AS4/3501-6 is  $X_p = 2002.5$  MPa and the corresponding  $CV_p = \sigma_p/X_p$  is 0.05855 [117] from which  $\sigma_p$  can be determined. Note that the strength value is the average over the bleed and no-bleed versions of the material reported in [117] and the CV is the average across environments and across the two material forms (bleed and no-bleed). The average fiber strength for fiber lengths between 1 and 10 cm was calculated as  $X_{fav} = 3849.5$  MPa. This was obtained by first interpolating, linearly, the values for 1 and 20 cm given in [109] to obtain the average strength of 10 cm long fibers, which is the approximate gage length of the specimens used in fatigue testing mentioned below. Then, the average strength of 1 and 10 cm long fibers (3849.5 MPa) gives a measure of the average strength of the fibers used in the specimens during fatigue testing. The average fiber strength for the shortest fibers (1cm length) is  $X_f = 4142$  MPa [109]. Then, the procedure just described gives 40  $\sigma_i$  values from which corresponding CV values can be obtained ranging from 0.018 to 0.155 with average  $CV_f = 0.0696$ . Therefore, for AS4/3501-6, the curve in Figure 6.4 is described by a mean fiber strength  $X_f = 4142$  MPa and a coefficient of variation  $CV_f = 0.0696$ . The fact that this value is close to  $CV = 0.0642$  found earlier for the effect of waviness and fiber diameter is, probably, entirely fortuitous.

### 6.2.3 Analysis procedure

A procedure to predict cycles to failure for a unidirectional ply under tension-tension loading can now be established. According to the modeling approach described in the previous section, the ply is divided into sections. Each section, represented in Figure 6.4 by a different bar, has a different strength

starting from very low to very high. Care was taken so that a large number of sections (in the cases run here 22 were sufficient) with different (increasing) strength  $X_{f_i}$  exceeding the stress applied to the fibers during the first cycle. For example, if the applied stress were  $\sigma_a = 1700$  MPa for AS4/3501-6 with  $v_f = 0.6$ , the applied fiber stress is  $\sigma = 2837$  MPa. Then, the range between 2837 MPa and  $1.05X_f = 4350$  MPa was divided in 22 sections with corresponding strength values (in MPa): 2900, 2960, 3000, 3050, 3100, 3150, etc. Note that the exact division into sections and the number of sections is arbitrary. The more sections are used the higher the accuracy but the solution was found to converge with approximately 20 sections. Convergence to within 3% can be obtained with 10 or less sections but the ease of computation and efficiency of the approach allowed a higher number to be used to obtain convergence within less than 1%.

Thus, the overall fiber strength distribution is determined by the effect of flaws in the fibers (or in general effects other than waviness and diameter variation). Within any given portion of that distribution, or section, the variation in strength is determined by the  $CV$  caused by waviness and diameter variation. This is valid since it is assumed that any fiber irrespective of its flaws and their severity can have any waviness or fiber diameter.

The required inputs are the fiber volume, the average fiber strength  $X_{fav}$  across all fiber lengths from 1 cm to the length of the ply, the average fiber strength for short fibers (approx. 1 cm), and the mean strength  $X_p$  and standard deviation  $\sigma_p$  for the tensile strength of a ply. In addition, data on the variation of fiber diameter (mean and standard deviation) are needed. The procedure is then as shown below.

1. A Monte Carlo simulation modeling the waviness and fiber diameter variation is performed to determine the  $CV$  of fiber strength.
2. A second Monte Carlo simulation is used to determine the  $CV_f$  of fiber strength resulting from factors other than in step 1.
3. An applied stress  $\sigma_a$  is selected.
4. The corresponding stress  $\sigma$  applied to the fibers is determined by dividing  $\sigma_a$  by the fiber volume fraction  $v_f$ .
5. The fibers with strength between  $\sigma$  and an arbitrary value higher than the mean fiber strength  $X_f$ , are divided arbitrarily into a number of sections (22 used here) each with different strength but constant coefficient of variation =  $CV$  (0.0642 for AS4/3501-6)
6. The fraction  $f$  of failed fibers under  $\sigma$  is determined using Eq. 6.12 with  $\sigma_f = X_f(CV_f)$ . Note here  $CV_f$  is used, related to flaws, and not  $CV$  which results from variations in diameter and waviness.

7. Load is redistributed to remaining fibers using Eq. 6.13.
8. Steps 6 and 7 are repeated until either all fibers fail and the ply fails or there is convergence to a value of  $f < 1$ .
9. If the ply has not failed in the previous step, for each section  $i$ , the cycle by cycle probability of failure  $p_i$  is determined using

$$p_i = cdf(\sigma_i, X_{si}, s_{si}) \quad (6.17)$$

where  $\sigma_i$  is the stress applied to the fibers of section  $i$ , obtained from step 7 (and is constant for all sections),  $X_{si}$  is the strength of the fibers of section  $i$ , obtained from step 5 (or step 11 below), and  $s_{si}$  is the standard deviation for the fiber strength in section  $i$ , obtained from  $s_{si} = CV(X_{si})$  or by using Eq. 6.18 below.

10. The number of cycles to failure  $N_i$  for section  $i$  is determined using Eq. 2.25. After  $N_1$  cycles, the first section fails. Then, section 2 becomes the new section 1, the yet unfailed section that is closest to the applied load. Thus, every time steps 6-11 are repeated, the section numbers decrease by one and the total number of unfailed sections decreases by 1. Each time,  $N_1$ , the number of cycles to failure for the fibers in the 1<sup>st</sup> section, is recorded and added to the previous sum of all  $N_1$  values. Of course, the value of  $N_1$  is not the same each time since it corresponds to a section with a different residual strength and coefficient of variation (and thus  $p$  value) each time.
11. For sections 2 to the maximum number of sections (22 was the starting number of sections used here), the new residual strength  $\sigma_r$  and  $CV$  are determined. The residual strength is obtained from Eq. 2.10. The new  $CV$  is determined from combining Eqs. 2.17 and 3.2 and solving for  $CV$ :

$$CV_{newi} = \frac{1.2478}{\frac{N_i-1}{N_i-N_1-1} \left( \frac{1.2478}{CV} - 0.9686 \right) + 0.9686} \quad (6.18)$$

where  $N_1$  is the number of cycles to failure for section 1. Note that this determination of  $CV$  is approximate as it assumes the normally distributed fiber strength within a section can also be approximated by a two-parameter Weibull distribution.

12. Since after  $N_1$  cycles the first section has failed, the applied fiber stress is adjusted to  $X_{s1}$ , the strength of the failed section, and the process steps 6-11 are repeated with the updated values of applied stress, strength, and  $CV$  of each section.

13. The sum of all  $N_1$  values until the ply fails (see step 8) gives the cycles to failure under applied  $\sigma_a$ .
14. Repeating steps 3-13 for different  $\sigma_a$  values gives the predicted S-N curve for this case.

### 6.2.4 Comparison with test results

The above procedure was applied to tension-tension fatigue ( $R \approx 0$ ) of AS4/3501-6 uni- directional laminates. This case was also examined in section 3.2 where a constant value of  $p$  was used until failure. Using the updated model,  $p$  is no longer constant. The predictions of the present approach are compared to test results, from Lee et al [74], in Figure 6.5 The original predictions from section 3.2 (Figure 3.1) are also included for comparison.

Note that all test data points are included in Figure 6.5, unlike Figure 3.1 where only the low and high cycle points were included for each stress level. It can be seen from Figure 6.5 that the improved model described in this section is an improvement over the simplified model developed in section 2.2 and is in excellent agreement with the test results. It is clear that the constant value of  $p$ , which gives the blue prediction curve in Figure 6.5, is not sufficient in this case. The reason for this is that the main form of damage, fiber breakage, changes drastically the cycle-by-cycle probability of failure  $p$ . The improved model accounts for this change in  $p$  and, as a result, gives much better predictions.

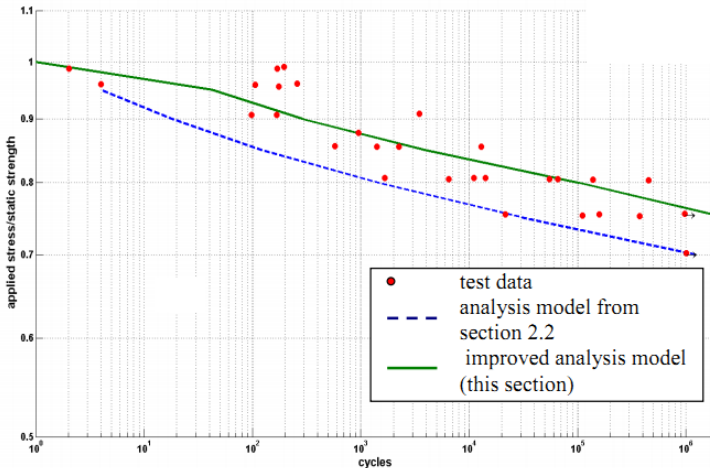


Figure 6.5: Analytical predictions compared to test results for uni-directional laminate ( $R \approx 0$ ). The test data is from [74]

### 6.3 Application 2 - cross-ply laminate under tension-tension loading

Conceptually, the case of a  $[0_n/90_m/0_n]$  under tension-tension loading would appear to be a simple extension of the model used in the previous section. However, as will be demonstrated, even for a simple laminate such as this, the damage created during cyclic loading, matrix cracks and fiber failures, can cause quite a complex stress state in the laminate. This stress state requires accurate analysis to determine local load redistributions from the 90 to 0 plies and, based on this, localized failure that will signal the creation of new damage as cyclic loading progresses. This might appear to contradict the discussion in section 2.2.1 where it was stated that as long as the spacing of matrix cracks in the 90° is large, the cycle-by-cycle probability of failure  $p$  is relatively constant. As the crack spacing gets smaller, adjacent cracks will interact and promote creation of additional cracks and fiber failure in the 0 plies. As a result, the residual strength will change the value of  $p$  will vary with cycles.

In order to apply the improved model just presented, the structure must be divided into sections. Accounting for the expected types of damage, the laminate should be divided into three main sections, the 0 plies, the 90 plies, and the 0/90 ply interfaces. Including the 0/90 ply interfaces is done to capture the creation of delaminations. The delaminations, even though limited in these laminates, may play an important role in determining cycles to failure for certain stacking sequences. As will be demonstrated later by analysis, the interlaminar normal stresses that develop are mostly compressive (which do not cause delamination) and the interlaminar shear stresses have too low a magnitude to cause delamination. There is only one case where the interlaminar normal stresses become tensile, the mid-point between successive matrix cracks in the 90° plies. This case will be discussed later. As a result, for the time being the 0/90 ply interface is not accounted for in detail. The main sections are the 0 and 90 plies and these may be divided into subsections as necessary.

In the above discussion the interlaminar stresses developing at the free edge, in particular the normal stress  $\sigma_z$ , which is tensile at the free edge, were not mentioned. The reason is that calculations of these stresses using the method in [118] show the maximum  $\sigma_z$  stress to be less than 6% of the applied average tensile stress and its effect is, therefore, neglected. This however does not account for any interaction of the free edge with a matrix crack which could lead to higher  $\sigma_z$  stresses locally.

Considering static loading, the types of damage that occur as tensile stress on the laminate  $\sigma_a$  is increased from 0 to final failure are determined. For a  $[0_n/90_m/0_n]$  laminate, the first damage that appears are matrix cracks in the 90° plies. These cracks extend the full width of the laminate and are confined

in the  $90^\circ$  plies by the fibers in the  $0^\circ$  plies which are tough and do not easily allow the matrix cracks to extend into the  $0^\circ$  plies. Two such cracks separated by a distance  $d$  are shown in Figure 6.6.

As  $\sigma_a$  is increased from 0, a level is reached at which the first matrix cracks will appear. This will occur at locations where local flaws are present such as small voids, resin rich areas, trapped volatiles or contamination, etc. While these locations act as stress risers that will cause the first matrix cracks, the local stress in the  $90^\circ$  plies when this happens is close to the in-situ, i.e. transverse, strength of the  $90^\circ$  ply.

As soon as the first matrix cracks appear in the  $90^\circ$  plies, the axial load in these plies must transfer to the  $0^\circ$  plies in the vicinity of the matrix cracks. As a result, interlaminar shear and normal stresses develop. Upon further increase of the applied load, these stresses combine with the axial stress to create further matrix cracks. The crack density will increase with increasing applied load. Depending on the relative thickness of the  $0^\circ$  and  $90^\circ$  plies, these matrix cracks at high crack densities may create delaminations at the  $0/90$  interface [74]. At some point fibers in the  $0^\circ$  plies will start to break and, eventually, the  $0^\circ$  plies will fail causing complete failure of the laminate.

Therefore, in order to predict cycles to failure in such a laminate, a model is needed that can determine when matrix cracks occur, how load is redistributed from  $90^\circ$  to  $0^\circ$  plies, and when failure occurs in the  $0^\circ$  plies. The problem, at least as far as determining when matrix cracks occur and at what density, has been addressed by several investigators. Berthelot, [119] used a shear lag model based on a displacement formulation. A stress-based approach using energy minimization was used by Hashin [120]. In another attempt, Berthelot and his colleagues used finite elements to determine the stresses in cross-ply laminates with matrix cracks [121]. Berthelot also gives a good summary of work done in this field in [122].

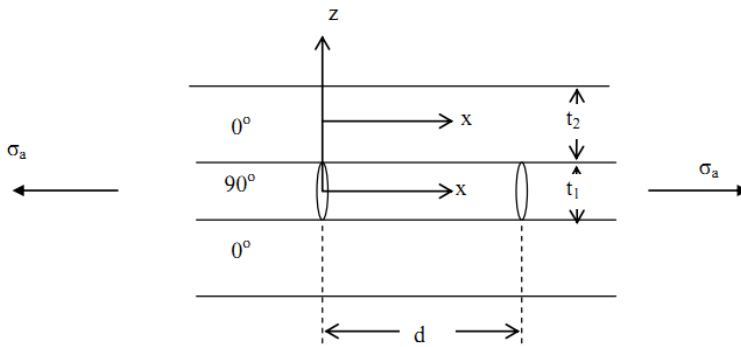


Figure 6.6: Matrix cracks caused in a cross-ply laminate under tension

### 6.3.1 Determination of stresses in a cross-ply laminate with matrix cracks under tension

A stress-based solution is developed here by minimizing the complementary energy in the laminate using calculus of variations. This approach is similar to the solution by Hashin [120], and it is analogous to the method presented before [ [123], [124]] for determining interlaminar stresses at skin/stiffener interfaces of stiffened composite panels and straight free edges of composite laminates.

The situation to be analyzed is shown in Figure 6.6. The thickness of the  $90^\circ$  plies is  $t_1$  and the thickness of the  $0^\circ$  plies is  $t_2$ . First, the stress at which one matrix crack appears in pristine  $90^\circ$  plies is determined. This is done by determining when the applied stress in the  $90^\circ$  plies equals the in-situ strength of these plies. Using the in-situ strength of the  $90^\circ$  plies is important because, depending on the relative thickness of  $0^\circ$  and  $90^\circ$  plies, it is anywhere from 20-40% higher than the transverse strength of the material. The presence of the  $0^\circ$  plies on either side of the  $90^\circ$  plies slows down the growth of transverse cracks in the  $90^\circ$  plies. Dvorak and Laws, [125], have developed curves that relate the energy release rate to laminate geometry, which are applicable to the present case. The in-situ strength of  $90^\circ$  plies can be determined by equating the energy release rate to the critical energy release rate and back-calculating the corresponding applied stress.

Once the first crack has appeared, the problem in Figure 6.6 with two cracks can be solved. The results from that problem can be matched to the case of a single crack by allowing the crack spacing  $d$  to go to infinity.

Due to symmetry, the 0 plies below the mid-plane need not be considered. Two coordinate systems are set up, one for the  $0^\circ$  and one for the  $90^\circ$  plies as shown in Figure 6.6 The stresses are then determined separately in the 0 and 90 plies using the respective coordinate system. It is assumed that the laminate is very long in the  $y$  direction (perpendicular to the plane of Figure 6.6) and, therefore, there is no dependence of stresses on the  $y$  coordinate. It is also assumed that the shear stresses  $\tau_{xy}$  and  $\tau_{yz}$  are zero. The stress equilibrium equations, either in the 0 or the 90 plies, with the  $y$  dependence neglected, have the form:

$$\begin{aligned} \frac{\partial \sigma_x}{\partial x} + \frac{\partial \tau_{xz}}{\partial z} &= 0 \\ \frac{\partial \tau_{xz}}{\partial x} + \frac{\partial \sigma_z}{\partial z} &= 0 \end{aligned} \tag{6.19}$$

It is now assumed that the  $\sigma_x$  stress in the  $0^\circ$  or the  $90^\circ$  plies is given by:

$$\sigma_x = \sigma_{x_{ff}} + A_i f(x) \tag{6.20}$$

where  $\sigma_{x_{ff}}$  is the far-field stress (large  $x$ ) when only one crack is present, which is the same as the stress when there are no cracks at all. This far-field stress can be determined considering strain compatibility (all plies extend by the same amount) of an uncracked laminate. Respectively, for the 90 and 0 plies,

$$\sigma_{x_{ff}}^{(90)} = \frac{E_{22}(t_1 + 2t_2)}{E_{22}t_1 + 2E_{11}t_2}\sigma_a \quad \sigma_{x_{ff}}^{(0)} = \frac{E_{11}(t_1 + 2t_2)}{E_{22}t_1 + 2E_{11}t_2}\sigma_a \quad (6.21)$$

The constant  $A_i$  ( $i = 1$  for 90 plies and 2 for 0 plies) is different for the two sets of plies and is determined by requiring that the total axial load at any location  $x$  along the laminate equals the applied load. Setting  $A_1 = 1$  with no loss of generality,  $A_2$  (in the 0 plies) is determined from force equilibrium, per unit width  $y$  of the laminate:

$$\int_{-t_1/2}^{t_1/2} (\sigma_{x_{ff}}^{(90)} + f)dz + 2 \int_{-t_2/2}^{t_2/2} (\sigma_{x_{ff}}^{(0)} + A_2f)dz = \sigma_a(t_1 + 2t_2) \quad (6.22)$$

where the factor of 2 in front of the second integral accounts for both sets of 0 plies, above and below the mid-plane. Using Eq. 6.21 to substitute in Eq. 6.22 and solving for  $A_2$  gives:

$$A_2 = -\frac{t_1}{2t_2} \quad (6.23)$$

The function  $f$  is still unknown at this point. The remaining stresses, except  $\sigma_y$ , are determined by using the equilibrium equations, the stress-free boundary conditions at the top of the laminate,

$$\begin{aligned} \tau_{xz}^{(0)}\left(z = \frac{t_2}{2}\right) &= 0 \\ \sigma_z^{(0)}\left(z = \frac{t_2}{2}\right) &= 0 \end{aligned} \quad (6.24)$$

and the stress continuity conditions at the interface between the  $0^\circ$  and  $90^\circ$  plies:

$$\begin{aligned} \tau_{xz}^{(90)}\left(z = \frac{t_1}{2}\right) &= \tau_{xz}^{(0)}\left(z = -\frac{t_2}{2}\right) \\ \sigma_z^{(90)}\left(z = \frac{t_1}{2}\right) &= \sigma_z^{(0)}\left(z = -\frac{t_2}{2}\right) \end{aligned} \quad (6.25)$$

Using Eqs. 6.19 to determine  $\tau_{xz}$  and  $\sigma_z$  and applying conditions 6.24 and 6.25 the stresses are found to be:

$$\sigma_x^{(90)} = \sigma_{x_{ff}}^{(90)} + f(x) \quad (6.26)$$

$$\tau_{xz}^{(90)} = -zf'(x) \quad (6.27)$$

$$\sigma_z^{(90)} = \left(-\frac{t_1 t_2}{4} - \frac{t_1^2}{8} + \frac{z^2}{2}\right) f''(x) \quad (6.28)$$

$$\sigma_x^{(0)} = \sigma_{x_{ff}}^{(0)} - \frac{t_1}{2t_2} f(x) \quad (6.29)$$

$$\tau_{xz}^{(0)} = \left(-\frac{t_1}{4} + \frac{t_1}{2t_2} z\right) f'(x) \quad (6.30)$$

$$\sigma_z^{(0)} = \left(-\frac{t_1 t_2}{16} + t_1 \frac{z}{4} - \frac{t_1 z^2}{4t_2}\right) f''(x) \quad (6.31)$$

where primes next to  $f$  denote differentiations with respect to  $x$  and  $\sigma_{x_{ff}}^{(90)}$  and  $\sigma_{x_{ff}}^{(0)}$  are given by Eqs. 6.21.

The transverse stress  $\sigma_y$  is still unknown. It is determined by using the inverted stress- strain equations and strain compatibility, following the procedure in [124], [125]. This finally leads to:

$$\sigma_y = k_0 + k_1 z - \frac{S_{12}}{S_{22}} \sigma_x - \frac{S_{23}}{S_{22}} \sigma_z \quad (6.32)$$

where  $k_0$  and  $k_1$  are unknown constants determined from classical laminated plate theory, at large  $x$ , away from the crack for a single-crack case. Eq. 6.32 is applied to both the 0 and 90 plies provided the compliances  $S_{ij}$  and stresses are evaluated accordingly.

The only unknown left, is the unknown function  $f(x)$ . It is determined via energy minimization and calculus of variations [124], [125]. The energy expression to be minimized is:

$$\Pi_c = \frac{1}{2} \int \int \int_V \underline{\sigma}^T \underline{S} \underline{\sigma} dx dy dz - \int \int_A \underline{T}^T \underline{\bar{u}} dx dz \quad (6.33)$$

where underscores denote matrices or vectors.  $S$  is the compliance tensor for the portion of the laminate being evaluated in Eq. 6.33, for example 0° or 90° plies,  $\underline{T}$  are the tractions corresponding to the prescribed displacements  $\underline{\bar{u}}$ .  $V$  is the volume of the laminate and  $A$  is the area over which displacements are prescribed.

Eq. 6.33 includes the unknown function and its derivatives. It turns out the second term in Eq. 6.33 does not contribute to the solution. It affects the particular solution of  $f$  which is already fixed by requiring that the stresses in Eq. 6.20 recover the far-field classical laminated-plate theory solution. For the remaining part of the complementary energy  $\Pi_c$  the  $y$  and  $z$  integrations can be carried out easily, leaving the  $x$  integration. Thus,  $\Pi_c$  has the form:

$$\Pi_C = \frac{1}{2} \int_0^d H(f, f', f'') dx \quad (6.34)$$

where  $H$  is the integrand in Eq. 6.34 containing  $f$  and its first two derivatives along with the compliances and geometry of the problem resulting from the  $y$  and  $z$  integration of Eq. 6.33.

To minimize the energy, one must find the function  $f$  that minimizes the integral in the right hand side of Eq. 6.34. This is a classic problem in calculus of variations. The unknown function  $f$  is determined by solving the Euler equation:

$$\frac{d^2}{dx^2} \left( \frac{\partial H}{\partial f''} \right) - \frac{d}{dx} \left( \frac{\partial H}{\partial f'} \right) + \frac{\partial H}{\partial f} = 0 \quad (6.35)$$

This turns out to be a fourth order ordinary differential equation for  $f$  that is solved subject to the boundary conditions at  $x = 0$  ( $\sigma_x = \tau_{xz} = 0$ ) and  $x = d/2$  ( $\tau_{xz} = d\sigma_z/dz = 0$ ). The solution is in terms of exponentials. Note that as this solution must be valid for large values of  $d$ , any exponentials with positive exponents will lead to ever increasing stress values and are thus neglected.

### 6.3.2 Comparison of analytically determined stresses to finite element results

Comparison of this solution to finite element results taken from [121] shows excellent agreement for relatively large crack spacing and some discrepancy for very small crack spacing ( $d < 10t_1$ ). This comparison is shown in Figure 6.7.

The stresses are now combined in a Hashin-type failure criterion [126] including the interlaminar stresses to determine failure at any given point in 0 or 90 plies. It should be noted that, for the transverse strength of the 90° plies, the in-situ strength mentioned earlier is used. As an additional check of the accuracy of the improved model, the number of cracks as a function of applied stress in various cross-ply laminates made with T300/934 predicted by the analysis method presented are compared to test results obtained by Wang [127], in Figure 6.8.

As already mentioned, the first cracks typically appear at locations where local flaws or inconsistencies act as stress concentrations. Therefore, some discrepancy between the present method and test results is to be expected at low crack densities. This discrepancy is most pronounced in the case of the [0/90<sub>2</sub>/0] laminate. The rest of the predicted curves are in reasonable agreement for the [0/90<sub>4</sub>/0] and [0/90<sub>3</sub>/0] laminates. At higher crack densities, the problem already highlighted in Figure 6.7 becomes significant. It is

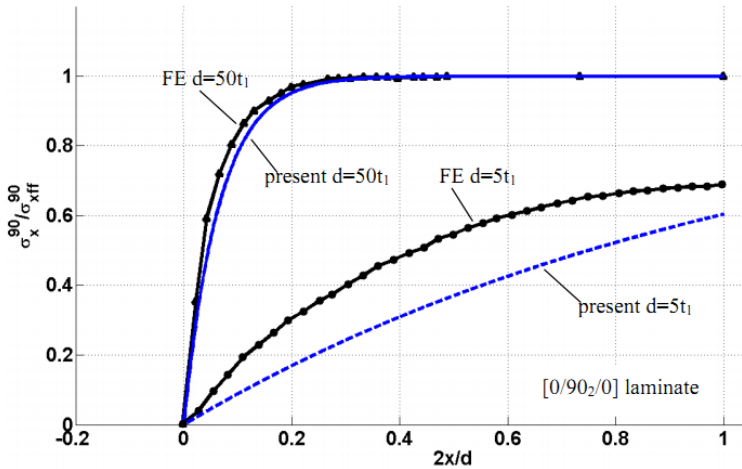


Figure 6.7: Normal stress  $\sigma_x$  in  $90^\circ$  ply compared to finite element results from [121]

suspected, that the implicit assumption of the analytical model that the  $\sigma_x$  stress does not vary with  $z$ , is no longer valid for higher crack densities. In any case, while it is understood that the analytical model needs some improvements, it is much easier to use than finite element solutions and, for the time being, is considered sufficient for using to generate predictions of strength evolution under cyclic loading.

To proceed with fatigue life predictions, knowledge of the critical locations in the  $0^\circ$  and  $90^\circ$  plies is needed. Typical plots of the stresses in these plies are shown in Figure 6.9. The axial stress  $\sigma_x$  in the  $0^\circ$  plies is zero at the two matrix cracks and goes through a maximum at the mid-point between the cracks. The interlaminar normal stress  $\sigma_z$  is compressive at the two matrix cracks and slightly tensile at the mid-point between them. It should be noted that as the crack spacing decreases, the tensile  $\sigma_z$  value half way between adjacent cracks keeps increasing and it is possible that at very high crack densities it might affect further damage creation by causing delaminations at the  $0/90$  ply interface. For most crack densities, however, this tensile value is quite low and does not alter the damage evolution. The interlaminar shear stress  $\tau_{xz}$  is zero at two matrix cracks and zero at the mid-point between them. It reaches a maximum (or a minimum) at two intermediate points symmetrically located with respect to the mid-point of the distance between the two cracks. The maximum interlaminar shear stress is very low and does not lead to failure of the ply.

The axial stress  $\sigma_x$  in the  $0^\circ$  plies is maximum at the location where the two cracks are (recall the cracks are confined in the  $90^\circ$  plies) and goes through a

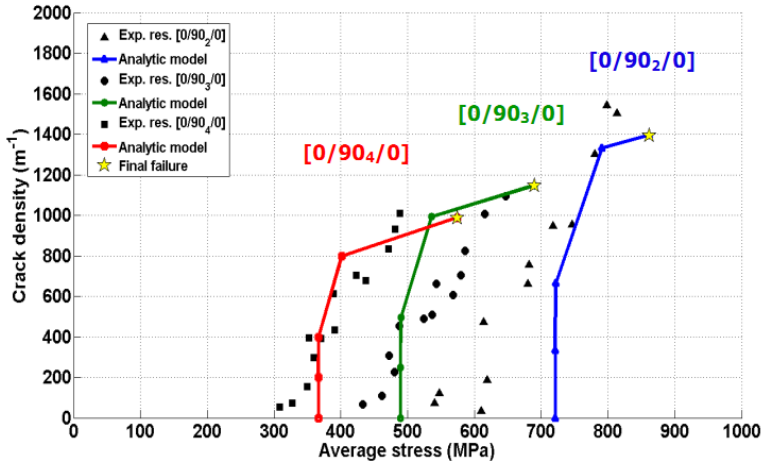


Figure 6.8: Crack density versus applied stress for cross-ply laminates Test versus theory. (Test results from [127])

minimum half-way between them as is shown in the bottom part of Figure 6.9. The interlaminar stresses  $\sigma_z$  and  $\tau_{xz}$  in the  $0^\circ$  plies have very similar shapes as in the  $90^\circ$  plies but their peak magnitudes are much lower than in the  $90^\circ$  plies. The stresses in the  $0^\circ$  plies at the bottom of Figure 6.9 are plotted at the  $0/90$  interface for two reasons: one because as one moves towards the top of the laminate, which is stress free, the interlaminar stresses become negligible and two, because the  $0/90$  interface is the only interface where delaminations may occur if the magnitude of the interlaminar stresses is sufficiently high. As it turns out, for the laminates examined here, this was not the case and no delaminations are predicted. This is not in complete agreement with the test results reported in [74] where some delaminations appeared at high crack densities.

### 6.3.3 Predictions of cycles to failure compared to test results

The above discussion and the stress shapes in Figure 6.9 help determine the critical locations where damage might be created during cyclic loading. To quantify this better, the Hashin failure criterion (modified to include interlaminar stresses) was used to determine the critical location in  $0^\circ$  and  $90^\circ$  plies. Two locations came out as the most critical: (a) The interface between  $0$  and  $90$  plies at  $x = 0$  (next to a matrix crack) and (b) The same interface at  $x = d/2$  (midway between matrix cracks). At the first location,  $\sigma_x$  in the  $0$  plies reaches its maximum value,  $\sigma_z$  reaches its maximum compressive value, and  $\tau_{xz} = 0$ . At the second location,  $\sigma_x$  in the  $0$  plies reaches its minimum

value (which is close to the maximum),  $\sigma_z$  reaches its maximum tensile value, and  $\tau_{xz} = 0$ . The first location was always more critical in predicting failure than the second for all the cases examined.

The fatigue approach described in the previous sections will now be combined with the stress analysis presented in this section to predict the cycles to failure for cross-ply laminates made with AS4/3501-6. The laminates examined were  $[0/90_2]_s$ ,  $[0_2/90_2]_s$  and  $[0/90_4]_s$ . Each laminate was divided in two sections, the 0 and 90 plies. The 0 plies were then divided into sub-sections in exactly the same way as described in section 6.2.1 for the laminate with all  $0^\circ$  plies. As already mentioned, the critical location for all laminates and load levels was the 0/90 interface next to a matrix crack ( $x = 0$ ). Then, the results from the previous section on the uni-directional plies can be applied here directly. This neglects any effects of the compressive  $\sigma_z$  stress at the critical location.

The analytical predictions are compared to test results obtained by Lee et al [74] in Figs. 6.10 - 6.12. The best fit curve to the test data is also included for comparison. The agreement is good for the  $[0/90_2]_s$  laminate (Figure 6.10) but not as good for the  $[0_2/90_2]_s$  laminate (Figure 6.11). The comparison for the  $[0/90_4]_s$  laminate in Figure 6.12 shows that the present method needs improvement.

As can be seen from Figs. 6.10 - 6.12, the predictions from the present model are always conservative (below the best fit curve) and they get progressively worse (more conservative) as the thickness of the  $90^\circ$  plies increases. It is believed that the main reason for the discrepancy is that, within each section ( $0^\circ$  and  $90^\circ$  plies)  $\sigma_x$  is independent of  $z$ . Work by Berthelot [122] suggests that for low crack spacings this assumption is no longer valid. An improved stress model is expected to improve the fatigue life predictions.

Another reason for the discrepancies in Figs. 6.11 and 6.12 is that the model evenly redistributed load from failed fibers to all unfailed fibers in the 0 plies. As mentioned in the previous section, in a real situation only the nearest fibers to a failed fiber will participate in load sharing. This would localize load redistribution and keep fibers from failing early. As a result, the predicted lives will increase raising the analytical predictions higher and closer to the test data.

## 6.4 Discussion

The improved model described in the previous sections brought to the surface what is, perhaps, the most important issue in developing predictive tools for fatigue performance of composites: The need for accurate static analyses that can quantify the strength and stiffness of a composite structure given its damage state. This was shown in section 6.2 where by tracking fiber breakage,

excellent predictions were obtained. As soon as the level of complexity went up, in the  $[0_n/90_m/0_n]$  laminates, section 6.3, the shortcomings of the stress analysis model translate to inaccuracies in the predictions.

The analytical framework for predicting fatigue strength of composite structures works extremely well if the associated (static) stress analysis models that account for the types and extent of damage are accurate. Future efforts should concentrate on improving these models. The basic models for residual strength and cycles to failure may need improvements but this is secondary compared to the issues that arise when the static analysis models needed for the method to work are not accurate or available.

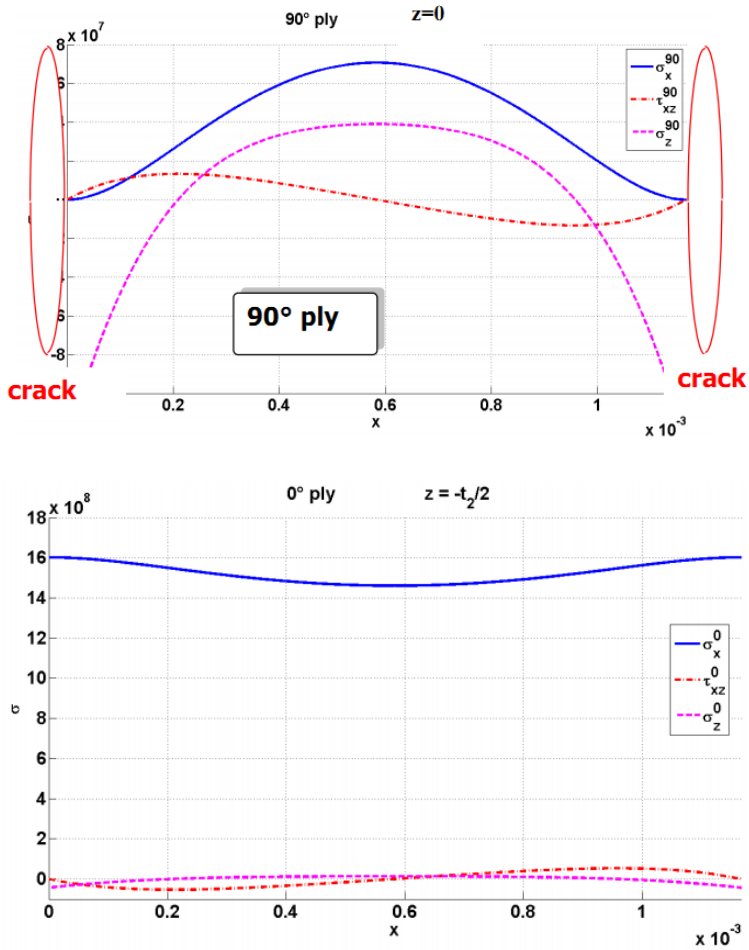


Figure 6.9: Stresses in a [0/90<sub>2</sub>/0] laminate under tension with two matrix cracks in the 90° plies

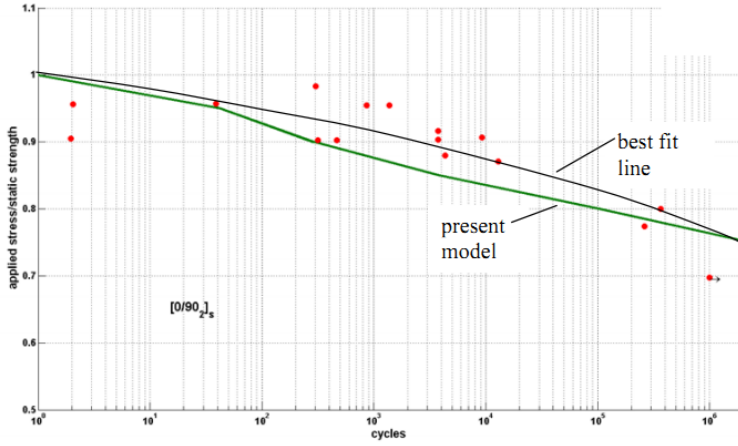


Figure 6.10: Analytical predictions compared to test results for  $[0/90_2]_s$  AS4/3501-6 laminate. (Test results taken from [74])

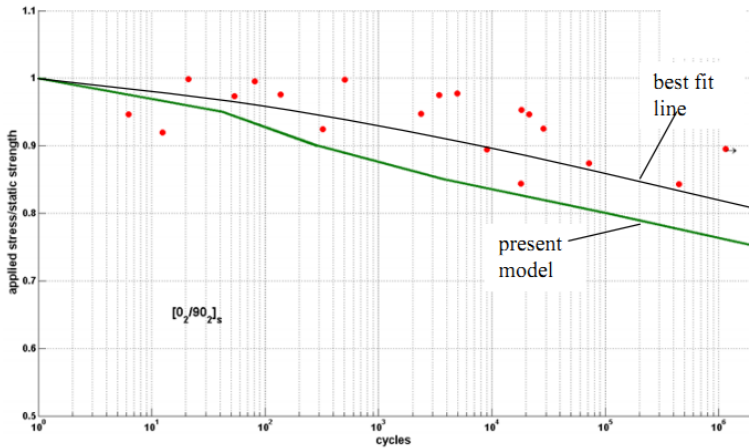


Figure 6.11: Analytical predictions compared to test results for  $[0_2/90_2]_s$  AS4/3501-6 laminate. (Test results taken from [74])

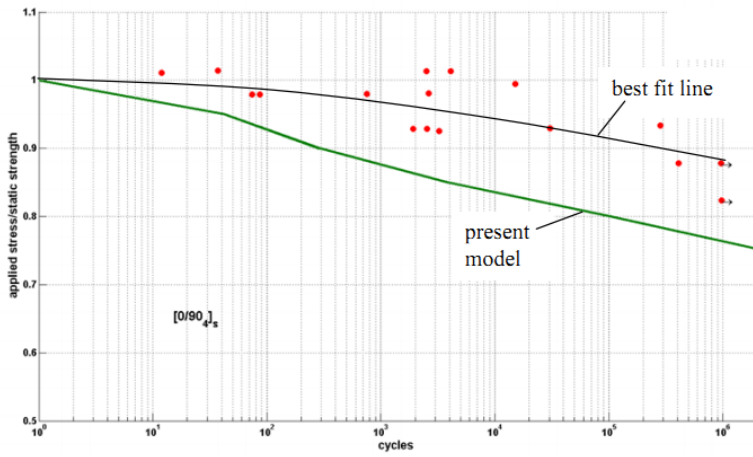


Figure 6.12: Analytical predictions compared to test results for  $[0/90_4]_s$  AS4/3501-6 laminate. (Test results taken from [74])

# 7

## *Conclusions and recommendations*

An analytical model that can be used to predict cycles to failure of composite structures under constant amplitude or spectrum loading was presented in the previous chapters. First, a simple model for determining the residual strength as a function of cycles, applied load, and the strength distribution at the beginning of the cyclic loading was created. This model was used to determine the cycle-by-cycle probability of failure  $p$  for a composite structure under cyclic loading. The cycles to failure were then determined as the cycles at which the probability  $p$  that failure has occurred is maximized. The cycle-by-cycle probability of failure  $p$  was shown to be constant if the static strength follows a two-parameter Weibull distribution and the residual strength obeys the residual strength model presented here. The model was extended to spectrum loading by tracking the evolution of residual strength as different loads (in terms of amplitude, direction, type) are applied and creating an equivalence between spectrum and constant amplitude loading.

The model developed is purely analytical and, as such, requires no fatigue or other calibration tests or empirical or semi-empirical parameters or curve fitting. It is therefore, very efficient and versatile and can be used not only as a predictive tool but also as a means for establishing design guidelines and curves in the form of Goodman diagrams, omission levels for fatigue test programs, cycles to failure curves with a specific reliability, and reduced number of test cycles. Predictions for the cycles to failure based on a constant  $p$  match test results very well in many cases but deviate from test results when multiple forms of damage and complex stress states are present in the structure. A correction to the model, still based on the same residual strength and cycles-to-failure equations was created to account for the fact that, in general, the cycle-by-cycle probability of failure  $p$  does not remain constant during a fatigue test. This improved the accuracy of the predictions but also identified some areas where more work is needed.

The main issue that must be addressed so that the model can have more general applicability, is the need to track multiple types of damage as they are created and transition to other damage types. If one form of damage dominates the fatigue behavior, the model presented here is adequate. If more than one types of damage are present and each affects structural performance by locally or globally changing strength and stiffness, the model must be modified. Areas

where modifications are needed and some suggestions for these modifications are briefly given in the two sections that follow.

## 7.1 Conclusions

A summary of the conclusions drawn from the analytical model follows. While there is experimental evidence to support most of them, some of them have not yet been experimentally verified or have been only partially verified. The status of experimental verification is indicated at the end of each conclusion with, accordingly, the word(s), “verified”, “partially verified”, or “not verified”.

- 1 The proposed model relating the rate of change of residual strength to the current value of the residual strength gives very good prediction for residual strength as a function of cycles as long as the residual strength is a monotonic function of cycles. (Verified)
- 2 It is possible to obtain excellent predictions for the cycles to failure provided the statistical distribution for the static and residual strength are accurately known and one type of damage dominates the fatigue behavior. (Verified)
- 3 It is possible to extend the model to spectrum loading, giving very good predictions for the blocks to failure for tension-dominated spectra, by mapping the residual strength to a number of cycles and loading type. This requires that one type of damage dominates the behavior. (Partially Verified)
- 4 The cycle-by-cycle probability of failure is constant if the static strength distribution is two-parameter Weibull and the residual strength model introduced here holds. (Not Verified).
- 5 The cycle-by-cycle probability of failure will change when significant load redistribution occurs and/or new types of damage appear in the structure. This has been incorporated in the model with excellent results but also identified the need of accurate static strength models that account for the damage present in the structure as a necessary requirement for the model to be accurate. (Partially Verified)
- 6 The scatter of the residual strength decreases with cycles. As the number of cycles increase, only the stronger specimens remain in a population and the scatter becomes narrower. (Not Verified)
- 7 The Miner sum of applied cycles divided by the cycles to failure  $\sum \frac{n_i}{N_i}$  can be less than, equal to, or greater than 1 depending on the sequence

- of applied loads. According to the present model, low-high sequences add up to less than 1 and high-low sequences add up to more than 1. (Partially Verified)
- 8 Changing the order of application of load segments in a fatigue test does not change the residual strength but it does change the number of cycles to failure. The cycles to failure will not change as long as the final load segment in the sequence remains the same irrespective of how all previous load segments are ordered. (Not Verified)
  - 9 The present model can be successfully used to construct Goodman diagrams without the use of any fatigue testing. The accuracy of the resulting diagrams ranges from good (tension-dominated loading with one type of damage dominating behavior) to poor (compression-dominated loading). (Verified)
  - 10 The present model can be used to determine the number of fatigue cycles or fatigue lives to which a specimen should be tested to provide B-Basis life reliability. Depending on the assumptions, this number of lives ranges from 8.9 to 17.9. (Verified)
  - 11 The proposed model can be used to determine omission levels for test programs. These are the load levels below which, cycling up to a prescribed number of cycles will cause no damage beyond that already in the structure, will cause no growth of the damage already present, and will cause no failure. (Verified)
  - 12 The proposed model can be used to derive an exchange law to determine a reduced number of test cycles at a slightly increased applied load as a function of the required number of service cycles and applied loads (Not verified).

## 7.2 Recommendations

As with every new model that attempts to be general and cover all possible cases, there are several areas where more work is needed to improve the model's accuracy. For convenience, the section or sections where a specific issue arose is also included at the end of each recommendation.

- 1 Currently, the cycles to failure are obtained as the cycles that maximize the probability  $P$  that there has been (one and only one) failure between 1 and  $N$  cycles. It should be examined whether using the mean (which is twice the modal value) instead of the mode, gives a better prediction. At the same time, physical reasoning for making this change should be provided. (Section 2.2)

- 2 The determination of experimental scatter for static and residual strength must be accurate. The information available was not sufficient for some of the tests compared to the analytical predictions.(Sections 3.2, 3.3, and 5.2)
- 3 The main difficulty in the proposed method is in determining the residual strength given a level of damage. If more than one interacting types of damage are present, for example matrix cracks and delaminations, analytical modeling of this interaction and its effect on strength and stiffness is necessary. This is a static analysis that can be quite complex. If this analysis is accurate, marching onwards in cycles to the next major damage event using the methodology presented here is easy and accurate. (Sections 6.2 and 6.3).
- 4 The effect of damage caused during the tensile part of the cycle on the compressive residual strength and, vice versa, the effect of damage caused during the compressive part of the cycle on the residual strength in tension are, currently, not modeled as accurately as it would have been desirable for cyclic loads with significant tensile and compressive components, ( $R < 0$ ). More work is needed in this area where more than one types of damage interact. (Section 5.2.2)
- 5 Correcting for the R-ratio was done here using simple multiplicative factors to credit the structure when the load excursion does not go through zero. More accurate methods are needed (Section 2.3)
- 6 A small discrepancy is introduced for two-parameter Weibull static strength distributions if  $p$  is calculated using the cumulative distribution function and then the predictions are forced to go through the mean static strength after one cycle. This inconsistency must be reconciled. (Section 2.2)
- 7 In updating the cycle-by-cycle probability of failure  $p$ , it was assumed that the residual strength distribution at any given point can be made into an “equivalent” two-parameter Weibull distribution. This is valid in many cases but not always and no rigorous description of when this breaks down was given. Multiple types of damage and their interaction would change the distribution parameters or, even, the type of the distribution. (Section 6.2.3)
- 8 It is assumed that  $p$  is piecewise constant while residual strength changes. This is meant to represent evolving damage mechanisms at smaller scales than accounted for in the model. The extent to which this assumption is valid must be examined. (Section 6.1)

- 9 Under spectrum loading, the analysis presented suggests that the order of load application can change without any effect on the number of cycles (or blocks) to failure as long as the last segment in the sequence remains the same. This is, probably, not as widely applicable as the equations suggest. It relates to the fact that loading in tension creates a damage state that will affect the subsequent behavior of the structure in compression. If the situation is reversed this will give a different answer (see section 5.2.3) . More work is needed in this area accounting for multiple types of damage and their interaction.
- 10 A one-to-one correspondence between damage state and residual strength of the structure was assumed with the requirement that if a certain residual strength is reached, the uniquely defined damage state corresponding to it also occurs. The range of applicability of this assumption has not been fully explored. (Sections 2.1 and 6.1)
- 11 The redistribution of load from failed fibers to adjacent fibers was done by distributing the load of the failed fibers evenly to all other fibers. This is conservative. Three-dimensional finite element models of the load redistribution from one fiber to its neighbors [114] show that the stress concentration factor in adjacent fibers is lower than what was used here. Improved load sharing models should be investigated. (Sections 6.2.1, 6.2.2).
- 12 An improved stress solution, for example with a  $\sigma_x$  that is a function of the out-of-plane coordinate  $z$ , is needed for more accurate predictions of fatigue lives of cross-ply laminates. (Section 6.3.1)
- 13 The residual strength at any cycle level was obtained as a solution to a simple first order differential equation. This was an assumption that needs experimental verification beyond what is presented here. In addition, different assumptions for this dependence on cycles and damage state should be investigated.



## Bibliography

- [1] MIL-HDBK-5H. October 2001. Figure 3.7.6.1.8e.
- [2] Kensch C.W. Fatigue of composites for wind turbines. In *3d International Conference on Fatigue of Composites*, Kyoto Japan, 13–15 Sep 2004.
- [3] Bansemir H. and Emmerling S. Fatigue substantiation and damage tolerance evaluation of fiber composite helicopter components. In *the RTO AVT Specialists' Meeting "Applications of Damage Tolerance Principles for Improved Airworthiness of Rotorcraft"*, Corfu Greece, 21–22 April 1999.
- [4] MIL-HDBK-5H. October 2001. Figure 3.7.6.1.10b.
- [5] McCarty J.E. Johnson R.W. and Wilson D.R.M. *737 Graphite-Epoxy Horizontal Stabilizer Certification*. Proceedings of 23d AIAA/ASME/ASCE/AHS Structures, Structural Dynamics, and Materials Conference, 1982. 307-322.
- [6] Brandecker B. and Hilgert R. *A-320 Full-scale Structural Testing for Fatigue and Damage Tolerance Certification of Metallic and Composite Structure*. Proceedings of 16th Congress of the International Council of the Aeronautical Sciences, ICAS-88-5.8.1, 1988.
- [7] Schijve J. *Fatigue of Structures and Materials*. Kluwer Academic Publishing, 2001. chapter 20.
- [8] Rouchon J. *Fatigue and Damage Tolerance Evaluation of Structures: The Composite Materials Response*. 22nd Plantema Memorial Lecture, May 2009. NLR Report NLR-TP-2009-221.
- [9] Talreja R. *Fatigue of Composite Materials*. Technomic Publishing Co., Lancaster PA, 1986.
- [10] Lorenzo L. and Hahn HT. *Fatigue Failure Mechanisms in Unidirectional Composites*. *Composite Materials: Fatigue and Fracture, ASTM STP 907*. Hahn HT editor. ASTM, Philadelphia, 1986: 210-232.
- [11] Charewics A. and Daniel IM. *Damage Mechanisms and Accumulation in Graphite/Epoxy Laminates*. *Composite Materials: Fatigue and Fracture, ASTM STP 907*. Hahn HT editor. ASTM, Philadelphia, 1986: 274-297.

- 
- [12] Reifsnider KL. Sculte K. and Duke JC. *Long-Term Fatigue Behavior of Composite Materials. Long-Term Behavior of Composites, ASTM STP 813*. O'Brien TK editor. ASTM, Philadelphia, 1983: 136-159.
- [13] Reifsnider KL. and Stinchcomb WW. *A Critical-Element Model of the Residual Strength and Life of Fatigue-Loaded Composite Coupons. Composite Materials: Fatigue and Fracture, ASTM STP 907*. Hahn HT editor. ASTM, Philadelphia, 1986: 298-313.
- [14] Bakis CE. Yih HR. Stinchcomb WW. and Reifsnider KL. *Damage Initiation and Growth in Notched Laminates Under Reversed Cyclic Loading. Composite Materials: Fatigue and Fracture, Second Volume, ASTM STP 1012*. Lagace PA editor. ASTM, Philadelphia, 1989: 66-83.
- [15] Peters PW. *The Influence of Fiber, Matrix, and Interface on Transverse Cracking in Carbon Fiber-Reinforced Plastic Cross-Ply Laminates. Composite Materials: Fatigue and Fracture, Second Volume, ASTM STP 1012*. Lagace PA editor. ASTM, Philadelphia, 1989: 103-117.
- [16] Guynn EG. Bradley WL. and Elber W. *Micromechanics of Compression Failures in Open Hole Composite Laminates. Composite Materials: Fatigue and Fracture, Second Volume, ASTM STP 1012*. Lagace PA editor. ASTM, Philadelphia, 1989: 118-136.
- [17] Black NF. and Stinchcomb WW. *Compression Fatigue Damage in Thick, Notched Graphite/Epoxy Laminates. Long-Term Behavior of Composites, ASTM STP 813*. O'Brien TK editor. ASTM, Philadelphia, 1983: 95-115.
- [18] Russel AJ. and Street KN. *Predicting Interlaminar Fatigue Crack Growth Rates in Compressively Loaded Laminates. Composite Materials: Fatigue and Fracture, Second Volume, ASTM STP 1012*. Lagace PA editor. ASTM, Philadelphia, 1989: 162-180.
- [19] Ramkumar RL. *Effect of Low-Velocity Impact Damage on the Fatigue Behavior of Graphite/Epoxy Laminates. Long-Term Behavior of Composites, ASTM STP 813*. O'Brien TK editor. ASTM, Philadelphia, 1983: 116-135.
- [20] Beheshty MH. and Harris B. *A Constant-Life Model of Fatigue Behaviour for Carbon-Fibre Composites: The Effect of Impact Damage. Composites Science and Technology*. 1988; 58: 9-18.
- [21] O'Brien TK. Murri GB. and Salpekar SA. *Interlaminar Shear Fracture Toughness and Fatigue Thresholds for Composite Materials. Composite*

---

*Materials: Fatigue and Fracture, Second Volume, ASTM STP 1012.*  
Lagace PA editor. ASTM, Philadelphia, 1989: 222-250.

- [22] Mohlin T. Blom AF. Carlsson LA. and Gustavsson AI. *Delamination Growth in a Notched Graphite/Epoxy Laminate Under Compression Fatigue Loading. Delamination and Debonding of Materials, ASTM STP 876.* Johnson WS editor. ASTM, Philadelphia, 1985: 168-188.
- [23] Gustafson C-G. Jilkèn L. and Gradin PA. *Fatigue Thresholds of Delamination Crack Growth in Orthotropic Graphite/Epoxy Laminates. Delamination and Debonding of Materials, ASTM STP 876.* Johnson WS editor. ASTM, Philadelphia, 1985: 200-216.
- [24] Bathias C. and Laksimi A. *Delamination Threshold and Loading Effect in Fiber Glass Epoxy Composite. Delamination and Debonding of Materials, ASTM STP 876.* Johnson WS editor. ASTM, Philadelphia, 1985: 217-237.
- [25] O'Brien TK. *Generic Aspects of Delamination in Fatigue of Composite Materials.* J. American Helicopter Society, 1987; 32: 13-18.
- [26] Harris CE. and Allen DH. *A Continuum Damage Model of Fatigue-Induced Damage in Laminated Composites.* SAMPE Journal, 1988: 43-51.
- [27] Subramanian S. Reifsnider KL. and Stinchcomb WW. *A Cumulative Damage Model to Predict the Fatigue Life of Composite Laminates Including the Effect of a Fibre-Matrix Interphase.* Int. J. Fatigue, 1995;17(5):343-351.
- [28] Yang JN. Lee LJ. and Sheu DY. *Modulus Reduction and Fatigue Damage of Matrix Dominated Composite Laminates. Composite Structures.* 1992;21:91-100.
- [29] Lee LJ. Yang JN. and Sheu DY. *Prediction of Fatigue Life for Matrix-Dominated Composite Lamintes. Composites Science and Technology.* 1993;46:21-28.
- [30] Badaliance R. and Dill HD. *Compression Fatigue Life Prediction Methodology for Composite Structures.* NADC-78203-60, 1982.
- [31] Ratwani MM. and Kan HP. *Compression Fatigue Analysis of Fiber Composites.* J. Aircraft, 1981;18:458-462.
- [32] Schaff JR. and Davidson BD. *Life Prediction Methodology for Composite Structures. Part I - Constant Amplitude and Two-Stress Level Fatigue.* J. Composite Materials, 1997;31(2):128-157.

- 
- [33] Schaff JR. and Davidson BD. *Life Prediction Methodology for Composite Structures. Part II - Spectrum Fatigue*. J. Composite Materials, 1997. 158-181.
- [34] Kedward KT. and Beaumont PWR. *The Treatment of Fatigue and Damage Accumulation in Composite Design*. Int. J. Fatigue, 1992;14(5):283-294.
- [35] Philippidis TP. and Vassilopoulos AP. *Fatigue Strength Prediction Under Multiaxial Stress*. J. Composite Materials, 1999;33(17):1578-1599.
- [36] Whitney JM. *Fatigue Characterization of Composite Materials*. Report AFML-TR-79-4111, 1979.
- [37] Whitney JM. *A Residual Strength Degradation Model for Competing Failure Modes. Long-Term Behavior of Composites, ASTM STP 813*. O'Brien TK editor. ASTM, Philadelphia, 1983:225-245.
- [38] Sendekyj GP. *Fitting Models to Composite Materials Fatigue Data. Test Methods and Design Allowables for Fibrous Composites*, ASTM STP 734. Chamis CC editor. ASTM, Philadelphia, 1981:245-260.
- [39] Schulte K. *Damage monitoring in polymer matrix structures*. J. Physique IV, Colloque C7, supplement au Journal de Physique III, 3, 1993, pp. 1629-1636.
- [40] Schulte K. *Stiffness reduction and development of longitudinal cracks during fatigue loading of composite laminates*. Proc. European Mechanics Colloquium 182, Mechanical Characterisation of Load Bearing Fibre Composite Laminates, 29-31 Aug. 1984, Elsevier Science Publisher, London, 1985 pp. 36-54.
- [41] Schulte K. *Damage development under cyclic loading*. Proc. European Symposium on Damage Development and Failure Processes in Composite Materials, 4-6 May 1987, Leuven Belgium, 1987 pp. 39-54.
- [42] Ronold KO. and Echtermeyer AT. *Estimation of Fatigue Curves for Design of Composite Laminates*. Composites Part A, 1996;27A:485-491.
- [43] Chamis CC. and Ginty CA. *Fiber Composite Structural Durability and Damage Tolerance: Simplified Predictive Methods. Composite Materials: Fatigue and Fracture, Second Volume, ASTM STP 1012*. Lagace PA editor. ASTM, Philadelphia, 1989: 338-355.
- [44] Lee J. Harris B. Almond DP. and Hammett F. *Fibre Composite Fatigue-Life Determination*. Composites Part A, Philadelphia, 1997;28A:5-15.

- 
- [45] Diao X. Ye L. and Mai. Y-W. *Simulation of Fatigue Performance of Cross-Ply Composite Laminates*. Applied Composite Materials, 3, 1996. 391-406.
- [46] Turon A. Costa J. Camanho P.P. and Dávila C.G. *Simulation of delamination in composites under high-cycle fatigue*. Composites Part A, 38, 2007. 2270-2282.
- [47] Lian W. and Yao W. *Fatigue life prediction of composite laminates by FEA simulation method*. Int. J. Fatigue, 32, 2010. 123-133.
- [48] Mandell J.F. Samborsky D.D. and Sutherland H.J. Effects of material parameters and design details on the fatigue of composite materials for wind turbine blades. In *Proceedings of the European Wind Energy Conference*, Nice, France, 1-5 March 1999.
- [49] Kawai M. and Koizumi M. *Nonlinear constant fatigue life diagrams for carbon/epoxy laminates at room temperature*. Composites: Part A, 38, 2007. 2342-2353.
- [50] Vassilopoulos A.P. Manshadi B.D. and Keller T. *Influence of the constant life diagram formulation on the fatigue life prediction of composite materials*. Int. J. Fatigue, 32, 2010. 659-669.
- [51] Filis P.A. Farrow I.R. and Bond I.P. *Classical fatigue analysis and load cycle mix-event damage accumulation in fibre reinforced laminates*. Int. J. Fatigue, 26, 2004. 565-573.
- [52] Andersons J. Hojo M. and Ochiai S. *Empirical model for stress ratio effect on fatigue delamination growth rate in composite laminates*. Int. J. Fatigue, 26, 2004. 597-604.
- [53] Kim S.J. and Hwang I.H. *Prediction of fatigue damage for composite laminate using impact response*. Int. J. Fatigue, 28, 2006. 1334-1339.
- [54] Post N.L. Bausano J. Case S.W. and Lesko J.J. *Modeling the remaining strength of structural composite materials subjected to fatigue*. Int. J. Fatigue, 28, 2006. 1100-1108.
- [55] Shivakumara K. Chena H. Abalib F. Leb D. and Davis C. *A total fatigue life model for mode I delaminated composite laminates*. Int. J. Fatigue, 28, 2006. 33-42.
- [56] Boerstra G.K. *The Multislope model: A new description for the fatigue strength of glass fibre reinforced plastic*. Int. J. Fatigue, 29, 2007. 1571-1576.

- 
- [57] Harper P.W. and Hallett S.R. *A fatigue degradation law for cohesive interface elements Development and application to composite materials*. Int. J. Fatigue, 32, 2010. 1774-1787.
- [58] Verhoef R.C. *Residual Strength of FRP Materials*. Master Thesis, Department of Aerospace Engineering, Delft University of Technology, September 2001. 1774-1787.
- [59] Bhat N.V. *Delamination Growth in Graphite/Epoxy Composite Laminates under Tensile Loading*. Ph.D. Thesis M.I.T., September, 1993.
- [60] Shim D.J. and Lagace P.A. *Damage and Delamination Characteristics in Composite Laminates with Ply Dropoffs under Static and Cyclic In-plane Loads*. Proceedings of the American Society for Composites 19th Technical Conference, Atlanta, Georgia, October, 2004.
- [61] Hahn HT. Kim RY. *Proof testing of composite materials*. J Composite Materials, 1975. vol 9, 297311.
- [62] Sendekyj G.P. *Fitting Models to Composite Materials Fatigue Data*. Test Methods and Design Allowables for Fibrous Composites, ASTM STP 734, Chamis, C.C. editor, ASTM, Philadelphia, 1981. 245-260.
- [63] *Guidance Material for Fatigue Limit Tests and Composite Blade Fatigue Substantiation*.
- [64] Mandell J.F. Samborsky D.D. Wang L. Wahl N.K. *New Fatigue Data for Wind Turbine Blade Materials*. Transactions of the ASME J of Solar Energy Engineering 125, 2003. 506-514.
- [65] Lagace P.A. and Nolet S.C. *Effect of Ply Thickness on Longitudinal Splitting and Delamination in Graphite/Epoxy Under Compressive Cyclic Load*. Composite Materials, Fatigue and Fracture, ASTM STP 907, Hahn H.T. editor. ASTM, Philadelphia, 1984. 335-360.
- [66] *Composite Materials Handbook 17-2F, vol 2, Polymer Matrix Composites Material Properties*. June 17, 2002.
- [67] Pavia EG and OBrien JJ. *Weibull Statistics of Wind Speed over the Ocean*. J. Climate and Applied Meteorology, 25.
- [68] Simar S. and Vanhems A. *Probabilistic Characterization of Directional Distances and Their Robust Versions*. Technical Report 10044. <http://www.stat.ucl.ac.be/IAP>.

- 
- [69] Yang JN and Jones DL. *Load Sequence Effects on Graphite/Epoxy Laminates, Long Term Behavior of Composites, ASTM STP 813*. O'Brien, TK editor, ASTM Phila PA, 1983. 246-262.
- [70] Wedel-Heinen. J. Et al. *Optimat Blades- Reliable Optimal Use of Materials for Wind Turbine Rotor Blades*. Report OB-TG6-R002, 2006. chapter 13.2.
- [71] Dvorak G.J. Laws N. and Hejazi M. *Analysis of Progressive Matrix Cracking in Composite Laminates I. Thermoelastic Properties of a Ply with a Crack*. J. Composite Materials, 19, 1985. 216-234.
- [72] O'Brien TK. *Characterization of Delamination Onset and Growth in a Composite Laminate in Damage in Composite Materials*. ASTM STP 775, 1980. 140-167.
- [73] *Metallic Materials and Elements for Aerospace Vehicle Structures*. MIL-HDBK-5J, January 2003. 9-253.
- [74] Lee J-W. Daniel I.M. and Yaniv G. *Fatigue Life Prediction of Cross-ply Composite Laminates. Composite Materials: Fatigue and Fracture 2nd Vol. ASTM STP 1012*. Lagace PA editor, ASTM, Philadelphia, 1989. 19-28.
- [75] Gathercole N. Reiter H. Adam T. and Harris B. *Life Prediction for Fatigue of T800/5245 Carbon-fibre Composites: I. Constant Amplitude Loading. Int J. Fatigue*. 1994;16. 523-532.
- [76] Maier G. Ott H. Protzner A. and Protz. B. *Damage Development in Carbon Fibre-Reinforced Polyimides in Fatigue Loading as a Function of Stress Ratio, Composites, vol 17, No 2*. April 1986. 111-120.
- [77] Amijima S. Fujii T. and Hamaguchi M. *Static and Fatigue Tests of a Woven Glass Fabric Composite Under Biaxial Tension-Torsion Composites*. 1991. 22(4):281-289.
- [78] Cvitkovich MK. O'Brien TK. Minguet PJ. *Fatigue Debonding Characterization in Composite Skin/Stringer Configurations. Composite Materials, Fatigue and Fracture, 7th vol, ASTM STP 1330*. Cucinell, RB editor. ASTM, 1998. 97-121.
- [79] O'Brien TK. *Fatigue Delamination Behavior of PEEK Thermoplastic Composite Laminates. J. Reinforced Plastics and Composites*. 1988:7. 341-359.

- 
- [80] O'Brien TK. Rigamonti M. and Zanoti C. *Tension Fatigue Analysis and Life Prediction for Composite Laminates. NASA Technical Memorandum 100549.* 1988.
- [81] Gerharz JJ. Rott D. and Schuetz D. *Schwingfestigkeitsuntersuchungen an Fuegungen in Faserbauweise. BMVg-FBWT. 79-23.* 1979.
- [82] Sheikh AK. Ahmed M. and Badar MA. *Fatigue Life Prediction of Assemblies of Rotating Parts, Int. J. Fatigue, 17.* 1995. 35-41.
- [83] Whitehead RS. Kan HP. Cordero R. and Saether ES. *Certification Testing Methodology for Composite Structures Task I, Report No NADC-87042-60 (vol I) and DOT-FAA-CT-86-39.* 1986.
- [84] *Composite Materials Handbook 17-1E, vol 1, Guidelines for Characterization of Structural Materials.* January 12, 1997. Section 8.3.
- [85] *MIL-HDBK-5H.* October 2001. Section 9.2.2.1.
- [86] Gerharz JJ. Rott D. and Schuetz D. *Schwingfestigkeitsuntersuchungen an ungekerbten und gekerbten Faserverbundwerkstoffproben aus multidirektionalem Laminat, Report No BMVg-FBWT 79-22.* Laboratorium fuer Betriebsfestigkeit, Darmstadt Germany, 1979.
- [87] Ramkumar RL. *Compression Fatigue Behavior of Composites in the Presence of Delaminations, Damage in Composite Materials ASTM STP 775.* Reifsnider KL ed., 1982. 184-210.
- [88] Badalianc R. and Dill HD. *Damage Mechanisms and Life Prediction of Graphite/Epoxy Composites, Damage in Composites Materials ASTM STP 775.* Reifsnider KL. ed., 1982. 229-242.
- [89] Bakis CE. and Stinchcomb WW. *Response of Thick Notched Laminates Subjected to Tension-Compression Cyclic Loads, Composite Materials Fatigue and Fracture ASTM STP 907.* Hahn, HT editor, ASTM, Philadelphia, 1986. 314-334.
- [90] Simonds RA. Bakis CE. and Stinchcomb WW. *Effects of Matrix Toughness on Fatigue Response of Graphite Fiber Composite Laminates, Composite Materials: Fatigue and Fracture 2nd vol, ASTM STP 1012.* Lagace PA, editor, ASTM, Philadelphia, 1989. 5-18.
- [91] Mahinfalah M. Skordahl RA. *The Effects of Hail Damage on the Fatigue Strength of a Graphite/Epoxy Composite Laminate.* Composite Structures 42, 1998. 101-106.

- 
- [92] Hahn HT. *Fatigue Behavior and Life Prediction of Composite Laminates, Composite Materials: Testing and Design ASTM STP 674*. Tsai SW editor, ASTM, 1979. 383-417.
- [93] Ramani SV and Williams DP. *Notched and Unnotched Fatigue Behavior of Angle Ply Graphite/Epoxy Composites, Fatigue of Filamentary Composite Matls, ASTM STP 636*.
- [94] Shimokawa T and Hamaguchi Y. *Distributions of Fatigue Life and Fatigue Strength in Notched Specimens of a Carbon Eight Harness Satin Laminate*.
- [95] Kan HP Shah, CH and M Mahler. *Certification Methodology for Stiffener Terminations*. DOT/FAA/AR-95-10, 1996.
- [96] *Composite Materials Handbook, volume 3, Polymer Matrix Composites, Materials Usage, Design and Analysis*. MIL-HDBK-17-3F, June 2002.
- [97] Broutman L.J. and Sahu S. *A New Theory to Predict Cumulative Fatigue Damage in Fiberglass Reinforced Plastics in Composite Materials Testing and Design, (2nd Conference) ASTM STP 497*. American Society for Testing and Materials, 1972. 170-188.
- [98] Hwan W. and Han K.S. *Cumulative Damage Models and Multi-Stress Fatigue Life Prediction*. J Composite Materials, 20, 1986. 125-153.
- [99] Revuelta D. Cuartero J. Miravete A. and Clemente R. *A New Approach to Fatigue Analysis in Composites Based on Residual Strength Degradation*. Composite Structures, 48, 1999. 183-186.
- [100] Epaarachchi J.A. and Clausen P.D. *A New Cumulative Fatigue Damage Model for Glass Fibre Reinforced Plastic Composites Under Step/Discrete Loading*. Composites Part A: Applied Science and Manufacturing 36, 2005. 1236-1245.
- [101] Adam T. Gathercole N. Reiter H. and Harris B. *Life Prediction for Fatigue of T800/5245 Carbon-Fibre Composites: II Variable Amplitude Loading*. Fatigue, 16, 1994. 533-547.
- [102] Shokrieh M.M. and Zakeri M. *Generalized Technique for Cumulative Damage Modeling of Composite Laminates*. J Composite Materials 41, 2007. 2643-2656.
- [103] Wahl N.K. *Spectrum Fatigue Lifetime and Residual Strength for Fiberglass Laminates*. Montana State University, Mechanical Engineering Department, 2001. PhD thesis.

- 
- [104] [www.taygeta.com/random/weibull.xml](http://www.taygeta.com/random/weibull.xml).
- [105] Composite Materials Handbook. *Mil-Hdbk-17-1F, vol 1, Polymer Matrix Composites*. Guidelines for Characterization of Structural Materials, 1997. chapter 8.3.4.
- [106] Agarwal B.D. and Broutman L.J. *Analysis and Performance of Fiber Composites*. Wiley, 1980. 20.
- [107] Hexcel product data on as4/8552 hexply material. [www.hexcel.com/resources/datasheets/carbon-fiber-datasheets/as4.pdf](http://www.hexcel.com/resources/datasheets/carbon-fiber-datasheets/as4.pdf).
- [108] Rangaraj S.S. and Bhaduri S.B. *A Modified Rule-of-Mixtures for Prediction of Tensile Strengths of Uni-directional Fibre-Reinforced Composite Materials*. J. Materials Science, 29, 1994. 2795-2800.
- [109] Beyerlein I.J. and Phoenix S.L. *Statistics for the Strength and Size Effects of Microcomposites with Four Carbon Fibers in Epoxy Resin*. Composites Science and Technology, 56, 1996. 75-92.
- [110] Lee J-W and Harris C.E. *A Micromechanics Model for the Effective Youngs Modulus of a Piecewise-Isotropic Laminate with Wavy Patterns*. J. Composite Materials, 22, 1988. 717-741.
- [111] Kassapoglou C. Fantle S.C. and Chou J.C. *Wrinkling of Composite Sandwich Structures Under Compression*. J. Composites Technology and Research, vol 17, 1995. 308-317.
- [112] Kyriakides S. Arseculeratne R. Perry E.J. and Liechti K.M. *On the Compressive Failure of Fiber Reinforced Composites*. Int. J. Solids and Structures, 32, 1995. 689-738.
- [113] Varelidis P.C. McCullough R.L. and Papaspyrides C.D. *The Effects of Temperature on the Single-Fiber Fragmentation Test with Coated Carbon Fibers*. Composites Science and Technology, 58, 1998. 1487-1496.
- [114] Qian C. *phD thesis work on fatigue of uni-directional fiber-glass composites*. progress presentation, Sep 2010.
- [115] Hedgepeth J.M. and van Dyke P. *Local Stress Concentrations in Imperfect Filamentary Composite Materials*. J. Composite Materials, 1, 1967. 294-309.
- [116] Zho X.-F. and Wagner H.D. *Stress Concentrations Caused by Fiber Failure in Two-Dimensional Composites*. Composites Science and Technology, 59, 1999. 1063-1071.

- 
- [117] Composite Materials Handbook. *Mil HDBK-17-2E*. Vol 2: Polymer Matrix Composites Materials Properties. Chapter 4.
- [118] Kassapoglou C. *Determination of Interlaminar Stresses in Composite Laminates under Combined Loads*. J. Reinforced Plastics and Composites, vol 9, January 1990. 33-59.
- [119] Berthelot J.-M. *Analysis of transverse cracking of cross-ply laminates: a generalized approach*. J. Composite Materials, 31, 1997. 1780-1805.
- [120] Hashin Z. *Analysis of Cracked Laminates: A Variational Approach*. Mechanics of Materials, 4, 1985. 121-136.
- [121] A. Berthelot J.-M. Leblond P. El Mahi and Le Corre J.-F. *Transverse Cracking of Cross-ply Laminates: Part 1. Analysis*. Composites Part A, 27, 1996. 989-1001.
- [122] Berthelot J.-M. *Transverse Cracking and Delamination in Cross-ply Glass-fiber and Carbon-fiber Reinforced Plastic Laminates: Static and Fatigue Loading*. Applied Mechanics Review, 56, 2003. 111-147.
- [123] Kassapoglou C. *Stress Determination at Skin Stiffener Interfaces of Composite Stiffened Panels Under Generalized Loading*. J. of Reinforced Plastics and Composites, vol 13, 1994. 555-572.
- [124] Kassapoglou C. *Determination of Interlaminar Stresses in Composite Laminates under Combined Loads*. J. Reinforced Plastics and Composites, vol 9, January 1990. 33-59.
- [125] Dvorak G.J. and Laws N. *Analysis of Progressive Matrix Cracking in Composite Laminates II. First Ply Failure*. J. Composite Materials, 21, 1987. 309-329.
- [126] Hashin Z. *Failure Criteria for Unidirectional Fiber Composites*. J. Applied Mechanics, 47, 1980. 329-334.
- [127] Wang A.S.D. *Fracture Mechanics of Sublaminar Cracks in Composite Materials*. Composites Tech Review, 1984. 6-45.

---

## Biographical Note

Christos Kassapoglou (with two “ss” and not one) was born in Athens Greece on November 27 of the year that the Boston Celtics won their 8th straight NBA Championship by sweeping the Lakers (then Minnesota Lakers) 4-0. All in all that was a good year. It was the same year the Celtics scored 173 points against the Lakers in a single game and it was the year of the first transcontinental jet flight from Los Angeles to New York. Cost: \$301. It was also the year that Elvis entered the UK music charts for the first time with “Heartbreak Hotel”. And Richard Starkey (aka Ringo Star) was given his first drum set. Even the spectacular eruption of the Kilauea volcano in Hawaii on November 14 (contrary to what some might think, totally unrelated to the events of November 27) was a good omen. In high school he started hang-gliding. After finishing Athens College High School in Athens, Christos went to MIT in Boston for undergraduate and graduate studies (BS in Aeronautics and Astronautics and two MS degrees one in Aeronautics and Astronautics and one in Mechanical Engineering). It was there that he saw a hamburger for the first time (and unfortunately not the last). He passed the PhD qualifying exam at MIT but opted for work in industry and did not even start the PhD program. He worked for three years at Beech Aircraft in Wichita KS on the all-composite Starship I. One of the most rewarding and educational experiences of his life. It was there that he learned how to drive in ice-storms. He had no choice on the matter. He then left the Midwest for the East Coast. He worked for almost 15 years in the Structures Research Section of Sikorsky Aircraft. It is there that he met some of the best engineers on this planet and is indebted to them for teaching him how to be an engineer and a human being. He also learned how to figure skate and managed to pull off some double jumps. All good things come to an end, hopefully giving way to other good things, and he left Sikorsky in 2001 to return to Greece. He spent the next 8 years consulting for US companies on structural analysis of composite structures. In 2008 he was talked into joining the faculty of Aerospace Engineering at the Delft University of Technology, first part time and, since 2010, full-time. He still does consulting. He does not hang-glide any more. He figure skates occasionally. And he is trying to break the world record for the longest time span between an MS and a PhD degree (28 years). He won the lottery twice: The first time when he got married to Annie and the second when his son George was born.



